Advanced Microwave Filter Design

By

Marjan Mokhtaari

B.Sc. in Systems and Communications, Sharif University of Technology, IRAN, 1998
M.Sc. in Electromagnetic and Microwaves, Sharif University of Technology, IRAN, 2000

A Thesis Submitted in Partial Fulfillment of the Requirement for the Degree of

Doctor in Philosophy

In the Department of Electrical and Computer Engineering

Advanced Microwave Filter Design

by

Marjan Mokhtaari

B.Sc. in Systems and Communications, Sharif University of Technology, IRAN, 1998
M.Sc. in Electromagntics and Microwaves, Sharif University of Technology, IRAN, 2000

Supervisory Committee

Dr. Jens Bornemann, Department of Electrical and Computer Engineering

---

Supervisor

Dr. Smain Amari, Department of Electrical and Computer Engineering

---

Co-supervisor, Royal Military College of Canada

Dr. Wolfgang Hoefer, Department of Electrical and Computer Engineering

---

Departmental Member

Dr. Zuomin Dong, Department of Mechanical Engineering

Outside Member

Supervisory Committee

Dr. Jens Bornemann, Department of Electrical and Computer Engineering
Supervisor

Dr. Smain Amari, Department of Electrical and Computer Engineering, Royal Military College
Co-supervisor

Dr. Wolfgang Hoefer, Department of Electrical and Computer Engineering
Departmental Member

Dr. Zuomin Dong, Department of Mechanical Engineering
Outside Member

ABSTRACT

This thesis presents new procedures and guidelines for the design of advanced microwave filters. Practical implementations include dual-band, multi-band and ultra-wideband filters for applications in wireless and telecommunication systems. The traditional narrow-band coupling-matrix approach is extended to include multiple and out-of-band resonances, which allows the model to accurately predict and design the filter performance over a wide frequency range. A variety of coupling scenarios are presented and their advantages over current designs demonstrated. The approach includes the placement of transmission zeros in order to obtain quasi-elliptic responses, improve stopband performance and generate sharp transitions from the passbands to their adjacent stopbands.

In order to contribute to filter miniaturization, bandwidth enhancement and manufacturing simplicity, a new class of step-impedance resonators is proposed and their harmonic tuning properties utilized. Advanced coupling configurations are realized, which are applicable to single- or multi-band filter operations with bandwidths ranging from a few percent to fifty percent. Moreover, the developed design procedures are applied to ultra-wideband filters covering bandwidths of up to 150 percent.

All filters designed with the procedures developed in this thesis are validated by several commercially available electromagnetic field-solver packages, in-house numerical codes and/or measurements. The excellent overall agreement between computational and experimental results verifies the advanced filter design procedures presented in this thesis.

Dedication to

The memory of my beloved and sacrificed mother, ***Fatima,***

The best father in the world, ***Abbas,***

and to my lovely sisters, ***Malih*** *and* ***Mojgan.***

Acknowledgments

During my study and research at the University of Victoria, I have been extremely blessed by God to meet and collaborate with many people who were so supportive and helpful in this research.

I would like to deeply thank my advisor, Prof. Jens Bornemann for his strong knowledge and continuos support, patience and extemplary courage to embark on research avenues. He has been my best research advisor ever and it has been a privilege collaborating and working with him within past years. He has been source of ideas and understanding, yet, his wisdom allowed me to direct and finish my research successfully.

I would also like to extend my special appreciation to my co-advisor, Prof. Smain Amari for introducing me to this wonderful research group at the University of Victoria and his support and fruitful discussions. I would like to thank Prof. Wolfgang Hoefer and Prof. Zomin Dong for serving on my commitee and providing me with their different aspects and useful comments on this thesis. I am also grateful to Prof. Nayeb Denidni for seving as External Examiner.

I would like to acknowledge breath and dept of help I have recieved from my friends at the University of Victoria, specifically at the Numerical Electromagnetics and Microwave Laboratories. The spirit of perseverance and cooperations with Prof. Bornemann's group produces a unique environment that nurtures academic excellence. I wish to thank, in particural, Dr. Rambabu Karumudi, who generously provided me with his help on the fabrication of the dual-band filters and his useful discussion on different aspects of my thesis; Mr. Albie Thiart, Dr. Seng Yong Yu, Dr. Huilian Du and Dr. Jinye (James) Zhang, who helped me feel comfortable in the new environment. My next appreciation goes to the secretory of the group, Mrs. Donna Shannon, who indebtly supported me within the past years.

Also, I am greatly thankful to my friends for their constant support and friendship. I would like to thank, in particular, Dr. Farshad Khunjush, Mrs. Maryam Mizani and Miss Yasi Barzi for countless and true support.

Finally, it is time to mention the most important people in my life, my parents, who did everything that is humanly possible, so that I could reach *any* goal I dreamed of throughout my life. I learned not to settle for anything but the best from my beloved mom, who was always the pillar of strength, support, patience and unconditional love for the whole family. My dad showed me how hard work and patience always pays off. My loving sisters, Malih and Mojgan, should know that I am very proud of them as sisters and persons for what they do everyday. Without their continued sopport, I would have not accomplished this effort. *Merci and I love you all !*

List of Contents

List of Figures

CHAPTER 1

Introduction

1.1 Motivation and Background

Filters are among the most important components of wireless and communications networks, and as far as efficiency and size are concerned, they may impose stringent restrictions on the performance of any mobile or stationary communication system. With recent advances in Low-Temperature Co-fired Ceramic (LTCC) and Micro-Electro-Mechanical System (MEMS) technologies, high-performance transmit and receive modules are now realizable. Although significant efforts have been devoted towards achieving compact low-power electronic and radio frequency (RF) components, issues related to design and fabrication of efficient, compact and integrable filters have hardly been addressed. This remains true also for antennas and all passive distributed microwave components such as couplers, hybrids and multiplexers, whose dimensions are considered in terms of required specifications. The performance dependence stems from the fact that all of the aforementioned distributed components are composed of one or more resonant structures. Therefore, the main objective of this dissertation is to embark on the challenging issues of microwave filter design and performance for next generation wireless communication systems.

In addition to the need for compactness, low-power characteristics of such transmit/receive modules are extremely important and require highly efficient low-loss components. In order to reach minimum power consumptions in micro-circuits, smaller numbers of devices are preferred.

As a result of shared medium in wireless communications, the valuable frequency

spectrum has been divided to serve a diverse range of applications. Conventionally, wireless devices operate at a frequency band allocated for a particular application. Since received signals from other wireless devices act as undesirable interference, transceivers are often designed for narrow frequency bandwidth. The limited operation bandwidth of these systems makes them incapable of functioning at frequency bands other than their own. On the other hand, wireless systems capable of operating at multiple frequency bands are useful in numerous applications and are in great demand. Mobile phone terminals with ability of wireless connection to the Internet are examples of multi-band systems.

Channels of traditional communications satellite systems are assigned contiguously in frequency, and each channel is provided by a channel filter, amplified, and transmitted. Therefore, filters in such systems have one passband illustrating the active channel. Such conventional filters can be synthesized using different methods, e.g., image parameter or insertion loss methods [1]. The connection of the parts operating at each single band is a critical issue for single input/output ports and can ultimately impact on the final performance. As a result, this approach leads to a bulky and costly structure with minimum compatibility in various technologies.

The overall concepts of advanced filters started in the 20^{th} century when Matthaei, Young and Jones introduced the coupling scheme in terms of the structural parameters between square and cylindrical cavities [2]. For a general multi-cavity structure, three types of couplings are typically present: magnetic and electric field coupling at the end of the cavity as well as electric field coupling in the cavity's center. Later, Atia and Williams reported a coupling network demonstrating a method of coupling elements extraction, which is governed by successive similarity transformations in form of plane rotations to the coupling matrix [3]. The angle of rotation is coordinated in order to minimize the sum of the squares of the coupling components affected by the plane rotation; then they are enforced to vanish. The computation of the input/output structure, inter-cavity slots and cavity dimensions in terms of the coupling parameters, matching resistors, center frequency and bandwidth represents a practical synthesis for waveguide filters. Particularly, Atia and Williams [3] employed Matthaei's theory in combination with Bethe's theory [3], which holds for small apertures and zero wall thickness, in

order to estimate all structural parameters. However, significant difficulties between experimental performances and computations were observed, and fine-tuning was an essential requirement [2]. The concept of quasi-dual mode resonators both in waveguide and planar technologies has reduced the number of utilized resonators and improved performance in a bandpass filter design [4-5].

Modern communication systems often use a complex arrangement of frequency plans and spatial coverage. Such systems require multi-band modules including filters with multiple passbands. Multi-band filters used to be developed in distinctive parts demonstrating each single band for convenience. Dual-band filters specifically, as a example of multiband filters, have been studied in several papers on various technologies and attracted attention worldwide [6-9]. The conventional concept of the design refers to combinations of switches between two separated filters operating at two distinctive frequencies [6-7]. This architecture dramatically impacts on size, cost, efficiency and power dissipation of the entire structure compared to a single passband filter. Alternatively, several stubs are utilized in order to generate attenuation poles to separate the bands, thus contributing to wide stopband regions [8], [10-11]. The dual-behavior resonators (DBR's) associated with different parallel open-ended stubs allow the designers in [10-11] to independently control the in-band and out-of-band responses of filters. The dual-behavior resonators include step-impedance resonators (SIRs), and stubs of different lengths lead to narrow-band filters with required operating bands. A concurrent dual-band filter integrates the characteristics of each passband filter in a single circuit, which automatically produces two passbands located at any two desired frequencies without increasing power consumption or a significant potential in cost and size. The semi-lumped prototype in [12] facilitates the split resonating frequencies of coupled resonator pairs to realize the dual-band response. The dual-band feature for multi-mode wireless Local-Area Network (LAN) systems can also incorporate step-impedance resonators with special input/output ports [13-14]. The coupling schemes on SIRs reported in [15-16] achieve dual-band characteristics with enhanced coupling excitation and additional matching network. The common disadvantages of aforementioned references are asymmetric multiple spurious responses of the fundamental passband within narrow bandwidths.

Recent multi-band filters explore the existence of resonators operating at multiple

frequencies. The final dimensions of the entire structure decrease drastically, but the interactions between the individual bands increase. A different way is to generate multiple stopbands within a broad-band filter through cross-coupling techniques [17]. This meditates the multi-passband filter synthesis and projects high efficiency on filter performance due to the significant attenuation on the sides of each single band. However, the number of single resonators utilized is at least two times higher than those filters with multi-harmonic resonators. The combination of aforementioned techniques accelerates both multi-band filter synthesis and is a breakthrough to enhancing efficiency and performance, which exclusively assist to capture the advantages of both techniques.

Various configurations have been proposed for realizing dual-band filters in printed-circuit technologies and mostly are uniplanar structures [13-14], [8-9]. The coalesced single-input single-output filter in [9] incorporates so-called frequency-selective resonators that are composite in structure, cascaded microstrip lines (resonators) on a two-dimensional periodical surface or so-called photonic bandgap (BPG) ground planes. It achieves an asymmetric dual-band behavior through additional degrees of freedom for controlling the relative positions of the passband center frequencies. In [14], the second resonance mode of quarter-wave or half-wave resonators is adjusted to operate at the second passband of the dual-band filters. Quendo *et.al.* describe a four-pole dual-band filter, whose wideband performance is separated by three transmission zeros generated by three open-end stubs [8]. The authors also report a dual-behavior resonator based on the parallel association of two different band-stop structures, which implies a constructive combination of two types of stubs utilizing step-impedances with different stub lengths [10-11].

The generation of a transmission zero or attenuation pole can be displayed in terms of field distributions within a filter structure. Consider the waveguide dual-band filter consisting of four resonators as shown in Fig. 1.1a. Its design concept will be described in the next chapters. The center frequencies of the first and second passbands are located at 14.15 GHz and 15.95 GHz, respectively, with multiple transmission zeros between and out of passbands. These transmission zeros are generated by source/load coupling and cross coupling between higher-order harmonics (see Chapter 3).

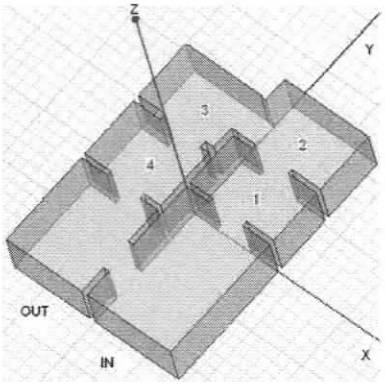

(a)

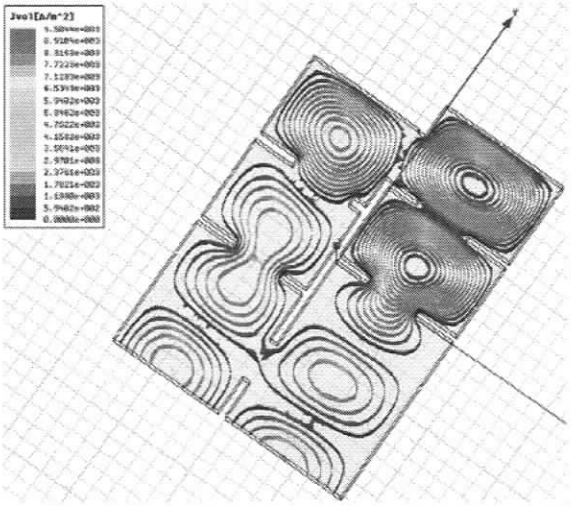

(b)

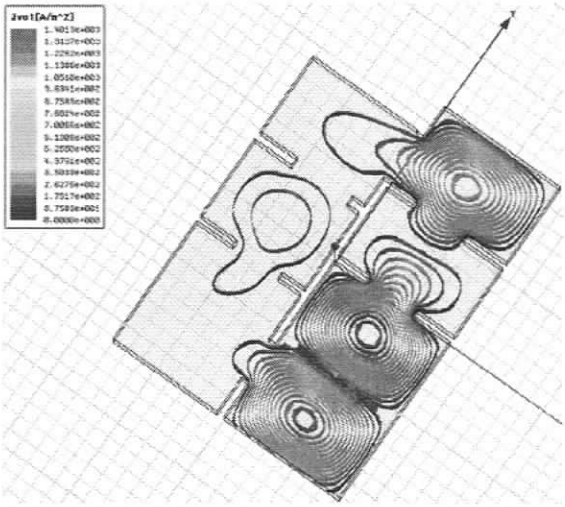

(c)

Fig. 1.1 Dual-band filter structure (a); field distributions in second passband at 15.95 GHz (b); transmission zeros at 15 GHz (c) and 17.6 GHz (d).

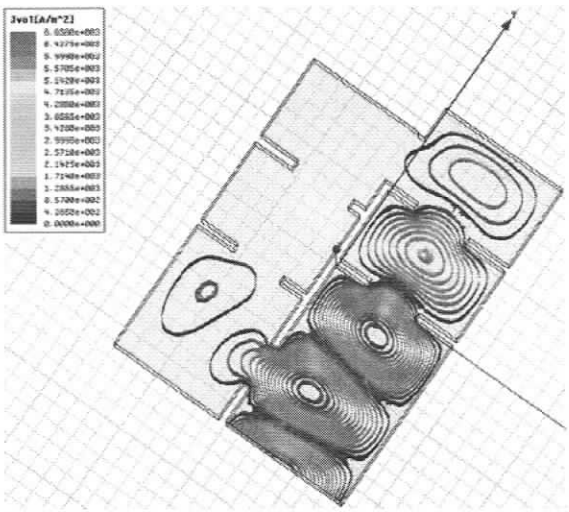

(d)

Fig. 1.1 Continued.

The fundamental mode excited at the input is TE_{10}. Fig. 1.1b shows the magnetic field distribution within the filter structure in the second passband at 15.95 GHz. Fig. 1.1c displays the distribution at the transmission zero located between the passbands at 15 GHz, which is generated through source/load coupling. Fig. 1.1d depicts the field distribution of another transmission zero produced through cross coupling between higher-order harmonics in the upper suppression region at 17.6 GHz. The density of the field distribution for transmission-zero frequencies is much smaller than that in passbands. Therefore, no field is observed at the output for transmission zeros, which defines the existence of high attenuation at those frequencies. Note that there is a small output signal in Fig. 1.1d. However, upon inspection of the related phases, this is a TE_{20}-like mode which is below its cutoff frequency for the Ku-band (12-18 GHz) filter.

The work by Tsai and Hsue investigates a dual-band filter composed of wideband and bandstop filters in a cascade connection, wherein the transfer functions of both passband and bandstop filters are expressed in the Z-domain [17]. Coupled-serial-shunted line structures and serial-shunted line configurations are the main elements for bandpass and bandstop filters, respectively. So far, the highly selective dual-band effect is accomplished by the step-impedance resonators due to their tunable harmonic response property in a planar structure inter-coupled in the same topology as a classical bandpass filter (BPF) [18]. The coupling coefficients play an essential role in the design of a dual-band filter. However, it is often difficult to achieve the

proper coupling coefficients and required quality factors for a multi-harmonic coupled transmission line resonator in two separate frequency bands [15-16].

Various architectures of step-impedance resonators, such as hairpin, folded or open loop configurations, are also presented in a number of publications [13-16] to model the dual-band characteristics. Chen [12] documents a novel dual-band filter configuration that employs two identical pairs of hybrid coupled quarter-wave transmission lines. Gradually, each pair of coupled resonators is designed such that its lower and higher split resonating frequencies are located at two designated passbands and utilized as the resonating mode of the dual-band filter. Transmission zeros, also referred to as attenuation poles and causing sharp skirts on the sides of each passband, are realized in these papers; however, the degree of freedom to appropriately select the relative positions of attenuation poles is missed. The above-mentioned publications demonstrate novel designs in planar filters structures, but most of them are not appropriate for miniaturized realization in a multi-layered circuit, such as LTCC, in which both active and passive components can be integrated for system-in-package (SIP) implementation. The dual-band filter developed in the LTCC technology combines in shunt two bandpass filters operating at different frequency bands via matching networks at termination ports. The performance of these filters degrades due to the thickness, dual-band matching network and multiple input/output ports in a compact layer. On the other side, these approaches come with additional expenses in terms of stacked filter size and added complexity [7].

In waveguide applications, in-line type elliptic response filters were first presented for frequency selectivity enhancement, mass and volume reduction of filters for satellite transponders [2-3]. Rigorous systematic design procedures for folded waveguide filters with cross coupling later eliminated the need for global optimization and resulted in a quasi-elliptic function response with sharper transition from passband to stopband [19].

Due to ease of fabrication and tuning, in-line type dual-mode filters, with termination ports positioned on opposite sides of the structures have been investigated widely for satellite applications [20-22]. Alternatives of conventional dual-mode filter designs are revealed via independent variables into a filter's coupling topology through a sequence of plane rotations or

similarity transformations. This technique is applicable to any reciprocal filter having multiple signal paths [21]. Non-degenerate modes of physical resonators instead of degenerate modes are also employed in dual- to triple-mode pseudo-elliptic filter designs in order to eliminate intra-cavity couplings. This design is ideal for situations, where real transmission zeros are required in the vicinity of the passband [22]. Asymmetric realization of dual-mode waveguide filters outlined in [20] also provides a comprehensive solution in the area of microwave filter design.

The n-pole in-line type dual-mode filter can realize $n/2$ transmission zeros at the most. The possible solution to increase the number of attenuation poles up to n is simply formed by employing a canonical structure. Holme in [23] outlines the realization of an in-line type dual-mode dual-band filter with elliptic response by allowing zeros to subdivide the filter into multiple passbands. A letter on a dual-mode canonical filter commences on the design of dual passbands [24]. The filter adopts conventional dual-mode techniques for mass and volume reduction. Besides, the canonical structure is also adopted for the maximum zero realization, which can be applied to commercial filter design.

A part of this dissertation presents a new coupling network approach to realize and synthesize in-line / folded type multi-band filters. Cross-coupled resonator filters are typically achieved via waveguide cavities or dielectric-resonator loaded cavities due to their low loss. On the other hand, in order to minimize volume, weight and cost, planar structures are most appealing. The method for the rigorous calculation of the coupling coefficients of the basic coupling structures encountered in the type of dual-band filters is developed in the same way as that for a single passband filter. This technique is also applicable to dual-mode or quasi-dual-mode filters and can be extended to the design of multi-band filters. The disadvantage of high conductor loss of planar filters using conventional conducting thin films can be overcome by replacing them with high-temperature super-conducting (HTS) thin films. It is also possible to combine them with active monolithic microwave integrated circuit (MMIC) devices to compensate the loss in the receiver or transmitter [25].

The proposed cross-coupled network in this research manages to increase the number of transmission zeros up to the number of employed resonators, which assists in capturing advanced

filter performance. This novel approach can be implemented in both waveguide and planar structures. To validate the design technique, several dual/triple-passband filters in waveguide and microstrip technologies are designed and verified.

The design of filters in waveguide or planar technologies requires careful attention to the modeling of coupling phenomena [26-27]. Therefore, the intrinsic coupling limitation of implementation processes can be accounted for, and undesirable effects such as additional passbands or suppression regions within a broad frequency range can be minimized or eliminated. These phenomena will assist in the design of multi-pass/stopband components. Cross-coupled filter synthesis is simply accelerated through the general analytical approach combined with gradient optimization techniques [26]. The proposed method accompanied by coupling topology can achieve passband filters with quasi-elliptic function response and, at the same time, linear phase in the passband. The extracted-pole technique can be simply employed in the filter's coupling configuration for better performance specifications [19], [27]. The coupling phenomena also facilitate the split-resonating frequencies of coupled resonator pairs in dual-band response realizations [12]. A non-resonating node model (NRNM) containing both resonating and non-resonating nodes is introduced along with singlets as the smallest basic building blocks for modular quasi-elliptic filter design [29]. Longitudinal dual-mode dielectric resonators are revealed for alternative dual-mode filter designs by inserting independent variables into the coupling scheme [21]. Other dual- and triple-mode pseudo-elliptic filters introduced in [22] utilize the degenerate modes of a physical resonator and intra-cavity coupling elimination. The generated transmission zeros are simply controlled by a dedicated mode whose resonance frequency coincides with the frequency of the transmission zero, which ultimately makes the design ideal for situations, where real zeros are required in the immediate vicinity of the passband. Pseudo-highpass filters are also synthesized through dual-mode operation modeling, bypass coupling and minimum required numbers of physical cavities [34].

A high level of coupling modeling is necessary and can only be accomplished by full electromagnetic (EM) analysis of the entire structure over wide frequency ranges. The EM-based techniques, including Coupled Integral Equation and Mode Matching techniques (CIET and MMT) for waveguide structures and the Method of Moment (MOM) for planar structures, have

proven to be powerful tools for solving the electromagnetic field problems and have been successfully applied to the analysis of various complicated planar and general 3-D structures [19], [21], [28], [30-34].

The design of microwave components such as filters, couplers, power dividers, diplexers and multiplexers requires an efficient / extensive coupling scheme relating the coupling coefficients between all elements and generate/degenerate modes. An analytical method for the synthesis of multiport microwave networks formed by coupled resonators has been proposed in [35]. The method is based on the definition of coupling and includes resonant and no-resonant nodes and an arbitrary number of input/output ports. It is linked with a synthesis procedure analogous to the one used for filters. The combination of the aforementioned technique with EM-based computation as a hybrid technique is employed for the design of microwave diplexers and multiplexers [30].

An efficient and advanced coupling configuration exhibits the conventional coupling topology extended by additional nodes of all non-resonant and resonant modes excited in the microwave component structure [3]. The realization of such a coupling scheme is a difficult task due to the multiple coupling coefficients between generate/degenerate modes at each single discontinuity. The challenges of this part of the research lie in the following aspect: (1) the theory must have an efficient feature to model cross-coupled networks, which partly eliminates the narrow-band restriction found in the current coupling matrix approach; (2) it must have the capability to increase the performance accuracy; (3) it must possess the ability to model different microwave components such as multi-band filters; and (4) it must have the capability to extract coupling models from field simulations. The objective of the second part of this dissertation is to develop the extended coupling models for the advanced design of microwave filters.

The license-free assignment of the 3.1GHz to 10.6GHz frequency range by The United States Federal Communications Commissions (FCC) pioneered fundamental research on ultra-wideband (UWB) devices for low cost wireless systems in military or commercial applications [36], [67-68]. Ultra-wideband communication systems promise high bandwidth, reduced fading from multipath propagation and low power requirements with a power spectral density of -

41.3dBm/MHz [37]. In the design context, fabrication and characterization of effective UWB filters employed in UWB modules are challenging tasks when compared to those of narrow band systems [38]. A suitable UWB filter should be capable of operating over a very wide frequency range under low power. Therefore, it is essential to guarantee a good behavior of the filter in the entire band of interest in terms of filter properties. These properties include bandwidth, transfer function, passband skirt, spurious suppression regions, impedance matching and amplitude and phase linearity within the passband in order to avoid distortions of the transmitted/received signals [38].

UWB filter design was initiated by the utilization of multiple resonators to cover the entire bandwidth [39]. This model requires a large number of resonators and can hardly achieve the required filter specifications. The development of an UWB filter using ring resonators and a transmission line model is addressed in [39-40]. The adjustment of both the ring and stub impedances contributes to controlling the attenuation pole frequency and can accomplish 86 percent bandwidth with five cascaded resonators. Microwave and RF narrow-to-wideband Surface Acoustic Wave (SAW) filters are reported in [41] using high performance resonators with very small capacitance ratios. The disadvantage of this technology, however, is that a particular substrate structure is required to suppress spurious responses.

Menzel et. al. report and describe two types of suspended-stripline (SSL) ultra-wideband filters, one based on a standard lumped element (L-C) filter concept including attenuation poles and a second one consisting of the combination of a low-pass and a high-pass filter [42], [71]. Moreover, the insertion of a notch stub on the bottom layer of the SSL filter to tailor the UWB spectrum is demonstrated in [51]. Co-planar waveguide bandpass filters for UWB applications and up to 50 percent bandwidth are also addressed in [43]. An aperture compensation technique and an inserted pair of capacitively loaded line sections are developed to control coupling strength and to formulate multi-pole passband behavior, respectively. Broadside and edge-coupled coupled-line ultra-wideband differential-mode filters are found to exhibit up to 170 percent fractional bandwidth [44], [56]. The system is embedded with a self-complementary antenna, a notch and a lowpass filter. Ultra-wideband filters are also realized in LTCC technology through stacked coupled resonators and inductance feedback [45]. The achieved

fractional bandwidth is up to 48 percent, but a very compact structure is obtained which is suitable for integration on chip.

In 2005, a new generation of UWB filter design was introduced in hybrid microstrip and co-planar waveguide (CPW) technologies [46], [64]. A full-wavelength CPW nonuniform resonator or multi-mode resonator (MMR) is constructed to produce its first three resonant modes around the lower end, center and higher end of the frequency band. Then a microstrip/CPW surface-surface coupled line is formed and designed to allocate enhanced coupling around the center frequency. Later work proposed similar UWB filters using broadside-coupled microstrip-coplanar waveguide structures integrated with a lowpass filter for better upper-band rejection performance [47]. Single- or multi-notch bands for the purpose of avoiding interference between the UWB radio system and existing services are also realized [50]. The single- to multi-notch bands are implemented by integrating stubs in the broadside-coupled conductors. The authors of [46] also report a different multiple-mode resonator based on an aperture-backed microstrip line. With the backside aperture on the ground plane, a non-uniform resonator is constructed with the first three resonant modes occurring within the band of interest while the parallel coupling between a resonator and two feed lines improves performance [48], [68]. Other composite microstrip-coplanar waveguide UWB filter structures are addressed in [53], [62]. The microstrip-CPW transitions and the CPW shorted stubs are adopted as quasi-lumped circuit elements for realizing a three-pole highpass filter prototype. By using a cross-coupled capacitance between the input and output ports and suitably designing transition stubs, an ultra-wideband filter is implemented with two transmission zeros at the band skirts [53]. The ultra-wideband filter in [62] comprises a single CPW quarter-wavelength resonator, which is coupled to two quarter-wavelength microstrip open-circuited stubs on the reverse side of the common substrate. The structure is capable of producing attenuation poles due to the associated side-coupling arrangement of input/output ports. A dual-metal-plane filter structure with a microstrip to CPW feeding mechanism is also developed to provide strong enough capacitive coupling for bandwidth enhancement [66]. CPW split-mode resonators and a short-circuited stub to implement the shunt inductance between two quarter-wavelength step-impedance resonators are utilized.

The recent progress in UWB filter design demonstrated in [48] consists of a multi-mode

resonator (MMR), two outer arms in the interdigital lines and two capacitive-ended interdigital coupled lines [54]. Particularly, two outer arms in the tapered configuration improve the coupling strength and compensate for the phase imbalance near the upper band limit by relying on extra capacitive-ended stubs. They are designed to assign their attenuation poles towards the fourth-order resonant frequency of the MMR, thereby suppressing the first spurious passband. Another UWB configuration utilizes a stub-loaded multiple-mode resonator rather than capacitive-ended stubs in symmetrical locations, which contributes to wider upper-band rejection performance [59].

Modified Z-transform techniques in complement with parallel two-section open-circuit stubs were used in microstrip technology to form relatively wideband filters with multiple transmission zeros at the upper/lower band edges for sharp rejection [49], [65]. Good performance on the edge rejection and within the passband is observed, but relatively small fractional bandwidth and a large number of transformer sections and stubs are the disadvantages of the reported UWB filter. A piecewise frequency approximation for the complex distribution of structured parameters has also been proposed for UWB filter design. The synthesis relies on two-section open-circuited stubs of non-equal length [69]. Later, short-circuited stubs rather than open stubs separated by nonredundant connecting lines for filter selectivity were introduced [61]. The folded configuration facilitates source/load coupling for additional attenuation poles and results in compact structure [65]. Embedding open stubs in the source and load connecting lines enables a notch filter in order to reject an undesired existing radio signal, which may interfere with the UWB operation [70].

Highpass (HP) and lowpass (LP) section combinations are commonly used in the exact synthesis of UWB filtering responses, since it requires a fair number of resonators to cover a very broad frequency range [52]. The frequency spectrum in the rejection band seems to be free of spurious responses due to the implementation of a low-pass section. A defected ground structure with hybrid quasi-lumped elements as inter-digital capacitors illustrates another example of UWB filter design in this HP/LP combination category [58]. Cascaded microstrip square ring resonators loaded with open stubs are also reported for sub-millimeter UWB filters with up to 20 percent fractional bandwidth [55]. Semi-lumped parallel resonance circuits adopted in

conjunction with optimum distributed HP/LP filters are studied in LTCC technology [63]. The implemented ultra-wideband filter using an optimum distributed HP filter structure of 11^{th} order demonstrates compactness, good selectivity and suppressed spurious responses due to the employed lowpass filter.

The realization of UWB filters in waveguide technology is also reported based on silicon-on-insulator (SOI) multimode interferometer (MMI) couplers and a Mach-Zehnder interferometer (MZI) in nanometer wavelength [57]. Ridge waveguide resonators realized in LTCC technology achieve ultra-wideband filters by printing parallel planar conductors as top and bottom walls and closely spaced metal-filled vias for the lateral walls [60]. The development of stripline transitions for impedance matching is essential.

The introduction of the multiple-harmonic Step-Impedance Resonator (SIR) has clearly facilitated filter synthesis; however, conventional configurations of SIRs require extremely small gaps between the coupled segments. Hence, this emphasizes manufacturing accuracy and ultimately results in increased expenses. Furthermore, the poor transitions from the passband to the stopbands cannot be ignored.

Recent UWB filter research tends to focus on miniaturization as such structures are more practical in terms of easy manufacturing and fabrication, cost and integration with other system boards [71 - 73]. In the past few years, several planar broadband filter configurations have been reported for UWB applications; nevertheless, few efforts have been made to reduce the entire size, manufacturing cost, but improve performance simultaneously.

Cascading multiple SIRs can feature good performance of UWB filters in both passband and stopband regions, but the designs can be rather long and spacious. Filter miniaturization reinforces the utilization of compact resonators.

Another aim of this dissertation is to introduce simplified and compact step-impedance resonators, which facilitate stronger coupling between coupled segments. Hence, this presents a significant reduction of the requirement for relatively small gaps in coupled-line sections.

Meanwhile, a new generation of compact SIR composed of loaded parallel high-impedance segments and folded low-impedance segments, which differ from those in [48], is documented and applied to UWB filter design with and without source/load coupling.

The purpose of the proposed SIRs is not only to enable and assure UWB filter realization but also to target dual-band filter synthesis in narrow to ultra-wideband applications. The term of bandwidth for dual-band filter synthesis depends on the type of utilized coupling topology. The proposed in-phase and out-of-phase coupling schemes manage to model narrow to ultra-wide passbands, respectively. Moreover, they are capable of generating attenuation poles between the bands for high isolation. The performances within the rejection bands are improved through the cross-coupling methodology. The new generation of dual-band filters resolves former restrictions and difficulties and can combine excellent performance and compactness with ease of fabrication and low cost.

1.2 Thesis Overview and Contributions

The prospective and primary objective of this thesis is to develop, implement and test a new class of multi-band to ultra-wideband filters through novel generation and procedures of coupling configurations, and new schemes and solutions to enhance the efficiency of the filter design process. The new solutions minimize the synthesis burden, optimization complexity and are more compatible with fabrication technologies for integrated circuits. This task is divided into three main thrusts.

The first thrust addresses issues related to cross-coupled network modeling with higher/lower-order resonances. Generally, the conventional coupling configuration and coupling matrix is utilized to design filters either in waveguide or planar technologies. A new approach of cross-coupled networks is first proposed for the advanced design of microwave filters. By inserting additional nodes for higher-order mode resonances, a broadband model is obtained, which eliminates the narrowband restrictions found in conventional coupling matrix approaches. The proposed approach is shown to be effective for a variety of filter structures. The efficiency and accuracy of this broadband model is also demonstrated.

The second thrust addresses the design of miniaturized dual-band to multi-band filters. Attention is devoted to different aspects of this task, such as modeling the filter topology, enhancing the filter performance and introducing complementary realizations of the same topology.

The third piece of this work touches on the design of ultra-wideband filters with respect to the contribution of new, efficient and compact step-impedance resonators. Emphasis is placed on compact topologies and ease of fabrication.

In Chapter 2, the principles of filter synthesis are described. Fundamental circuit analysis is applied to a two-port single-band topology and can be extended to multi-port and multi-band microwave networks under specific circumstances.

In Chapter 3, a cross-coupled network model of filters is introduced. Conventional design approaches utilizing cross-coupled networks are valid only in the vicinity of the filter pass band. However, higher/lower-order mode resonances in waveguide filters can be advantageously utilized to create additional transmission zeros and/or passbands. It is thus of fundamental importance that such effects, which have a profound influence on the final filter performance, be included from the onset of the filter design procedure. Therefore, a new configuration of the cross-coupled network, which accounts for higher/lower-mode effects through a framework of resonating or non-resonating nodes, is presented in Chapter 3. It is demonstrated that the performance predicted from this model's coupling matrices is valid over a wide frequency range and not just within the conventional narrow-band assumption. The new cross-coupled approach is validated by comparison with in-house and commercially available field-theory-based codes for a variety of single or multi-mode waveguide filters.

Chapter 4 develops the extended concept of the conventional coupling matrix to include designs of dual- and triple-band filters. The multi-band response is created by either placing transmission zeros within the bandwidth of a wideband filter or using higher-order resonances. Realizable topologies both in planar or waveguide technologies can be imposed and associated coupling coefficients enforced during optimization. The design process is verified by

measurements and comparison with results of commercially available field solvers.

Chapter 5 delineates methodologies to enhance the performance of dual- and triple-band filters. These methods include the application of folded/cascaded and self-complementary step-impedance structures, both of which are shown to be very effective for performance and miniaturization improvement. Due to the tunable spurious response properties of asymmetric step-impedance resonators, the new filters feature two to multiple controllable passbands at desired frequencies, high out-of-band rejection as well as wide stop-band regions created by a zero-phase feed structure without input/output matching networks. In addition, in order to extend the number of attenuation poles in the vicinity of the passbands, negative and positive cross-coupling between the source and the load is applied. The new topologies occupy less space in comparison with traditional designs.

Chapter 6 focuses on the third thrust of this thesis, ultra-wideband filter design. Both folded and compact step-impedance resonators consisting of parallel open-end high-impedance and folded low-impedance segments are used to design different types of direct and cross-coupled UWB filters. Coupling between adjacent resonators as well as between input and output ports is intensified through parallel open-end high-impedance segments. Therefore, the requirement of relatively small gaps in coupled segments is significantly reduced. Having extracted frequency harmonics of employed resonators, design curves can be generated, and filter theory may be employed to design different UWB filters, where coupled-line sections play the role of inverter circuits. Effective techniques such as open impedance stubs and source-load cross coupling are utilized to create additional attenuation poles in the vicinity of the passband and in the upper/lower suppression band. The introduced filters are shown to be very compact compared with similar structures known hitherto. The roll-off performance of the proposed filters is demonstrated to be considerably higher than that of microstrip resonators of the same size. Moreover, in the last section of this chapter, a rigorous study will be conducted on the effect of the proposed step-impedance resonators using new coupling topologies for the design of quasi-elliptic dual-band filters for narrow to ultra-wideband applications. The new coupling techniques achieve up to 48 percent fractional bandwidth in each passband. Several different dual narrow-band to ultra-wideband filters are illustrated and fabricated. Professional EM based software

packages verify the individual responses.

Finally, Chapter 7 summarizes the contributions presented in this thesis and submits recommendations for the future work.

CHAPTER 2

Principles of Filter Synthesis

The current chapter explains the fundamentals of filter synthesis. The basic theory is applied to any two-port single band filter design and can be extended to multi-port and multi-band networks under circumstances.

2.1 Fundamentals of Coupling Schemes in Filters

2.1.1 Introduction

Coupled microwave resonators are crucial components in modern communication systems. To design a filter with increasingly stringent requirements, cross-coupled resonators are often used to generate finite transmission zeros [26], [79-82]. The general theory of coupled-resonator bandpass filters initially developed in 1970's by Atia and Williams [3], [83-85]. The proposed theory leads to a coupling configuration reproducing the system function and coupling elements to be synthesized; however, it can eventually lead to unwanted or unrealizable coupling components too. Repeated similarity transformations are then utilized to eliminate the unwanted couplings, which must be considered in final synthesis [86]. Unfortunately, this process does not always converge. A slightly different approach was developed by Cameron employing a predefined coupling configuration in order to determine the filtering function with arbitrarily placed transmission zeros. The design procedure of the filter proceeds by extracting element values of the coupling matrix, once the filter function is obtained [74-75] [87]. Low-order function filters were also analytically solved by Kurzrok [78] [88]. Besides, other literatures and studies demonstrated other techniques, e.g. [89-92].

In the recent decades, optimization has been employed to synthesize microwave filters structures. The entire elements of the coupling configuration are assumed to be independent variables as in former approaches, but a simple cost function along with unconstrained optimization techniques is employed.

Various optimization techniques have been widely introduced for the synthesis of the extended coupling scheme along with the utilized filtering function in terms of required accuracy and fast convergence. A fast procedure and an alternative solution in the synthesis of the extended coupling topology through solving the least squares problem were proposed in [82]. The technique relies on the definition of the cost function involving eigenvalues of the transversal coupling matrix and their principal upper and lower sub-matrices [93]. Analytically derived initial and gradient matrices of bordered tri-diagonal core matrices are implemented to improve convergence of the optimization method. The other method by Macchiarella features multiple rotations of the coupling topology extracted from a generic prototype, and the values of the rotation angles are specified through an efficient Guess-Newton optimization procedure [94-95]. Gajaweera and Lind addressed the application of Newton-Raphson methodology along with additional intelligent principles on the numerical procedure to assure fast convergence [96]. Other publications addressed the gradient-based synthesis method comprising an analytical expression of the derivatives of the cost function of multiple coupled resonator filters. This approach is insensitive and fast converging procedure and yields a coupling matrix with specified topology that produces attenuation and reflection poles of a prespecified characteristic function [26] [79].

2.1.2 Problem Statement and Circuit Analysis

2.1.2.1 Computation of Low-Pass Prototype Filtering Function

The performance of any type of filter is specified based on scattering parameters. The input scattering parameter is defined as the input reflection coefficient (S_{11}), which demonstrates the ratio of the reflected signal to the excited signal in the input port. The smaller this ratio, the better the input impedance matching. The transfer coefficient also defined as the scattering parameter (S_{21}), shows the ratio of transferred signal at the output port and the signal excited at the input port.

A low pass prototype of the transmission/characteristic function ($S_{21}(f')$) as a function of the frequency variable f' is defined by

$$S_{21} = \frac{1}{1+\varepsilon^2 F_N^2(f')} \tag{2.1}$$

where ε is a scale factor related to the passband ripple R by $\varepsilon = [10^{R/10} - 1]^{-1/2}$ [26]. The filtering function ($F_N(f')$) is given by

$$\begin{aligned} F_N(f') &= \cosh(\sum_1^N \cosh^{-1}(x_n)) \\ x_n &= \frac{f' - 1/f_n'}{1 - f'/f_n'}, \left|F_N(f' = \pm 1)\right| = 1 \end{aligned} \tag{2.2}$$

where $s_n = jf_n'$ is the location of the n^{th} attenuation pole in the complex s-plane.

The filtering function is basically a rational function with a dominator given by the product $D_N(f') = \prod_{n=1}^{N}(1 - f'/f_n')$; therefore, the prototype function can be expressed as the ratio on two polynomials [74]

$$F_N(f') = \frac{P_N(f')}{D_N(f')} \tag{2.3}$$

In order to calculate the numerator polynomial, a simple recursion relation can be established between P_{N-1}, P_N, P_{N+1} as [26]

$$\begin{aligned} P_{N+1}(f') &= -P_{N-1}(f')(1 - \frac{f'}{f'_N})^2 \frac{(1 - 1/f'^2_{N+1})^{1/2}}{(1 - 1/f'^2_N)^{1/2}} \\ &+ P_N(f')[f' - 1/f'_{N+1} + (f' - 1/f'_N).\frac{(1 - 1/f'^2_{N+1})^{1/2}}{(1 - 1/f'^2_N)^{1/2}}] \\ P_0(f') &= 1, P_1(f') = f' - 1/f'_1 \end{aligned} \tag{2.4}$$

Obviously, P_{N+1} is a polynomial of degree N+1 if P_N and P_{N-1} are polynomials of degree N and N-1, respectively.

2.1.2.2 Theory of Coupled Resonators

At microwave frequencies, lossless cavities or resonators are one of the basic circuit elements in narrow-band applications. A network will be composed of an interconnection of

cavities/resonators. The interconnection (or coupling) represents a means by which electromagnetic energy can be exchanged between the different cavities. The coupling coefficients are assumed to be frequency-invariant, which is a valid assumption for narrow bandwidths. In addition to the cavity and the coupling components, a third element, the load resistance will also be included. Since the main objective is the synthesis of filter networks, only two-port network consisting of N coupled lossless resonators terminated by resistances at both ports are considered. A typical network of this structure is displayed in Fig. 3.1 where the resonance frequency of each resonator is tuned close to the normalized center frequency f_0. Resonators are numbered from 1 to N with the input and output ports applied to resonator #1 and resonator #N, respectively. The frequency-independent coupling coefficient between i^{th} and j^{th} resonators is denoted by $M_{i,j} = M_{j,i}$. These coupling values are real numbers and can be positive, negative or zero.

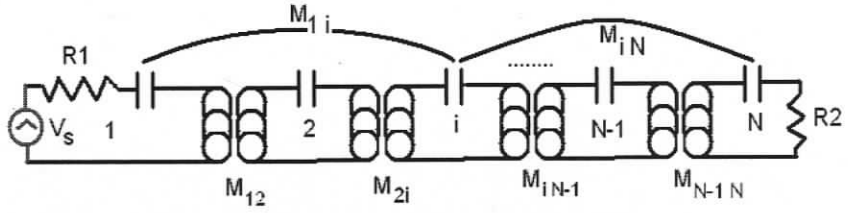

Fig. 2.1 The general configuration of a cross-coupled resonator filter

A voltage source of internal resistance R_1 and of a magnitude equal to unity excites the structure at the first resonator (#1). Resistor R_2, which is the load at the output port, is connected to the last resonator (#N). The normalized frequency f' is related to the real frequency f, the center frequency f_0 and the bandwidth Δf by

$$f' = \frac{f_0}{\Delta f}(f/f_0 - f_0/f) \tag{2.5}$$

For narrow-band filters, the shift in the resonance frequencies of the resonators is absorbed in frequency–independent diagonal elements of the coupling matrix $[M]$.

By taking the loop current in each resonator, the loop equations can be derived as

$$[f'U - jR + M]\,[I] = [A][I] = -j[e] \tag{2.6}$$

where R is the $\mathbf{N}_X\,\mathbf{N}$ matrix whose elements are all zero, except for the (1,1) and (N,N) entries which are equal to R_1 and R_2, respectively. M is also a real symmetric matrix whose (i,j) entry is $M_{i,j}$; U is the identity matrix, e is the input voltage ($[e]^t = [1,0,0...,0]$); I is the current vector, and

t represents the transposition operator. If the system of the above equation is solved for the currents, the transfer voltage ratio and the scattering parameters can be extracted as:

$$\begin{aligned} S_{21} &= -2j\sqrt{R_1 R_2}[A^{-1}]_{N1} \\ S_{11} &= 1 + 2jR_1[A^{-1}]_{11} \end{aligned} \tag{2.7}$$

Now, the synthesis problem can be formulated: determine the coupling matrix $[M]$ and termination resistors R_1 and R_2 such that the scattering parameters given by the above equations reproduce the insertion and reflection coefficients of the pre-specified prototype.

Optimization would be a robust tool to solve this problem due to the fact that it can be implemented on any desired filter topology. In other words, it eliminates the requirement for similarity transformation. In addition, any symmetric/non-symmetric and arbitrary odd/even order filter structure can be synthesized by optimization techniques. Furthermore, the coupling components of the filter structure can be limited to specific signs or certain magnitude ranges during optimization. The last feature will always provide an approximate solution to the problem if an exact solution is not possible due to the imposed limitations.

2.1.3 Synthesis

2.1.3.1 Cost Function

An optimization technique always requires a cost function in order to illustrate the accomplished convergence. A cost function is described based on the desired scattering parameters and those evaluated from the current trial matrix $[M]$. Due to the frequency dependence of the filtering function, the cost function is specified by the location of those desired frequencies such as attenuation poles or/and reflection zeros of the filtering function. Some scale factors contributed to the passband ripple as predefined in the insertion loss ratio is also assigned to the cost function to accelerate convergence. For a two-port network, the cost function (F) to be minimized is defined as equation (2.8) over all frequency samples.

$$F = \sum_{freq} \left\| S_{11}^{sorrugate} - S_{11}^{Simulated} \right\|^2 + \sum_{freq} \left\| S_{21}^{sorrugate} - S_{21}^{Simulated} \right\|^2 \tag{2.8}$$

The synthesis procedure starts with an initial guess for the coupling elements. The objective choice of the initial guess appears to yield measurable effects on the final response or the computation time in most cases. This indicates whether the process converges to the global or local minima. A typical initial guess for the coupling components exists in the topology matrix (see below). Other reasonable choice can be the Chebychev coupling elements for a filter of the same order without considering filter complexity. A search minimization algorithm based on the gradient calculation of the scattering parameters is utilized to gradually minimize the cost or error function.

2.1.3.2 Gradient Calculations

We assume that the entries of the coupling matrix are independent variables in the optimization process. The gradient of an error or cost function with respect to an independent variable x involves the derivatives of the scattering parameters. It can be shown that:

$$\frac{\partial|S_{11}|}{\partial x} = \mathrm{Re}\left[\frac{|S_{11}|}{S_{11}}\frac{\partial S_{11}}{\partial x}\right] \tag{2.9}$$

and a similar expression for S_{21} [97].

Using the above expression in terms of coupling components we get:

$$\frac{\partial S_{11}}{\partial x} = -2R_1\frac{\partial I_1}{\partial x}, \qquad x \neq R_1 \tag{2.10}$$

$$\frac{\partial S_{21}}{\partial x} = 2\sqrt{R_1 R_2}\frac{\partial I_N}{\partial x}, \qquad x \neq R_1, R_2 \tag{2.11}$$

These above derivatives can be calculated by taking the derivatives of the matrix equation [I]= -j [A^{-1}][e] to get:

$$\frac{\partial[I]}{\partial x} = j[A^{-1}]\frac{\partial[A]}{\partial x}[A^{-1}][e] \tag{2.12}$$

The topology of the filter network [T] is defined in terms of the components in the coupling matrix. If the element of the coupling matrix is zero, the corresponding element of the topology is zero too; otherwise, it would be specified as unity. It is the most valuable advantage for a design engineer that the topology of the filter network can be determined beforehand and will be enforced at each step in the optimization.

If x is replaced by the generic element of the coupling matrix $M_{p,q} = M_{q,p}$, the equations (2.10) and (2.11) convert to:

$$\frac{\partial S_{11}}{\partial M_{pq}} = -4jR_1T_{pq}[A^{-1}]_{1p}[A^{-1}]_{q1} \tag{2.13}$$

$$\frac{\partial S_{21}}{\partial M_{pq}} = 2j\sqrt{R_1R_2}T_{pq}([A^{-1}]_{Np}[A^{-1}]_{q1} + [A^{-1}]_{Nq}[A^{-1}]_{p1}) \tag{2.14}$$

where the M_{pq} is the off-diagonal element of the coupling matrix. The gradient of the scattering parameters with respect to the diagonal elements of the coupling matrix is achieved from the previous expressions by simply taking $p=q$ and dividing by a factor of two. The factor of two accounts for the fact that the diagonal elements of a symmetric matrix occur only once; however, off-diagonal elements occur twice.

$$\frac{\partial S_{11}}{\partial M_{pp}} = -2jR_1T_{pp}[A^{-1}]_{1p}[A^{-1}]_{p1} \tag{2.15}$$

$$\frac{\partial S_{21}}{\partial M_{pp}} = 2j\sqrt{R_1R_2}T_{pp}([A^{-1}]_{Np}[A^{-1}]_{p1}) \tag{2.16}$$

The values of the termination resistances R_1 and R_2 can be calculated both from theory and optimization. These values are obtained in the same way as the coupling coefficients. The computation of gradients of the reflection and transmission coefficients (S_{11} and S_{21}) with respect to the source resistance (R_1) following the aforementioned discussion contributes to the final result as

$$\frac{\partial S_{11}}{\partial R_1} = 2j[A^{-1}]_{11} + 2R_1([A^{-1}]_{11}[A^{-1}]_{11} + r[A^{-1}]_{N1}[A^{-1}]_{N1}) \tag{2.17}$$

$$\frac{\partial S_{21}}{\partial R1} = -2j\sqrt{r}[A^{-1}]_{N1} + 2R_1\sqrt{r}([A^{-1}]_{N1}[A^{-1}]_{11} + r[A^{-1}]_{NN}[A^{-1}]_{N1}) \tag{2.18}$$

where $r = R_2/R_1$ is the ratio of termination resistors. Note that the derivation demonstrated here is more general and can be even employed in cases where the adjoint network method is no longer applicable [98].

2.2 Synthesis of Multiple Microwave Networks

2.2.1 Introduction

Multi-port networks such as multiplexers, diplexers, couplers and hybrids are key components in communication systems. The design of diplexers is conventionally performed in two steps: firstly, each channel is independently synthesized; secondly, a power divider or manifold network is implemented in such a way that the responses for separated channels are minimally affected when integrated into the entire device. The extra lengths of the utilized transmission lines in the last part account for the phase shift for each channel [99-100].

Methods for the synthesis of multi-port microwave networks formed by coupled resonators are presented in the second part of this chapter. The fundamental feature of each method is the definition of a coupling topology representing resonant/non-resonant nodes and an arbitrary number of input and output ports. The application of the coupling matrix allows a synthesis procedure analogous to the one used for the filters in the previous section. The complete multi-port network performance must be expressed in the form of scattering or short-circuit admittance parameters. The resulting coupling matrix can be manipulated in the same way as coupling matrices for filters in order to generate the desired coupling topology [30] [35].

The new definition of the coupling matrix formed by n resonators and p non-resonant nodes including input and output ports was introduced in [35]. The matrix notations of the former definition of coupling matrix represent the loop current definition of the network. In the new method, the short-circuit admittance parameters are utilized for the entire synthesis and can be represented as rational polynomials with common denominator. The admittance matrix parameters can be computed from the specified scattering elements at discrete frequency values; then the final admittance functions are reconstructed from rational polynomials [101]. Besides, the admittance matrix can also be extracted from a canonical transversal network with a general topology. A circuit-based analysis of transversal networks contributes to an admittance matrix whose elements are related to the coupling components of the topology. By matching the elements of these two aforementioned admittance matrix functions, all the coupling elements are determined. In general, the transversal structure is not the desired coupling topology for the

network. In this case, a sequence of similarity transformations is applied in order to obtain the required structure [86].

The hybrid EM simulator based optimization is addressed in [30]. This method is implemented for microwave and millimeter-wave diplexers and multiplexers and can also be employed for any multi-port networks. The procedure relies on the combination of surrogate models with EM simulators to explore the definite coupling values for the model elements. All characteristics of the model parameters are extracted from an EM-based S-parameter computation of the full structure and are represented by a coupling matrix. The sensitivities of the model parameters with respect to the geometry parameters are obtained from n additional EM simulator runs, where n denotes the number of geometry elements to be optimized. The ideal coupling matrix is also extracted from the target transfer function representing the network characteristics. The optimization of the EM structure is then performed in the parameter space of the model, which is significantly faster than using the EM simulator exclusively performed the process [31].

2.2.2 Coupling Matrix Definition for Multi-Port Networks

The coupling scheme addressed in this section extends the former two-port modeling network. The network topology drawn in Fig. 2.2 consists of n resonators and p non-resonant nodes, which would be the input and output ports in this case.

For a multi-port network *(p>2)*, the conventional *(n+2)* x *(n+2)* coupling matrix is no longer valid. Therefore, it is essential to define a new format of coupling matrix suitable for networks with an arbitrary number of ports. The new coupling matrix is defined by

$$M = \begin{bmatrix} 0 & M_{01} & M_{0N+1} & M_{01(channel\#i)} & M_{0M+1} & M_{01(channel\#p-1)} & M_{0K+1} \\ M_{10} & [M_{(cahnnel\#1)}] & 0 & 0 & 0 & . & 0 \\ M_{N+1,0} & 0 & . & 0 & . & 0 & . \\ M_{1(channel\#i),0} & . & . & [M_{(channel\#i)}] & . & . & 0 \\ M_{M+1,0} & 0 & . & M_{M+1,1(channel\#i)} & . & . & . \\ M_{1(channel\#p-1),0} & . & 0 & & . & [M_{(channel\#p-1)}] & . \\ M_{K+1,0} & 0 & . & M_{K+1,1(channel\#i)} & . & . & 0 \end{bmatrix} \tag{2.19}$$

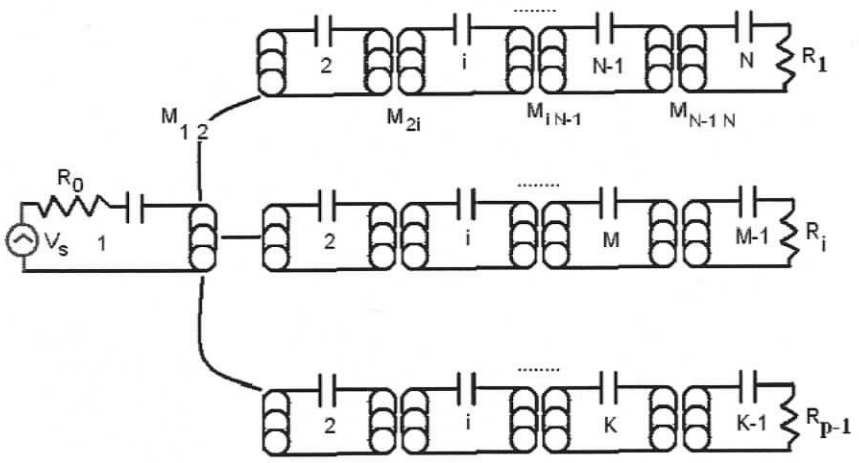

Fig. 2.2 Model of a multi-port network

where M consists of $(n+p)$ x $(n+p)$ elements which represent the coupling coefficients between all resonators and all ports.

The loop equations of the network are expressed analogously to two-port coupling scheme previously introduced in equation (2.6), where $s = j\frac{f_0}{\Delta f}(f/f_0 - f_0/f)$ is the normalized complex frequency variable and f_0 and Δf are the center frequency and the bandwidth used for the low-pass to band-pass transformation, respectively. I is also the vector of the loop current, E is the unit excitation vector $E^t = [1,0,0...,0]$ (depends on which port is excited) and U and R are diagonal matrices defined by blocks with the same dimension as M:

$$U = \begin{bmatrix} 0 & 0 & 0 & 0 & 0 & 0 \\ 0 & [U_{(channel\#1)}] & 0 & 0 & 0 & 0 \\ 0 & 0 & 0 & 0 & 0 & 0 \\ 0 & 0 & 0 & [U_{(channel\#i)}] & 0 & 0 \\ 0 & 0 & 0 & 0 & 0 & 0 \\ 0 & 0 & 0 & 0 & 0 & [U_{(channel\#p-1)}] \end{bmatrix} \tag{2.20}$$

$$U_{(channel\#i)} = \begin{bmatrix} 1 & & & 0 \\ & 1 & & \\ & & 1 & \\ 0 & & & 1 \end{bmatrix}_{MxM} \tag{2.21}$$

$$R = \begin{bmatrix} R_0 & & & & & & \\ & 0 & & & 0 & & \\ & & R_1 & & & & \\ & & & 0 & & & \\ & & & & R_i & & \\ & 0 & & & & 0 & \\ & & & & & & R_{p-1} \end{bmatrix} \tag{2.22}$$

where R_n corresponds to the reference impedance at each port.

Solving for the loop currents yields the symbolic coupling matrix $[A]$ in terms of coupling coefficients, resonance frequencies and load impedances at the input and output ports. The reflection and transmission coefficients can be expressed as:

$$\begin{aligned} S_{11} &= 1 + 2j[A^{-1}]_{11} \\ S_{k1} &= -2j[A^{-1}]_{k1} \qquad k \in \{2...p\} \end{aligned} \tag{2.23}$$

In general, the model parameters for a given EM structure are obtained by minimizing the difference between the computed S-parameters of the surrogate model and the simulated network response through the cost function.

2.2.3 Cost Function and Optimization

The cost function for the multi-port network synthesis is described via minimizing the difference between computed S-parameters of the surrogate model and the desired network performance at each single frequency.

$$F = \sum_{freq} \sum_{i=1}^{p} \sum_{j=1}^{p} \left\| S_{ij}^{sorrugate} - S_{ij}^{Simulated} \right\|^2 \tag{2.24}$$

This procedure yields the components of the coupling matrix of the initial EM structure. In order to optimize the elements of the coupling matrix, the sensitivity of the cost function with respect to all coupling elements and load impedances in each port must be evaluated. This can be achieved by computing the derivatives of the S-parameters in the cost function in terms of all variables in the network. The same procedure as that of the two-port filter network can be applied to a multi-port network to calculate the gradients of the S-parameters. A global search

minimization algorithm based on the gradient calculation of the scattering parameters is also utilized to minimize the cost function.

2.3 Summary

The coupling theory and modeling of two-port single-band networks is introduced for filter synthesis procedures. These fundamentals are extended to fulfill the coupling of multi-port networks. The desired specifications of the proposed networks are achieved through optimization of the cost function with respect to scattering parameters.

CHAPTER 3

Broadband Cross-Coupled Network

3.1 Introduction

The allocation of frequency bands corresponding to different usages or services imposes strict filter requirements and reflects their essential role in modern communications systems. Sharp roll-off skirts, low in-band insertion loss and asymmetric frequency responses can be created by cross-coupled or bypassed resonator arrangements, which produce attenuation poles at finite frequencies.

The first general theory of inter-coupled resonator passband filters presented in the 1970s is still widely employed [3]. A slightly different approach determines the filtering function for specified locations of transmission zeros [74-75]. Recent activities focused on the optimization techniques and synthesis of networks including source-load coupling [76-77]. Moreover, the concept of non-resonating nodes as a part of the coupling scheme was introduced in [29].

All filter design approaches utilizing cross-coupled networks are valid only in the vicinity of the filter passband. This is due to the fact that only those electric resonances are considered which describe the filter performance over an acceptable bandwidth. However, higher/lower-order mode resonances in filters, specifically in waveguide technology, can be advantageously utilized to produce additional transmission zeros and/or filters passbands. It is thus of fundamental importance that such effects, which have a profound influence on the final filter performance, be included from the onset of a filter design procedure.

Therefore, in the current Chapter, we demonstrate a new configuration of the cross-coupled network, which accounts for higher/lower-order mode resonances through a framework

of resonating and/or non-resonating nodes. This broadband model partly eliminates the narrow-band restrictions found in conventional coupling matrix approaches. It is also illustrated that the proposed broad-band cross-coupled topology correctly predicts all resonance/non-resonance effects over a wide frequency range. The process and accomplished performances are validated by comparison with in-house and commercially available field-theory-based codes.

3.2 Theoretical Approaches and Network Model

The basic concept of a cross-coupled network composed of N coupled lossless resonators and its governing equations are discussed in Chapter 2 and will not be repeated here. In order to improve the flexibility of this network, we are adding provisions for non-resonating nodes according to [29].

Within this framework, each actual cavity is modeled by its main resonance, which is associated with the filter passband, and by one or more higher/lower-order resonances, which are viewed as being completely detuned. As an example, consider the coupling scheme shown in Fig. 3.1.

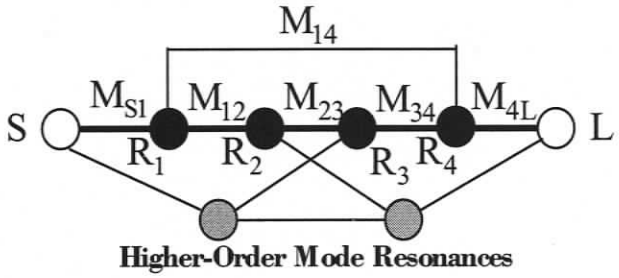

Fig. 3.1 Possible coupling scheme of a quadruplet with two higher-order mode resonances

The dark inline resonances together with the source and nodes represent the filter behavior in the vicinity of the passband. Since the gray higher-order nodes are tuned to higher-order mode harmonics, their influence on the filter passband is minimal. At their respective resonance frequencies, however, they dominate and might even use a path through the inline nodes of Fig. 3.1 as bypass coupling to create transmission zeros. Their connection to source, load or other nodes is determined by a comparison between the responses of the actual filter, i.e. using an EM field solver, and that from the coupling matrix. It will be shown that in order to meet the frequencies of some additional higher-order effects, only a certain connection of the higher-order

nodes is permitted.

In order to apply this technique to the broad/lower-band design procedure of filters, the additional passbands or attenuation poles attributed to higher-order harmonic resonances can be specified beforehand. The coupling matrix elements can then be obtained by optimization, keeping in mind that the coupling coefficient values for non-resonating nodes are constant and do not contribute a frequency term. In this work, the optimization of the coupling matrix is carried out using the Gauss-Newton Algorithm on the cost function:

$$F = \sum_{i=1}^{N_s}\left(\left|\frac{1}{GIL(f_i)}\right| - \left|\frac{1}{IL(f_i)}\right|\right)^2 + \sum_{i=1}^{N_p}\left(\left|\frac{1}{GRL(f_i)}\right| - \left|\frac{1}{RL(f_i)}\right|\right)^2 + \sum_{i=1}^{N_h}\left(\left|\frac{1}{GIL(f_i)}\right| - \left|\frac{1}{IL(f_i)}\right|\right)^2 + \sum_{i=1}^{N_c}\left(\left|\frac{1}{GRL(f_i)}\right| - \left|\frac{1}{RL(f_i)}\right|\right)^2 \tag{3.1}$$

where N_s, N_p, N_h and N_c are the number of frequency samples in the suppression band, passband, higher-order modes and cutoff frequency regions, respectively; GIL and GRL are the goal values for the insertion loss and return loss, and IL and RL are the actual values during optimization. Of course, the optimization procedure can lead to different solutions of the coupling matrix. Therefore, additional entries due to higher/lower order modes are individually limited to exclude solutions, which produce extra passbands in the frequency range of interest.

3.3 Realization and Performances

In the current section, we demonstrate how higher/lowers-order resonances and their correct representation within the coupling matrix approach aid in the wideband design procedure of filters.

The first example is an H-plane folded waveguide tri-section filter as shown in the inset of Fig. 3.2. In order to realize the performance with one transmission zero below the passband, the following standard coupling matrix and routing scheme (Fig. 3.3) was initially utilized (f_0=12.494GHz, b=0.25GHz):

$$M = \begin{bmatrix} 0.0000 & 1.0408 & 0.0000 & 0.0000 & 0.0000 \\ 1.0408 & -0.0821 & 0.9570 & -0.1150 & 0.0000 \\ 0.0000 & 0.9570 & 0.1022 & 0.9570 & 0.0000 \\ 0.0000 & -0.1150 & 0.9570 & -0.0821 & 1.0408 \\ 0.0000 & 0.0000 & 0.0000 & 1.0408 & 0.0000 \end{bmatrix} \tag{3.2}$$

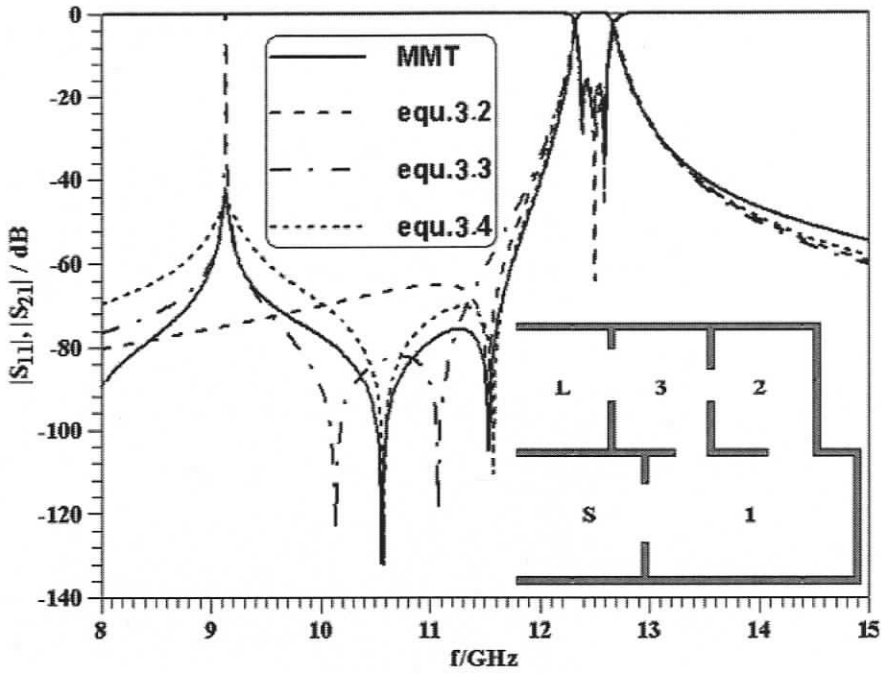

Fig. 3.2 Performances of the folded waveguide tri-section filter; comparison between EM field-theory analysis and different coupling schemes.

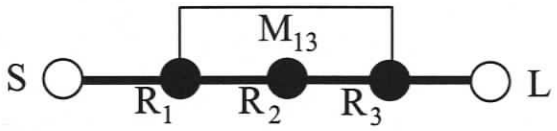

Fig. 3.3 Routing scheme for equation (3.2).

Cavity 1 operates in the TE_{102} mode to produce the correct cross coupling M_{13} (c.f. [78]). Upon realization of the actual filter, however, it is found that two transmission zeros always appear simultaneously (solid lines in Fig. 3.2) and that this behavior is not predicted by the original coupling scheme (dashed lines in Fig. 3.2). Apparently, the fundamental resonance of the TE_{102} cavity (9.3 GHz) creates another path for cross coupling. The first approach to include this behavior in the coupling matrix is shown in equation (3.3) and Fig. 3.4, assuming that a coupling

between the two resonances in cavity 1 (the fundamental one being heavily detuned) exists and that a second bypass coupling to resonator 3 is created.

$$M = \begin{bmatrix} 0.0000 & 1.0400 & 0.0000 & 0.0000 & 0.0000 & 0.0000 \\ 1.0408 & -0.0820 & 0.9570 & -0.1150 & -1.0000 & 0.0000 \\ 0.0000 & 0.9570 & 0.1022 & 0.9570 & 0.0000 & 0.0000 \\ 0.0000 & -0.1150 & 0.9570 & -0.0820 & 0.7500 & 0.0000 \\ 0.0000 & -1.0000 & 0.0000 & 1.0408 & 31.750 & 1.0400 \\ 0.0000 & 0.0000 & 0.0000 & 1.0400 & 0.0000 & 0.0000 \end{bmatrix} \tag{3.3}$$

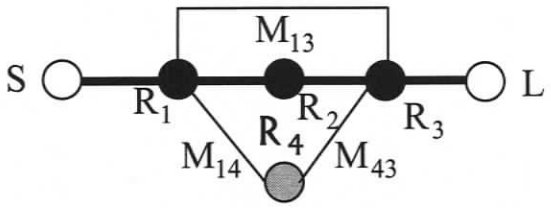

Fig. 3.4 Routing scheme for equation (3.3).

While this approach (dash-dotted line in Fig. 3.2) captures the fundamental resonance and the two attenuation poles, the values in (3.3) cannot be adjusted to match their exact positions. Therefore, the following coupling scheme (Fig. 3.5 and equation (3.4)) is derived. It is based on a simultaneous excitation of the two resonances in cavity 1 through the S-R_1 iris and correctly predicts the locations of the transmission zeros and all resonances (dotted lines in Fig. 3.2). Note that the original coupling matrix (3.2) is changed only very slightly by the introduction of the higher-order mode resonance and related paths.

$$M = \begin{bmatrix} 0.0000 & 0.9837 & 0.0000 & 0.0000 & 0.4480 & 0.0000 \\ 0.9837 & -0.0695 & 0.9210 & -0.1280 & 0.0000 & 0.0000 \\ 0.0000 & 0.9210 & 0.1218 & 0.8849 & 0.0000 & 0.0000 \\ 0.0000 & -0.1280 & 0.8849 & -0.0791 & -0.1515 & 1.0301 \\ 0.4480 & 0.0000 & 0.0000 & -0.1515 & 31.800 & 0.0000 \\ 0.0000 & 0.0000 & 0.0000 & 1.0301 & 0.0000 & 0.0000 \end{bmatrix} \tag{3.4}$$

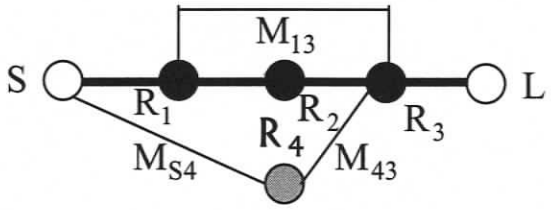

Fig. 3.5 Routing scheme for equation (3.4).

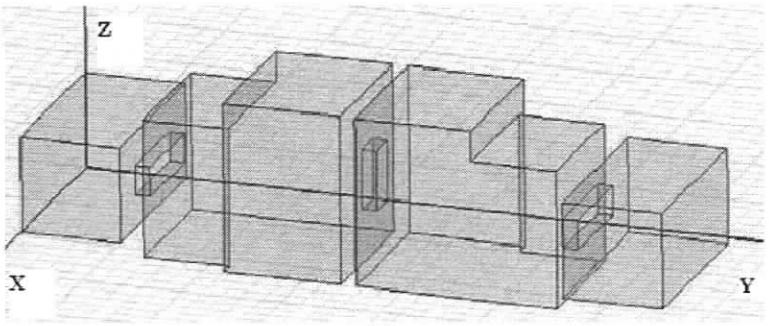

(a)

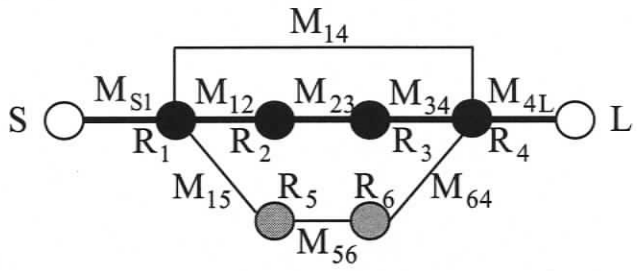

(b)

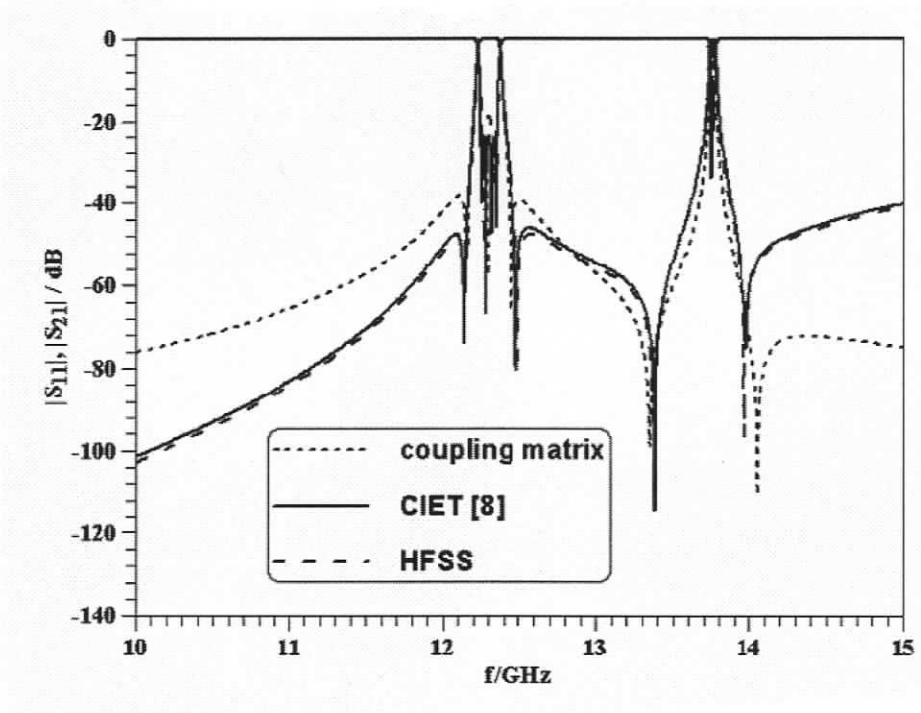

(c)

Fig. 3.6 Topology and performances of the four-pole dual-mode filter (quadruplet); topology (a); coupling scheme (b); comparison between coupling matrix, CIET and HFSS (c).

The next example applies to a dual-mode filter commonly known as a quadruplet. This

filter was originally presented in [28], and operates with TE_{101} and TE_{011} resonances. Its topology is shown in Fig. 3.6a. Cross coupling between resonators 1 and 4 in the main path of Fig. 3.6b provides two transmission zeros, one on each side of the passband. The part of the design procedure, which applies to the current investigation, is the second passband also displaying two transmission zeros (Fig. 3.6c). Upon studying the higher-order resonances in the two dual-mode cavities, the coupling scheme in Fig. 3.6b was used to evaluate the broadband filter performance. Fig. 3.6c compares the responses of two EM field-theory-based analyses (CIET and HFSS) with that obtained from the coupling scheme of Fig. 3.6b. Excellent agreement is observed. The new coupling scheme accurately predicts the second passband due to two higher-order-mode resonances and the additional two attenuation poles resulting from the bypass (Fig. 3.6b), which, since the coupling irises are small enough, operates in both frequency bands.

The third example in this section is a four-pole dual-mode filter based on TE_{101}- and TM_{110}-mode resonances (Fig. 3.7a). In the main path of the coupling configuration of Fig. 3.7b, input and output bypass couplings provide two transmission zeros above the passband (Fig. 3.7c). The second passband at 14.34GHz is generated by the next higher-order mode resonances in the two cavities, R_5 and R_6 in Fig. 3.7b, similar to the concept introduced in the previous example. However and contrary to the behavior of Fig. 3.6c, a bypass of R_5 and R_6 through the main path is not achieved here since the TE_{10}-mode coupling through the center iris is negligible. Thus no transmission zeros are produced close to the second passband. In addition to R_5 and R_6, resonances R_7 and R_8 represent the TE_{10}-mode cutoff frequencies in the two cavities. Their influence accounts for the spikes between 10.5 and 10.7 GHz (Fig. 3.7c). Note that the coupling matrix model of Fig. 3.7b accounts for all of the resonance effects within a broad bandwidth and that the performance agrees very well with the EM field-theory-based analyses of the actual filter structure (CIET and HFSS in Fig. 3.7c). Additional resonance effects in this filter occur between 14.5 and 15 GHz (not shown here). Their effects can be included as detuned resonances similar to those of R_5 to R_8 in Fig. 3.7b.

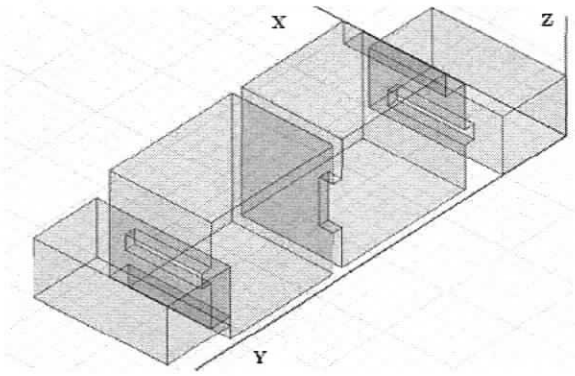

(a)

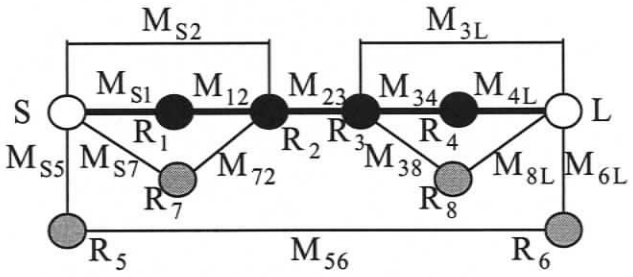

(b)

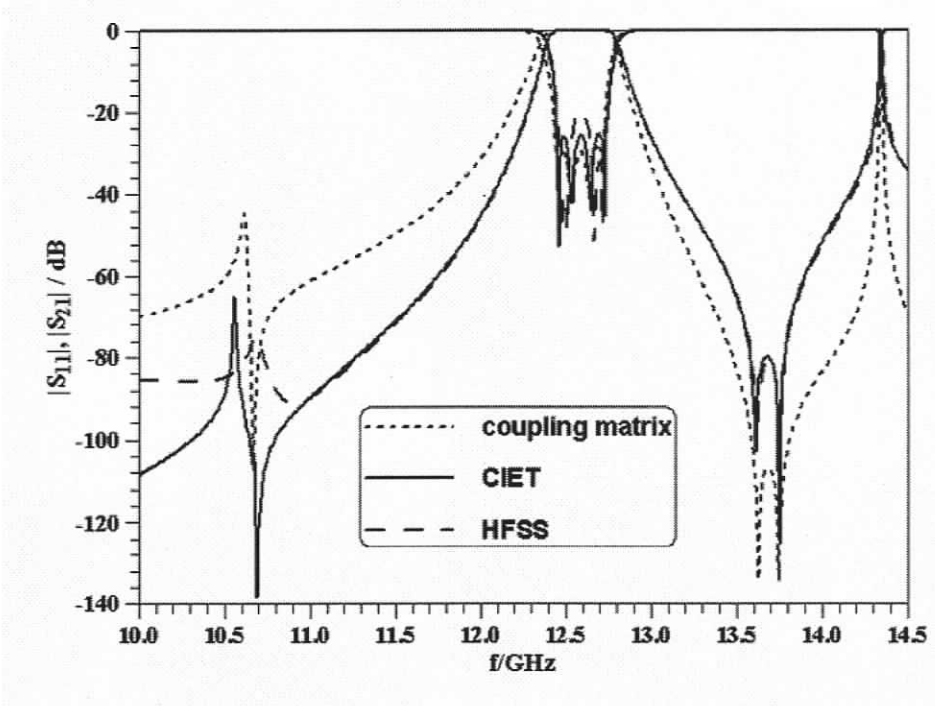

(c)

Fig. 3.7 Topology and performance of four-pole dual-mode filter with bypass coupling; topology (a); coupling scheme (b); comparison between coupling matrix, CIET and HFSS (c).

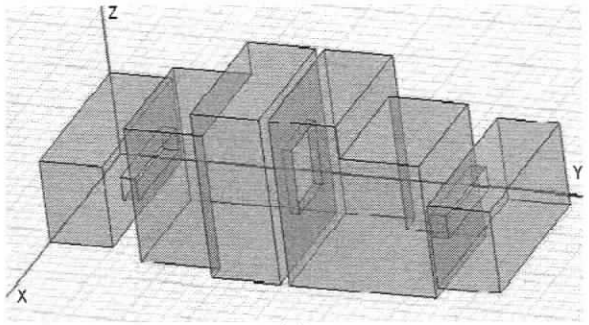

(a)

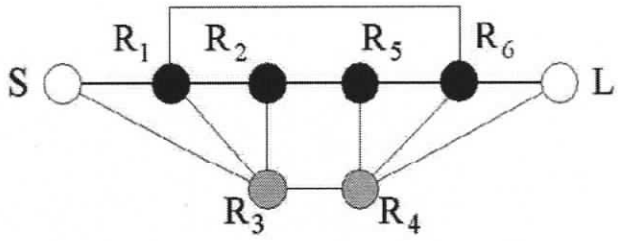

(b)

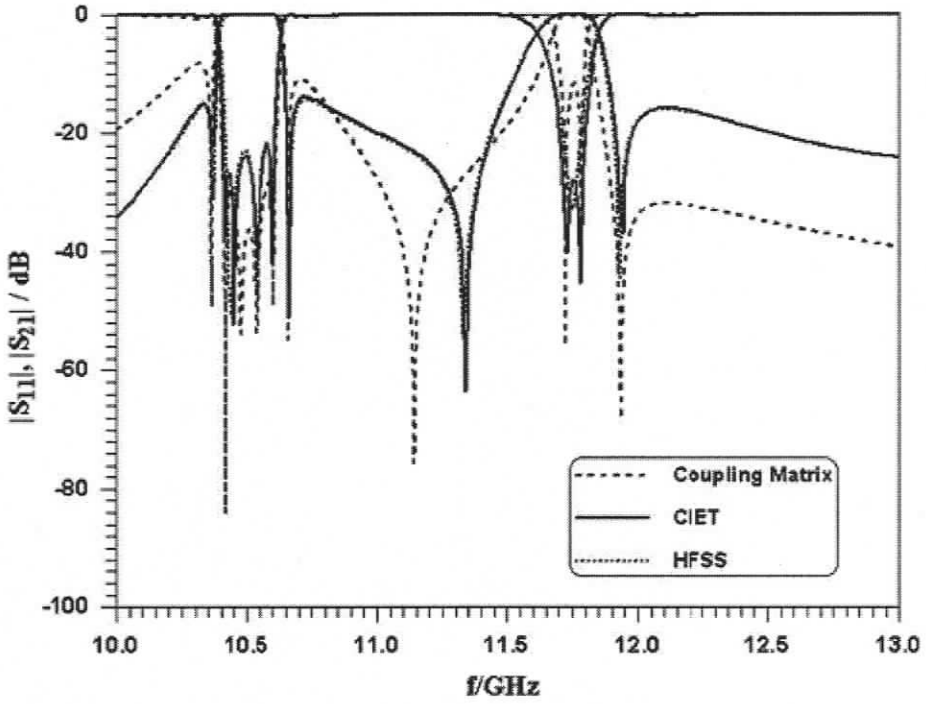

(c)

Fig. 3.8 Inline dual-band waveguide filter based on fundamental and higher-order mode resonances. (a) 3D-view of filter; (b) coupling scheme; (c) performances obtained from theory (dashed lines) and EM-based software (solid and dotted lines, which are almost indistinguishable).

In the final example, we will employ higher-order resonances in an inline configuration to create the second passband. Fig. 3.8a displays an inline dual-mode filter utilizing two modes (TE_{101}, TE_{011}) in the two cavities. This type of filter is a modification of Fig. 3.6a. Here we illustrate a design procedure for dual-band operation at 10.5 and 11.75 GHz. The second passband contributes to the next higher-order modes in the two cavities. In the coupling scheme of Fig. 3.8b, they are modeled as detuned resonators R_3 and R_4 in an attempt to maintain symmetry of the coupling matrix. Note that this design procedure differs from typical dual-band filter design approaches due to the fact that the second (higher) passband cannot be controlled independently. The higher-order resonances depend on the two cavities, whose dimensions are determined to obtain the first (lower) passband. Therefore, the midband frequency and bandwidth in this design are those of the lower passband (f_0 =10.5 GHz, b= 210 MHz). In the coupling scheme of Fig. 3.8b, the straight line from input to output, including 1–6 cross-coupling, forms a standard quadruplet for the lower frequency band. The addition and connection of the higher-order resonances in Fig. 3.8b are based on the following considerations.

In the first section of the dual-mode resonators, TE_{11} and TM_{11} are well below cutoff even in the upper frequency band. In the second (larger) section of the dual-mode resonators, both TE_{11} and TM_{11} are above cutoff. However, this section is too short for a TE_{111} resonance to occur and, therefore, nodes R_3 and R_4 represent TM_{110} resonances. Therefore, both fundamental resonances TE_{101} and TE_{011} couple to the TM_{110} higher-order resonance. Above 11.4 GHz, the input/output irises become propagating. That means that the input/output can couple directly to the TM_{110} resonances R_3 / R_4. Since the center iris of the filter is centered with respect to the two adjacent cavities, there is no $TE_{10/01}$ - TM_{11} coupling through the center iris, i.e., $M_{24} = M_{14} = M_{35} = M_{36} = 0$.

The coupling matrix obtained by following this scheme is given in equation 3.5. Its response is shown in Fig. 3.8c as dashed lines. The actual design as computed with HFSS (dotted lines) and the coupled integral-equation technique (CIET) (solid lines) agrees relatively well with the coupling-matrix prediction, shown in equation 3.5.

Except for small deviations between coupling matrix and full-wave codes, the only

notable discrepancy is the location of the transmission zero between 11–11.5 GHz. This is attributed to the fact that the TM_{11} – TM_{11} coupling through the center iris is highly frequency dependent in this frequency range. Such dependence is, of course, not captured by a coupling matrix approach, which assumes constant coupling coefficients. This is a limitation not only of this coupling-matrix design procedure, but of other coupling matrix designs as well. Moreover, the accuracy decreases with the frequency distance from the resonances considered in the coupling matrix. Nevertheless, this example demonstrates the flexibility of the coupling-matrix design routine presented in this chapter.

$$M = \begin{bmatrix} 0 & 1.3410 & 0 & 0.0024 & 0 & 0 & 0 & 0 \\ 1.3410 & -1.9990 & 0.7752 & 4.2254 & 0 & 0 & -1.0767 & 0 \\ 0 & 0.7752 & -0.0884 & 0.3869 & 0 & 1.0093 & 0 & 0 \\ 0.0024 & 4.2254 & 0.3869 & -9.3966 & 0.6955 & 0 & 0 & 0 \\ 0 & 0 & 0 & 0.6955 & -9.3966 & 0.3869 & 4.2254 & 0.0024 \\ 0 & 0 & 1.0093 & 0 & 0.3869 & -0.0884 & 0.7752 & 0 \\ 0 & -1.0767 & 0 & 0 & 4.2254 & 0.7752 & -1.9990 & 1.3410 \\ 0 & 0 & 0 & 0 & 0.0024 & 0 & 1.3410 & 0 \end{bmatrix} \tag{3.5}$$

3.4 Summary

In this chapter, a new and accurate class of cross-coupled networks for the advanced design of microwave filters has been proposed, and the concept of coupling-matrix filter design is extended to include a wide frequency range. By considering nodes for higher/lower-order resonances, a broadband model is obtained which partly eliminates the narrow-band restrictions found in current coupling approaches. In fact, the respective filters can be designed to include these parameters right from the start either in waveguide or planar technologies. Consequently, the related effects can be used to improve wideband filter performance and/or create additional characteristics such as, e.g., a second passband. The approach is validated through computation with in-house and commercially available field theory based codes. The simulated results from several band-pass filter examples for waveguide applications demonstrate that this approach correctly predicts all resonance effects over a wide frequency range.

CHAPTER 4

Coupling Matrix Design of Dual and Triple Passband Filters

4.1 Introduction

Recent developments in microwave filters have focused on many different topics, one of them being the design of dual- and triple-band filters. They are in heavy demand due to applications in modern wireless and satellite systems. Usually, theoretical design techniques are related to individual filter technologies. For instance, lumped-element or step-impedance approaches are used in low-temperature co-fired ceramic (LTCC) applications, e.g., [7], [102]. So-called dual-behavior resonators [8], [10] create attenuation poles at specific frequencies in order to separate individual passbands. The coupling between two modified open-loop resonators is used to create a dual-band filter in microstrip technology [103]. Polynomial approaches and coupling matrices are applied to the design of dual-bandpass [104] and bandstop filters [105] in waveguide technology.

In planar circuitry, dual- to multi-band filters can be typically designed using three basic approaches: First, by switching between two separated filters at two different frequencies [7], second, by employing stubs to generate attenuation poles which separate the passbands [8] as this is essentially a stopband approach; third, by utilizing multi-mode resonators, e.g. [13] or coupled-resonator pairs [12]. However, an efficient and compact dual- to multi-band filter is often difficult to achieve via proper coupling coefficients for a simultaneous, yet independent option for bandwidths and the location of transmission zeros.

Common to all such design procedures is the fact that they cannot immediately be used if the filter topology changes. Moreover, many approaches are limited with respect to the number of

transmission zeros and their locations over the frequency band of interest. Therefore, this chapter focuses on the design of dual- and triple-band filters by employing the coupling matrix and the optimization of its entries, which are similarly characterized as those used in waveguide technologies, e.g. [3]. One of the major advantages of this approach is that topologies and certain coupling elements can be controlled from the outset [77].

The basic approach of this method was introduced in [106]. In order to demonstrate that the basic design is an independent option of the type of resonators, three different commonly used resonator configurations in planar technologies are presented as planar examples: hairpin resonators [107], open-loop resonators [32] and quasi-dual-mode resonators [4]. However, measurements failed to confirm the transmission zeros between individual passbands. Here, we present new designs and measurements, which validate the design approach in microstrip technology. The same theory is applied to dual-band waveguide filters and shows that the inclusion of higher-order mode resonances aids in the design. It is thus demonstrated that the design process is generally applicable to multiband filter designs in varying topologies and technologies.

We are using hairpin resonators [107] and open-loop resonators [32] as triple/dual-band examples in microstrip technology. Dual-band waveguide designs include folded cavity filters, e.g., [108], and inline dual-mode configurations, e.g., [28], [109]. Folded waveguide filters make use of higher-order resonances in addition to the dual-band design. That is, the dual-band effect in inline configurations can also be created because of higher-order resonances [110].

4.2 Principles of Design Procedure

The basic approach to generate a coupling matrix for desired specifications of a single passband filter is presented in [26] and [77] and has been described in Chapter II. The principal advantages of this technique are, first, that the topology of any scheme of coupled resonators can be specified in advance and, secondly, that the signs and limits of coupling coefficients can be strictly enforced during optimization. For the design of dual- and triple-band filters, we assume first that a single wideband filter will be constructed whose bandwidth covers all bandwidths of

the dual- and/or triple-band filters.

Since the maximum number N of realizable transmission zeros is dictated by the topology, any number $n \leq N$ of transmission zeros can now be placed within the initial broad frequency band in order to separate individual passbands. Optimization [26] is then employed to adjust the entries of the coupling matrix. Their maxima and minima can be controlled via closed-form expressions for the electric and magnetic coupling coefficients of, e.g., open-loop resonators [111].

The basic design steps are shown here at the examples of dual/triple-band filters with four/six resonators and two/four transmission zeros, each two of which are located between adjacent passbands, respectively.

In case of a triple-band filter design, the individual passbands are centered at 2.65, 3, and 3.35 GHz, and more than 50-MHz bandwidth is to be retained in each of the bands.

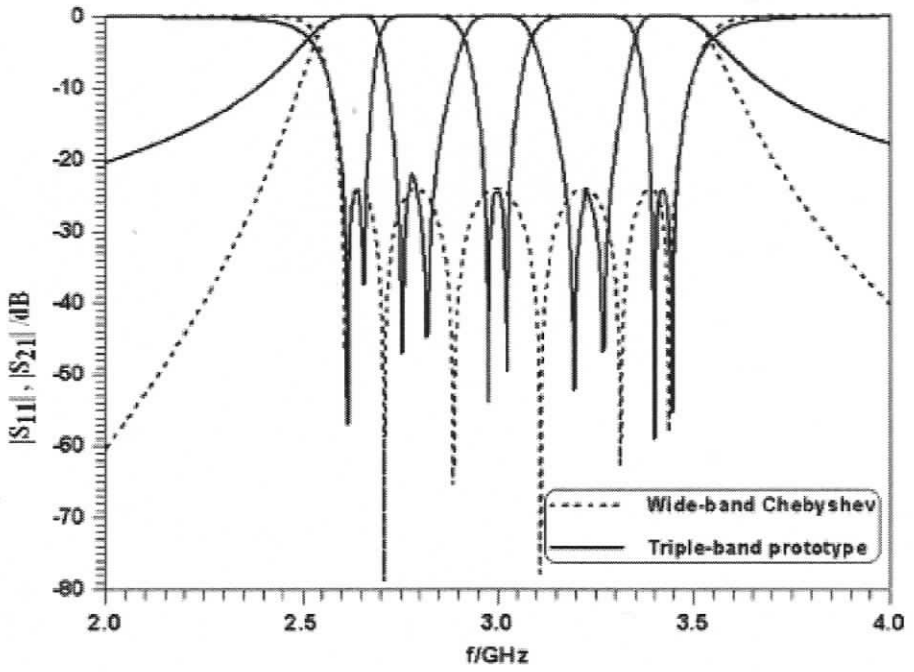

Fig. 4.1 Wideband Chebyshev and triple-band prototype responses of the design example.

We first design a standard Chebyshev response over the entire triple-band frequency range using 3 GHz as the center frequency, 800-MHz bandwidth, and 24-dB return loss. This

design is shown in Fig. 4.1 as dashed lines. To allow a coupling matrix to be optimized, we then require, first, a prototype function for the triple-band filter and, secondly, an initial coupling matrix to start the optimization. One possibility to obtain the prototype function is to optimize the coefficients of the numerator and denominator of the filtering function. This is usually done to determine the prototype function and the positions of the reflection and transmission zeros in particular. Our approach is different though. We obtain the prototype function from piecing together the functions of three individual filters, each of which is designed according to the single band-pass filter approach in [26].

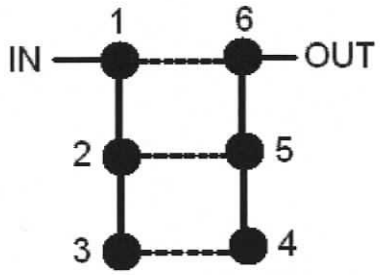

(a)

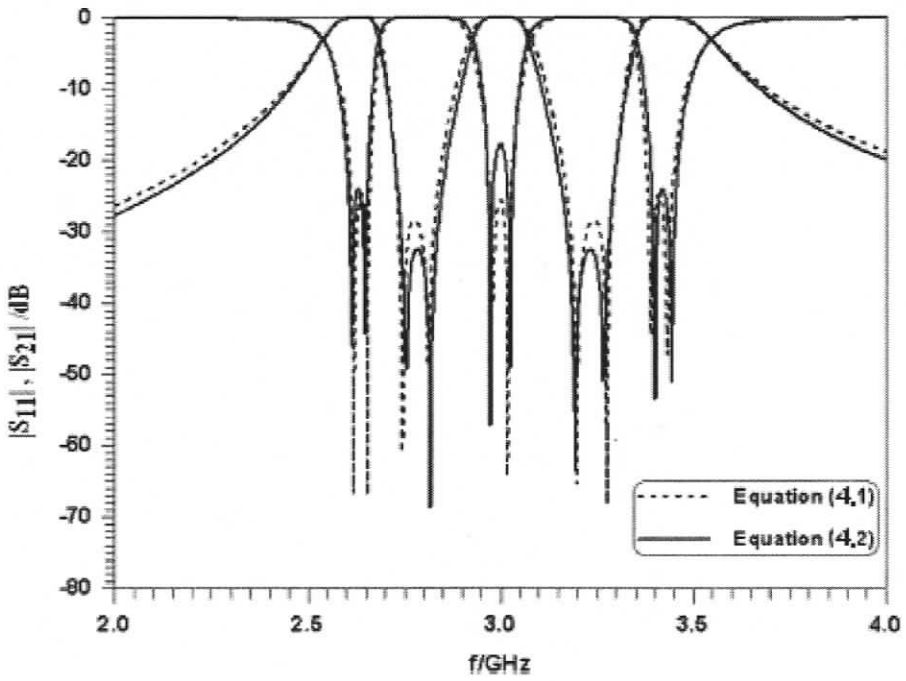

(b)

Fig. 4.2 (a) Topology of a triple-band filter including six hairpin resonators (filled circles); and (b) responses of triple-band coupling matrices obtained by optimization from different initial values.

For the triple-band filter considered in the first example, the left-most response is that of a two-pole filter with a transmission zero to the right, the center response corresponds to a two-pole elliptic-function filter (one transmission zero on each side), and the right-most response is that of a two-pole filter with one transmission zero on the left. The so-obtained overall prototype function is shown in Fig. 4.1 as solid lines. The three different parts are clearly distinguished by the discontinuous points between the passbands at 2.78 and 3.23 GHz. The choice of an initial coupling matrix involves the actual circuit topology. Let us assume that the triple-band filter be designed for microstrip technology on RT6006 substrate and that six hairpin resonators be employed (see Fig. 4.2a). The four transmission zeros are to be created by cross couplings between hairpin resonators 1 and 6, as well as 2 and 5, thus specifying a symmetric folded filter configuration.

One of the simplest initial coupling matrices is that of the standard wideband Chebyshev filter (cf. Fig. 4.1, dashed line) and allowing for the additional cross couplings 1–6 and 2–5. As the sign of the coupling is determined by the orientation of the hairpin resonators, we allow both magnetic and electric couplings in the optimization. For the given example, a quick calculation using the closed-form expressions in [111] advises that the magnitude of normalized inline coupling coefficients be less that 0.9 and that of the cross couplings be less than 0.5. With this initial coupling matrix, the optimization produces the following coupling matrix (including source and load), as shown in equation (4.1), whose performance is shown as dashed lines in Fig. 4.2b. Depending on the initial values, different coupling matrices are obtained. For instance, using direct and cross couplings to be 0.5 and 0.25 in magnitude, respectively, and specifying two couplings M_{12} and M_{25} as negative, a different final matrix is obtained, as shown in equation (4.2), and its performance is shown as solid lines in Fig. 4.2. Note that both approaches result in a very small coupling between resonators 3 and 4; it is actually much smaller than 0.0001 in the equation (4.2) and, therefore appears as zero. Whereas both matrices M_1 and M_2 adhere to the restrictions specified above, the filter governed by M_2 is attractive due to the fact that one of the coupling coefficients vanishes. A disadvantage compared to that given by M_1 is the reduced return loss in the center band. This filter can now be designed by translating the coupling

coefficients into line dimensions on an RT6006 substrate using commercial field solvers.

$$M_1 = \begin{bmatrix} 0 & 0.6541 & 0 & 0 & 0 & 0 & 0 & 0 \\ 0.6541 & 0 & 0.7689 & 0 & 0 & 0 & 0.4792 & 0 \\ 0 & 0.7689 & 0 & 0.5740 & 0 & -0.0112 & 0 & 0 \\ 0 & 0 & 0.5740 & 0 & -0.0157 & 0 & 0 & 0 \\ 0 & 0 & 0 & -0.0157 & 0 & 0.5740 & 0 & 0 \\ 0 & 0 & -0.0112 & 0 & 0.5740 & 0 & 0.7689 & 0 \\ 0 & 0.4792 & 0 & 0 & 0 & 0.7689 & 0 & 0.6541 \\ 0 & 0 & 0 & 0 & 0 & 0 & 0.6541 & 0 \end{bmatrix} \tag{4.1}$$

$$M_2 = \begin{bmatrix} 0 & 0.6251 & 0 & 0 & 0 & 0 & 0 & 0 \\ 0.6251 & 0 & -0.8128 & 0 & 0 & 0 & 0.4450 & 0 \\ 0 & -0.8128 & 0 & 0.5488 & 0 & -0.0200 & 0 & 0 \\ 0 & 0 & 0.5488 & 0 & 0 & 0 & 0 & 0 \\ 0 & 0 & 0 & 0 & 0 & 0.5488 & 0 & 0 \\ 0 & 0 & -0.0200 & 0 & 0.5488 & 0 & -0.8128 & 0 \\ 0 & 0.4450 & 0 & 0 & 0 & -0.8128 & 0 & 0.6251 \\ 0 & 0 & 0 & 0 & 0 & 0 & 0.6251 & 0 \end{bmatrix} \tag{4.2}$$

One difficulty in realizing cross-coupled microwave filters in planar technology is to identify and control the required electric and magnetic couplings for the non-adjacent resonators. Several cross-coupled planar structures have been proposed recently, including microstrip dual-mode resonators, dual-plane multi-coupled line structures, hair-pin structures and microstrip square open-loop resonators [32], [111-113], [114-117]. Microstrip square open-loop resonators can have a smaller size in comparison with microstrip dual-mode resonators. In addition, square open-loop and hairpin resonators are much simpler in structure than dual-plane multi-coupled lines. As they require no grounding and ground-plane coupling apertures. Furthermore, it appears that coupled square open-loop or hair-pin resonators are more flexible in implementation on a variety of cross-coupled planar filters, whose topologies are analogous to those of cross-coupled waveguide cavity filters [32], [117].

It is now desirable to adopt the synthesis technique demonstrated in last section on cross-coupled planar/microstrip filters. However, the application of such a design approach requires the knowledge of mutual couplings between coupled resonators. For cross-coupled waveguide cavity filters, similar procedures are widely employed in terms of inter-cavity couplings due to the

simplicity and accuracy [3], [19].

The next step is to characterize the couplings and external quality factors with respect to the elements in physical structures so that the physical dimensions of the filter topology can be extracted from coupling coefficients as design parameters. Fig. 4.3 depicts four different types of coupling schemes encountered in the filter design. These couplings may be described as the magnetic coupling, electric coupling, and mixed coupling or hybrid coupling [113].

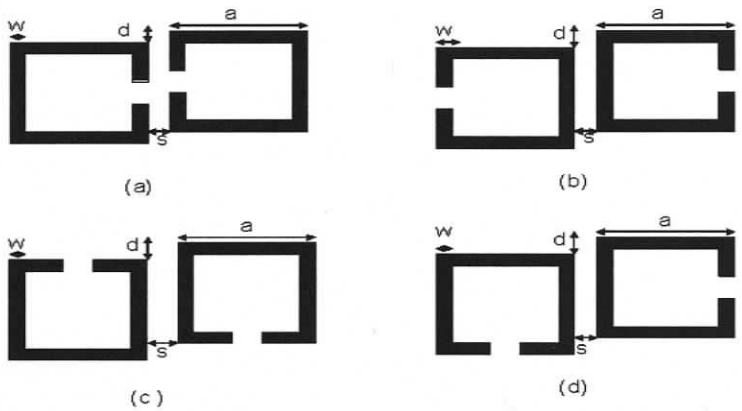

Fig.4.3 Basic planar/microstrip coupling schemes for square open loop resonators on a substrate; (a) electric coupling; (b) magnetic coupling; (c, d) mixed coupling topologies.

The coupling schemes are related to different orientations of a pair of identical square open-loop resonators, which are separated by a spacing *s* and may or may not be subject to an offset *d*. Any other coupling topology among those coupling schemes is that of the proximity coupling, which is basically through fringing fields. The nature and the extent of the fringing fields determine the nature and strength of the coupling coefficient. At the resonance frequency, each of the open-loop resonators has the maximum electric field density at the side with an open gap but the maximum magnetic field density at the opposite side. Due to the exponentially decaying character of the fringing field outside the region, the electric fringing field is stronger near the side which has the maximum electric field distribution. In other words, a negative coupling coefficient is obtained if the open sides of two coupled resonators are approximately placed as in Fig. 4.3a, whereas a positive coupling coefficient can be realized if the sides with the maximum magnetic field of two coupled resonators are approximately positioned as in Fig. 4.3b.

For the coupling schemes in Fig. 4.3c and Fig. 4.3d, the magnetic and electric fringe fields at the coupled sides may have comparative distributions so that both electric and magnetic couplings occur. These couplings may be designated as mixed or hybrid couplings.

It may be convenient for the design procedure of a planar/microstrip filter to estimate the coupling coefficients of the coupled open-loop resonators using some closed-form expressions. It is demonstrated that for a given substrate with a relative dielectric constant ε_r and thickness h, the coupling coefficients can be specified in terms of normalized dimensional elements such as s/h, w/h and a/h where s, w and a are the gap between coupled sides, the thickness of the employed resonators and the length of each side of resonators, respectively. The coupling coefficients may be fitted into the following models through numerical approximation [111]. For the electric coupling coefficient (K_e), the following closed-form functions can be used:

$$
\begin{aligned}
K_e &= \frac{\pi}{16} F_e \exp(-A_e)\exp(-B_e)\exp(-D_e) \\
A_e &= 0.2259 - 0.01572\varepsilon_r + 0.1\sqrt{\varepsilon_r + 1}\,\frac{w}{h} \\
B_e &= \left[1.0678 + 0.266\ln\left(\frac{\varepsilon_r + 1}{2}\right)\right]\left(\frac{s}{h}\right)^{pe} \\
pe &= 1.0886 + 0.03146\left(\frac{w}{h}\right)^4 \\
D_e &= \left[0.1608 - 0.06945\sqrt{\frac{a}{h}}\right]\left(\frac{s}{h}\right)^{1.15} \\
F_e &= \left[-.09605 + 1.4087\sqrt{\frac{a}{h}} - 0.2443\frac{a}{h}\right]
\end{aligned}
\tag{4.3}
$$

For the magnetic coupling coefficient (K_m), we have

$$
\begin{aligned}
K_m &= \frac{\pi}{16} F_m \exp(-A_m)\exp(-B_m)\exp(-D_m) \\
A_m &= \left[-0.06834 + 0.14142\frac{w}{h} + 0.08655(\frac{w}{h})^3 \right] \\
B_m &= 1.2(\frac{s}{h})^{pm} \\
pm &= 0.8885 + 0.1751\sqrt{\frac{w}{h}} \\
D_m &= \left[1.154 - 0.8242\sqrt{\frac{a}{h}} + 0.1417\frac{a}{h} \right](\frac{s}{h}) \\
F_m &= \left[-0.5014 + 1.0051\sqrt{\frac{a}{h}} - 0.1557\frac{a}{h} \right]
\end{aligned}
\tag{4.4}
$$

and the following expressions can be applied for the mixed coupling coefficient (K_B):

$$
\begin{aligned}
K_B &= K_m^{'} + K_e^{'} \\
K_m^{'} &= 0.5K_m \\
K_e^{'} &= 0.5K_e
\end{aligned}
\tag{4.5}
$$

The above formulas are able to quantitatively demonstrate that the magnetic coupling is predominant in this case, even though both electric and magnetic couplings occur. The above formulas are validated in [111] using a full-wave EM simulator.

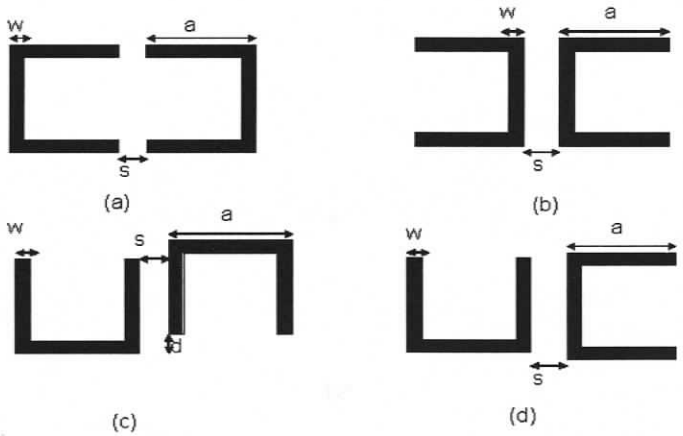

Fig. 4.4 Basic planar/microstrip coupling schemes for hair-pin resonators on a substrate; (a) electric coupling; (b) magnetic coupling; (c, d) mixed coupling topologies.

The other resonators used in the filter design are hair-pin (Fig. 4.4) and quasi dual-mode resonators (Fig. 4.5) [4-5]. The half-wavelength hairpin resonator, which is larger in size in comparison with the folded-square open-loop resonator, is addressed in several papers [112], [118]. The structural parameters of the cross-coupled hair-pin resonators in a filter coupling topology can be expressed by the same formulas employed for magnetic coupling in square open-loop resonators. The negative coupling coefficient in this case can be achieved via capacitive coupling between open-ended sides of coupled resonators. This capacitive coupling is described in most microstrip handbooks, e.g. [119].

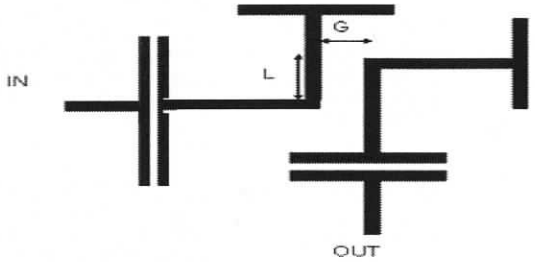

Fig. 4.5 Quasi dual-mode resonator

This quasi dual-mode resonator is characterized similar to a conventional dual-mode patch resonator, but with considerably smaller size [120-121]. Either changing the capacitance portion or the inductive portion of single mode resonators controls the resonance frequency in this case. The coupling length L and gap G in Fig. 4.5 adjust the sign and magnitude of the coupling coefficient between two excited modes. Furthermore, the type of housing and its proximity to the substrate strongly impact the quality factor (Q) in dual-mode patch resonators, whereas quasi dual-mode resonators are free from radiation problems. The filter layout of quasi dual-mode resonators allows the realization of cross coupling and thus supports elliptic filters.

4.3 Synthesis Approach

Let us go back to the triple-band filter example in section 4.2 and the coupling coefficient approximation in section 4.2.1. After equating the coupling coefficients of equation (4.2) with those in the actual structure (inset of Fig. 4.6), the response obtained by Ansoft Designer is shown as solid lines in Fig. 4.6. Of course, the achievable precision is limited in this step due to comparison of an equivalent circuit (coupling matrix) with a full-wave electromagnetic (EM) model. Therefore, slight differences between responses of the coupling matrix and that of the actual circuit must be accepted. Some minor fine-tuning in the EM-based code is also usually required. The design is verified by two different commercial packages, i.e., IE3D and Sonnet, whose responses are denoted as dashed lines in Fig. 4.6. (Note that slight differences between Ansoft Designer and IE3D results have been previously observed [122] and are attributed to the different approaches of the method-of-moments implementation in both packages.) In addition, due to the interpolation technique in IE3D, the simulation CPU time is at least ten times faster than that of Ansoft Designer and Sonnet. The passband insertion losses, as simulated with Ansoft Designer, are approximately 2.0, 2.3 and 2.1 dB; the minimum passband return loss is slightly below 10 dB. Depending on the actual filter topology and technology, tighter restrictions might have to be imposed on magnitudes and signs of individual coupling coefficients. For planar circuits, the closed-form expressions for the electric and magnetic coupling coefficients of, for example, open-loop resonators ((4.3)-(4.5)) are used. For waveguide-based filters, maximum aperture dimensions are determined in advance; and related coupling coefficients are calculated from simple mode-matching routines, e.g., [123].

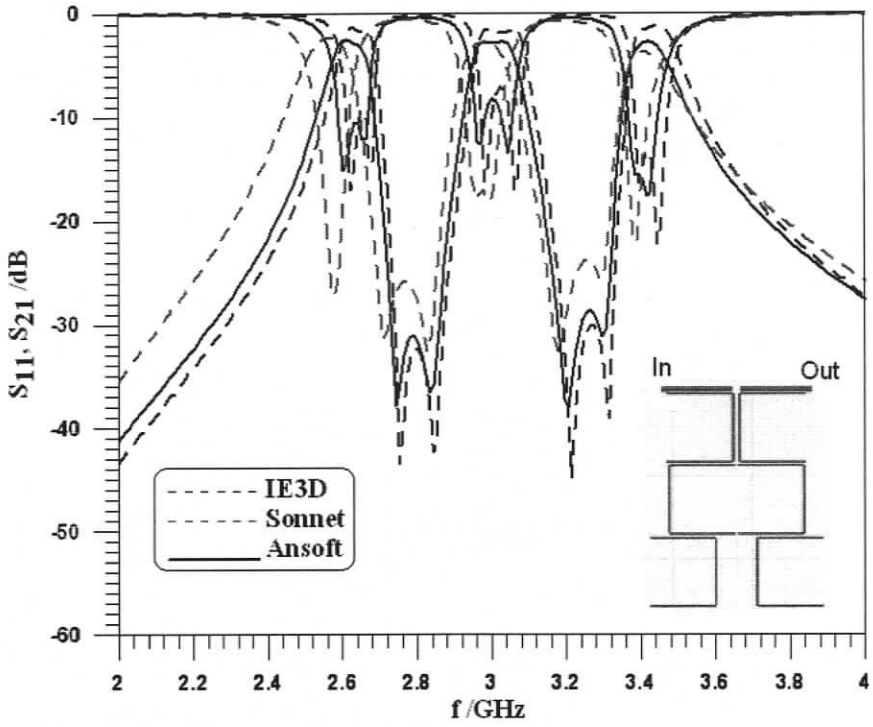

Fig. 4.6 Performances of the triple-band filter using hairpin resonators on RT 6006 substrate; Ansoft Designer (solid lines, data from [106]), IE3D and Sonnet (dashed lines).

Out-of-band rejection can be improved by placing transmission zeros not only between passbands but also to the left and/or right of all passbands. This is demonstrated in Fig. 4.7 using quasi dual-mode resonators. The coupling matrix performance in Fig. 4.7 displays four transmission and four reflection zeros. Each reflection zero is created by one resonator, and source-load coupling produces four transmission zeros. The coupling matrix for this type of quasi dual-mode filter is expressed as

$$M_3 = \begin{bmatrix} 0 & 0.77 & 0 & 0 & 0 & 0.073 \\ 0.77 & 0 & 0.99 & 0 & -0.72 & 0 \\ 0 & 0.99 & 0 & 0 & 0 & 0 \\ 0 & 0 & 0 & 0 & 0.99 & 0 \\ 0 & -0.72 & 0 & 0.99 & 0 & 0.77 \\ 0.073 & 0 & 0 & 0 & 0.77 & 0 \end{bmatrix} \tag{4.6}$$

with a center frequency at 3 GHz and four percent bandwidth in each passband. The elements in the coupling matrix are translated into actual coupling coefficients on RT6006 substrate and

thickness of 0.635mm. The results simulated with Ansoft Designer are illustrated in Fig. 4.7. The insertion loss within the passbands is less than 2.5 dB, and the return loss is better than 15dB. In addition and as an improvement over the coupling matrix response, the quasi-dual-mode structure achieves 30dB attenuation between the two passbands and in the stopbands to the left and right.

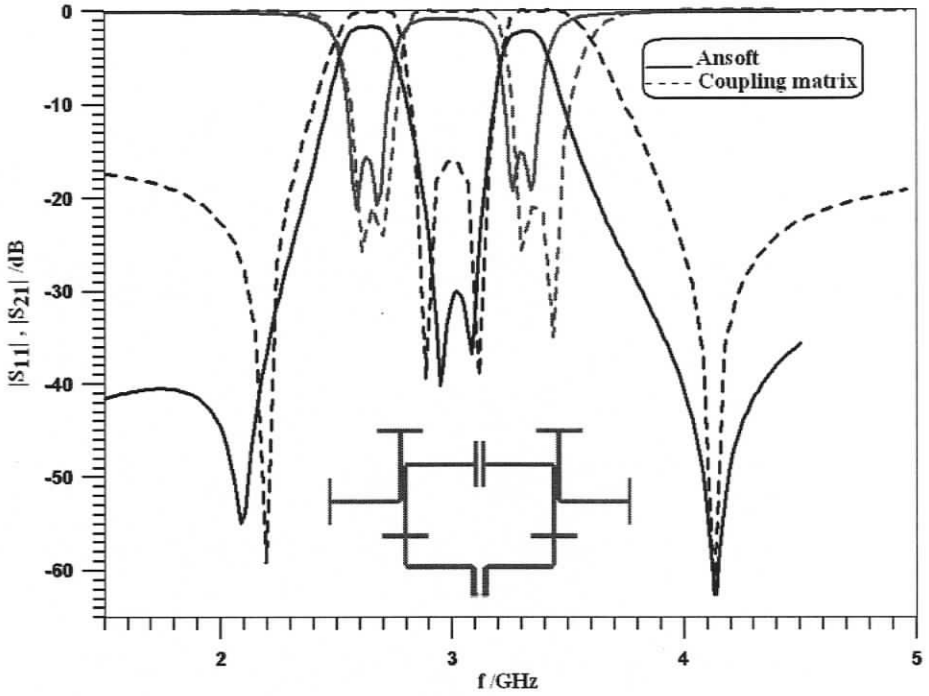

Fig. 4.7 Performance of a four-pole dual-band filter using quasi dual-mode resonator computed from the coupling matrix (dashed lines) and Ansoft Designer (solid lines).

4.4 Measurement Performances

The above theory is now applied to dual-band filters in microstrip and waveguide technologies. A few microstrip examples are presented in [106] and will not be repeated here. However, due to manufacturing tolerances, the transmission zeros between passbands are not experimentally confirmed in [106]. Therefore, a six-resonator dual-band microstrip filter with open-loop resonators is designed on an RT5880 substrate with a height of 508 μm. The design parameters are f_0=3GHz and b=500MHz and transmission zeros at 2.64, 2.94, 3.06, and 3.42 GHz. The initial coupling values in the coupling scheme shown in the inset of Fig. 4.8a are all 0.5, except for M_{16}= - 0.2. The optimized coupling matrix is

$$M_4 = \begin{bmatrix} 0 & 0.8719 & 0 & 0 & 0 & 0 & 0 & 0 \\ 0.8719 & 0 & 0.7001 & 0.6005 & 0 & 0 & -0.2373 & 0 \\ 0 & 0.7001 & 0 & 0 & 0 & 0.0700 & 0 & 0 \\ 0 & 0.6005 & 0 & 0 & 0.9440 & 0 & 0 & 0 \\ 0 & 0 & 0 & 0.9440 & 0 & 0 & 0.6005 & 0 \\ 0 & 0 & 0.0700 & 0 & 0 & 0 & 0.6986 & 0 \\ 0 & -0.2373 & 0 & 0 & 0.6005 & 0.6986 & 0 & 0.8719 \\ 0 & 0 & 0 & 0 & 0 & 0 & 0.8719 & 0 \end{bmatrix} \tag{4.7}$$

Fig. 4.8a shows the comparison between the performances of the coupling matrix and that of the actual circuits using Ansoft Designer. A prototype filter was built, and its response is shown in Fig. 4.8b together with a photograph and the Ansoft Designer data for comparison. The measurements confirm the basic shape of the computed filter characteristic, especially the existence of the four transmission zeros. However, the entire measurement is slightly shifted towards higher frequencies. After investigation, it was determined that this shift can be partly attributed to the fact that along the tracks (transmissions lines), the manufacturing process produces slightly deeper cuts into the dielectric. Therefore, the effective dielectric constant of the line will be lower than expected. Note that this effect is more pronounced for the thin lines used to form the open-loop resonators whose line widths are much smaller than those of the 50 ohm input and output sections. Fig. 4.8c displays the measurement data together with the Ansoft Designer performances when the effective dielectric constant is taken five percent lower than what is specified in the data sheet. Good agreement is observed between the simulation and measurements. The remaining discrepancies are attributed to manufacturing tolerances, which compare well with measurements presented in [106] for higher permittivity substrates. Measured passband insertion losses are 2.1 and 2.4 dB.

Single passband waveguide filters are traditionally modeled by coupling matrices, e.g., [3]. We are extending the dual-band design of Chapter 2 to waveguide technology by making use of two principles. The proposed example uses the same procedure as applied to the microstrip filters, but takes into account additional transmission zeros produced by the actual filter. This principle was first applied in [109]. Fig. 4.9a shows a dual-band filter in folded waveguide technology. The design parameters are f_0=15GHz, b=2GHz and transmission zeros at 12.94,

14.85, 15.09, and 16.31 GHz. In order to convert the optimized coupling matrix elements to actual aperture dimensions, we follow an approach given in [108]. Upon inspection of a first waveguide design, additional transmission zeros were observed resulting from the distance between the source/load aperture and the rest of the filter. The two additional resonances were included in the coupling scheme (see Fig. 4.9b) and result from the next higher-order modes in the input and output. They are modeled as as detuned resonator nodes R_5 and R_6 similar to [110] and in an attempt to maintain symmetry of the coupling matrix. The addition and connection of the other resonances in Fig. 4.9b can generate two more attenuation poles based on the following considerations. Note that this design differs somehow from all previous ones in this chapter due to the fact that the additional (left-most, right-most) attenuation poles cannot be controlled independently. The harmonic resonances depend on the input and output cavities, whose dimensions are determined to obtain all other transmission zeros. In the coupling scheme of Fig. 4.9b, the straight line from source to load forms a standard quadruplet transmission poles as well as four transmission zeros in the dual-band performance depicted in Fig. 4.9c.

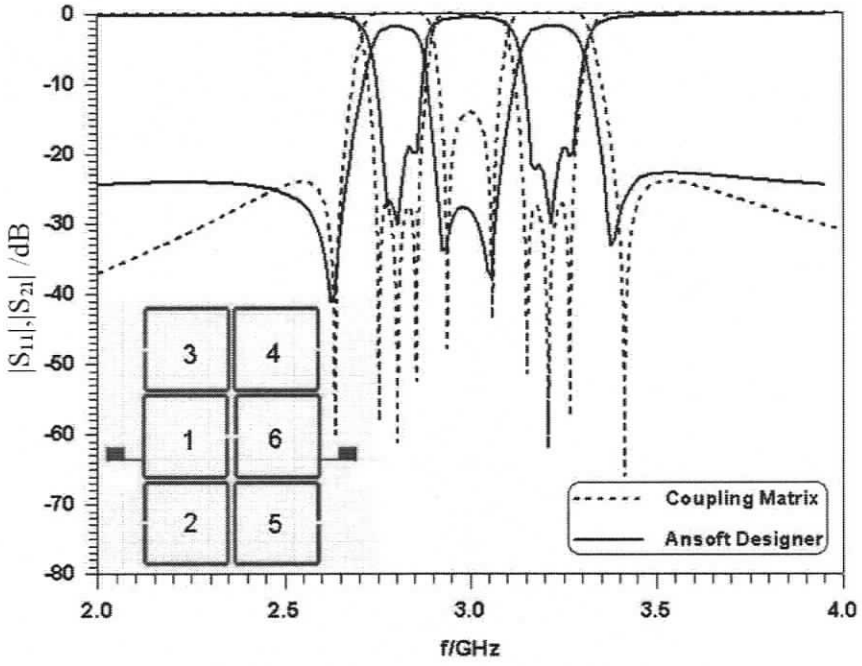

(a)

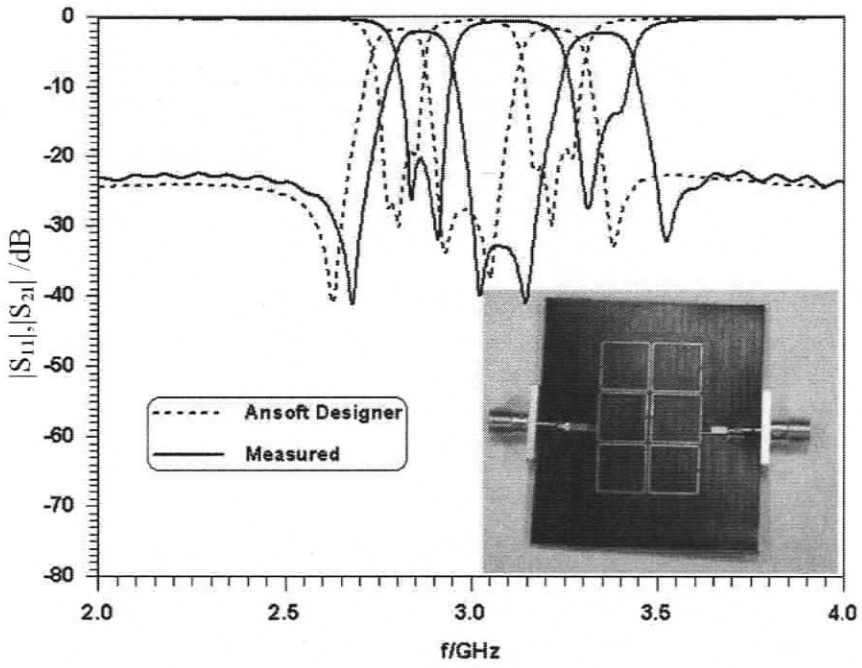

(b)

Fig. 4.8 Performance of a dual-band filter using six open-loop resonators on RT 5880 substrate (a) Comparison of coupling-matrix theory (dashed lines) with Ansoft Designer (solid lines); (b) prototype measurements (solid lines), photograph and Ansoft Designer data (dashed lines); (c) prototype measurements (solid lines) and Ansoft Designer data from -5% tolerance analysis on the substrate's ε_r.

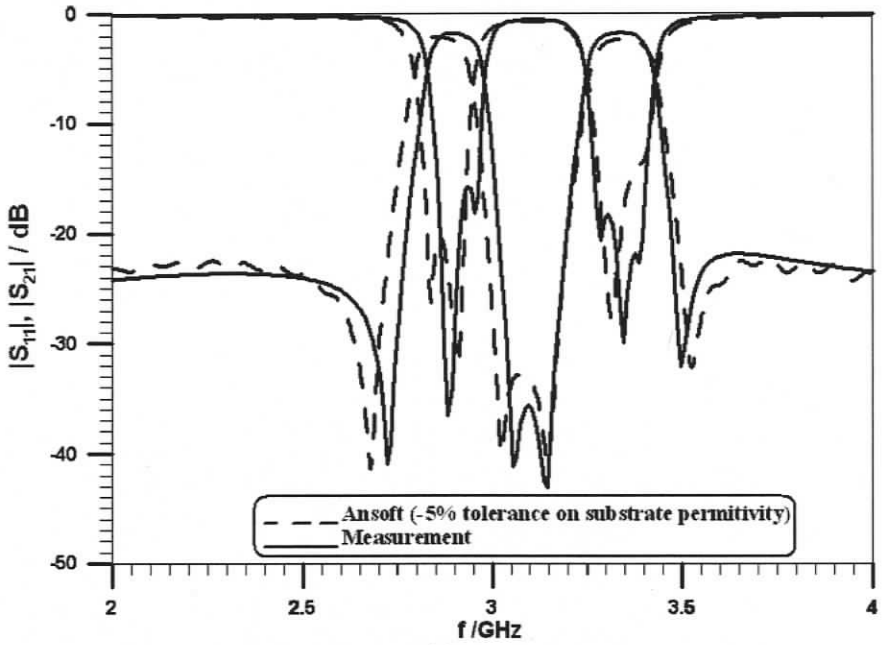

(c)

Fig. 4.8 Continued.

The optimized coupling matrix is shown in equation (4.8), and its response is shown as dashed lines in Fig. 4.9c.

$$M_4 = \begin{bmatrix} 0 & 0.3477 & 0 & 0 & 0 & 0.6000 & 0 & -0.0242 \\ 0.3477 & 0.0136 & 0.9000 & 0 & 0 & 0.0500 & 0 & 0 \\ 0 & 0.9000 & 0.0407 & 0.1588 & 0 & 0 & 0 & 0 \\ 0 & 0 & 0.1588 & 0.0407 & 0.9000 & 0 & 0 & 0 \\ 0 & 0 & 0 & 0.9000 & 0.0136 & 0 & 0.0500 & 0.3477 \\ 0 & 0.0500 & 0 & 0 & 0 & 2.2000 & 0.0050 & 0 \\ 0.6000 & 0 & 0 & 0 & 0.0500 & 0.0050 & -2.4000 & 0.7000 \\ -0.0242 & 0 & 0 & 0 & 0.3477 & 0 & 0.7000 & 0 \end{bmatrix} \tag{4.8}$$

Good agreement is obtained with the actual filter as modeled by the mode-matching technique (MMT) (solid lines) and the μWaveWizard (dotted lines), especially with respect to the location of the two additional zeros.

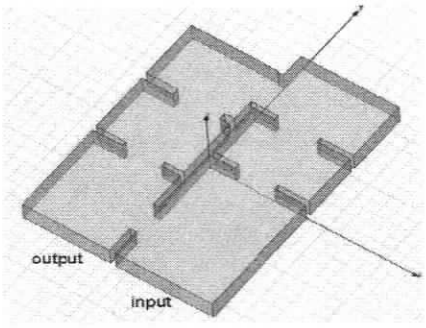

(a)

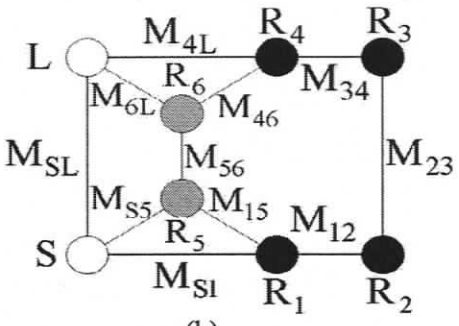

(b)

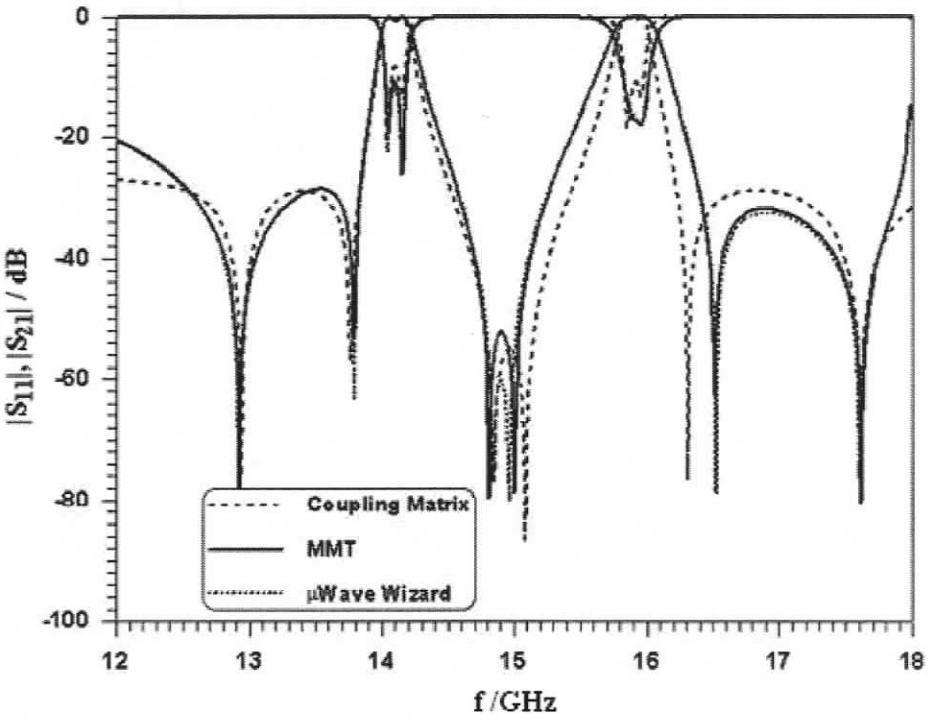

(c)

Fig. 4.9 A dual-band filter in folded waveguide technology. (a) 3D view of the filter; (b) coupling scheme; (c) Performances obtained from theory (dashed lines) and EM-based software (solid and dotted lines).

4.5 Summary

The proposed coupling matrix design method for dual- and triple-passband filters is a viable alternative to current multi-band filter design techniques. The method is flexible, not restricted to certain filter types or topologies, and is capable of including higher-order mode effects. The coupling scheme and limitations for the coupling coefficients can be enforced during the design. The feasibility of this technique is demonstrated for filter configurations in microstrip and waveguide technology. The designs are verified by measurements and a number of different EM full-wave codes.

CHAPTER 5

Advanced Dual-Band and Multi-Band Step-Impedance Filters

5.1 Introduction

The increasing demand for wireless communication applications requires RF components to operate in multiple separated frequency bands in order to access different services with a single multimode terminal. In addition, high speed wireless Local Area Networks (LANs) and other services such as the Worldwide Interoperability for Microwave Access (WiMAX) and Industrial, Scientific and Medical (ISM) spectrum allocation operate at frequencies between 2 GHz and 6 GHz with bandwidths up to 100 MHz. In order to accommodate this multi-band RF signal reception and transmission into a single RF transceiver, a dual-band or multi-band RF front-end circuit is required. This can be achieved by switching between separate filters, but such an approach leads to a high number of filter components, thus enlarging circuit size and increasing power consumption [6]. Concurrent dual-band or multi-band components are needed to integrate circuits operating in different bands into a single unit so that size, cost and component count can be reduced. Therefore, in this approach, all filter components must have the new feature of simultaneous passbands at separated center frequencies with adequate out-of-band and between-bands suppressions. Different configurations have been proposed for realizing dual-band filters. One of the preferred solutions involves shunt stubs and/or so-called dual-behavior topologies, [10], [11], [124-127]. In [12], the second resonating mode of a quarter-wave resonator is adjusted to resonate at the second passband of the dual-band filter. This prototype generates two transmission zeros on the upper side of the passbands and is suitable for miniature implementation.

Planar dual-band filter designs rely on the harmonic tuning properties of stepped-

impedance resonators (SIRs) as the other popular design approach [128]. Especially the second resonance of such resonators can be efficiently used to create dual-band filters, e.g. [125], [129-135]. Chang, Jeng and Chen [13] describe a dual-band filter with half-wave stepped-impedance resonator in a classical comb-line configuration, which creates a strong transmission zero between the two passbands. Alternatively, including the third resonance, SIRs are employed in triple-band filters [136-137] or ultra-wideband (UWB) filters, e.g. [138-141]. Several different designs in parallel-coupled or folded configurations have been presented, e.g. [13], [15], [142-143], and the control of additional attenuation poles in single-band filters is addressed in [112].

In order to create dual-band filters of varying bandwidths, multiple SIR's are connected and their coupling is appropriately adjusted. Therefore, the design of coupling coefficients for cascaded SIRs is of fundamental importance, e.g. [130], [139], [144]. However, the type of coupling between SIRs mainly determines the individual bandwidths and, therefore, influences the realization of coupling coefficients, e.g. [145], [146]. In certain coupling schemes, the coupling in the second passband cannot be controlled efficiently, or harmonic passbands cannot be suppressed effectively. Moreover, coupling schemes realized by different coupled-line segments can contribute to additional attenuation poles between the passbands or outside of the passbands, e.g. [134], [146] or, alternatively, can create additional resonances within the filter bands to increase bandwidth, e.g. [138], [140], [145].

Common to almost all dual-band designs presented so far is a poor stop-band characteristic towards higher frequencies. This is mainly caused by the fact that in certain coupling schemes, the coupling in the second passband cannot be controlled efficiently or those harmonic passbands cannot be suppressed.

Therefore, dual- to multi-band step-impedance resonator single-circuit filters with new coupling schemes, which support fully controllable passbands and feature wide stopbands towards higher frequencies, are presented for narrowband to wideband applications. Additional design features include inductive or capacitive cross coupling between source and load. These

new configurations are free of input and output matching networks and use stronger folding in order to reduce size and tight coupling.

This chapter presents advanced coupling topologies and their experimental verification. All circuits in [147] have been redesigned, fabricated and measured. The design approaches are verified by experiment and simulation with two electromagnetic field (EM) solver packages.

5.2 Fundamentals of Stepped-Impedance Resonators

A typical half-wavelength step-impedance resonator is depicted in Fig. 5.1 with Z_1 and Z_2 being the characteristic impedances of the transmission line sections of lengths θ_1 and θ_2, respectively. The resonance condition can be analyzed by deriving the input admittance viewed from an open end [16]. Ignoring the step discontinuities effect and fringing capacitances at the open-end gives

$$Yin = jY_2 \cdot \frac{2(R_z \tan(\theta_1/2) + \tan(\theta_2))(R_z - \tan(\theta_1/2)\tan(\theta_2))}{R_z(1-\tan^2(\theta_1/2))(1-\tan^2(\theta_2)) - 2(1-R_z^2)\tan(\theta_1/2)\tan(\theta_2)} \tag{5.1}$$

where $R_z=Z_2/Z_1$ is the impedance ratio. The resonance frequencies occur when the input admittance is zero ($Y_{in}=0$). Following standard transmission-line theory, the resonance conditions for the fundamental and second harmonic frequencies f_1 and f_2 with corresponding electrical lengths θ_{s1} and θ_{s2}, respectively, are calculated through odd- and even-mode resonance conditions [15]

$$R_z - \tan(\frac{\theta_1}{2})\tan(\theta_2) = 0 \quad \text{, odd mode} \tag{5.2a}$$

$$R_z \tan(\frac{\theta_1}{2}) + \tan(\theta_2) = 0 \quad \text{, even mode} \tag{5.2b}$$

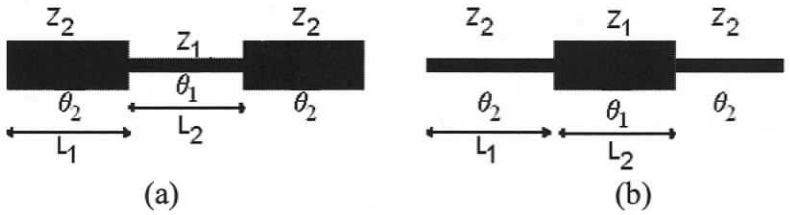

Fig. 5.1 Basic half-wavelength stepped-impedance resonator (from [16]) (a) if $f_2/f_1 > 2$ ($R_z<1$) and, (b) if $f_2/f_1 < 2$ ($R_z>1$).

The fundamental and harmonic frequencies of a step-impedance resonator occur alternatively in the odd and even modes. Thus any desired frequency ratio (f_n/f_1) of the higher-order harmonics (f_n) to that of the fundamental mode (f_1) occur when Y_{in}=0, and can be determined through (5.2) in terms of proper choice of impedance ratio R_z and U, which is expressed as the electrical length ratio:

$$U = \frac{\theta_2}{\theta_1 + \theta_2} \tag{5.3}$$

The first harmonic ratio (f_2/f_1) is defined such that

$$\begin{aligned} f_2 / f_1 &< 2 \qquad if R_z > 1 \\ f_2 / f_1 &= 2 \qquad if R_z = 1 \\ f_2 / f_1 &> 2 \qquad if R_z < 1 \end{aligned} \tag{5.4}$$

Note that the actual length ratio ($L_2/(L_1+L_2) \approx \theta_2/(\theta_1+\theta_2)$) depends on the effective permittivity, discontinuities and open-end effects.

The above essential conditions are utilized to design dual-band filters with different center frequency ratios. In the special case, where θ_1=2θ_2, equations (5.2a) and (5.2b) simplify to

$$\theta_{s1} = \tan^{-1}(\sqrt{R_z}), \qquad \theta_{s2} = \pi/2 \tag{5.5}$$

Therefore, the fundamental dual-band filter design function relating the ratio of both resonance frequencies is defined as

$$\frac{f_2}{f_1} = \frac{\pi}{2\tan^{-1}(\sqrt{Z_2/Z_1})} \tag{5.6}$$

This condition can be used as an initial value in optimization. Other initial values can be found in [142].

In a dual-band filter design procedure, R_z, θ_1 and θ_2 should be extracted so that equations (5.2a) and (5.2b) are satisfied. This implies that by appropriately determining the impedance ratio R_Z, and electrical length ratio U, two passbands with any desired frequency ratio can be achieved.

Fig. 5.2 displays the ratio of the harmonic frequencies to the fundamental mode f_n/f_1 of a basic SIR as a function of the electric length ratio U for different impedance ratios R_Z. In the design procedure of a dual-band filter with a single SIR in Fig. 5.1, the center frequencies of the

first and second passbands are recognized as the fundamental and first higher-order harmonics, respectively. The viable solutions for the length ratios of the SIR are typically demonstrated in Fig. 5.2 in terms of a given R_Z. Clearly, for a specific harmonic ratio (e.g., f_2/f_1=1.7 as shown in Fig. 5.2), two different solutions can be selected for the length ratio in terms of each impedance ratio. They are marked as B, C for R_z =1.55 and A, D for R_z =3.5 in Fig. 5.2. The optimum solution for the length ratio is eventually specified by the fact that the next higher-order harmonics should appear at a frequency as far as possible away. However, realizable impedance characteristics of the low- and high-impedance segments in the SIR topology must also be considered with respect to fabrication simplicity and size reduction.

Cascaded resonators with proper inter-resonator coupling circuits typically realize band-pass filters in the microwave frequency range. Filter design parameters, e.g. coupling coefficients and the number of stages, are derived from given filter specifications such as center frequency at fundamental resonance f_0, bandwidth Δf, and reflection and attenuation characteristics. Thus, the electrical parameters such as characteristic impedances, electrical lengths and impedance/admittance inverters are calculated. By assuming an open-end coupled segment of a SIR, the coupling coefficient k in the fundamental mode is given by [142]

$$k_{i,i+1} = \frac{\Delta}{\sqrt{g_i g_{i+1}}} \tag{5.7}$$

where Δ is the normalized bandwidth, and g_i are the filter coefficients.

The next step in the synthesis consists of generating a coupling matrix whose elements represent the normalized coupling coefficients between individual SIRs as well as to the source and load. The actual coupling coefficients k_{ij} are obtained from

$$\begin{aligned} k_{01} &= k_{N,N+1} = M_{01}\sqrt{\Delta f / f_0} \\ k_{ij} &= k_{ji} = M_{ij}\,\Delta f / f_0, \qquad i,j = 1,...,N;\ i \neq j \end{aligned} \tag{5.8}$$

where N is the number of resonators in the filter topology, and i=0 and j=N+1 represent the input and output ports, respectively. The actual coupling values between coupled segments are determined via even/odd-mode transmission line impedance characteristics

$$k_{ij} = (Z_{0e} - Z_{0o})/(Z_{oe} + Z_{0o}) \tag{5.9}$$

and must match those in (5.8) after proper adjustment of the coupled-line segments [119].

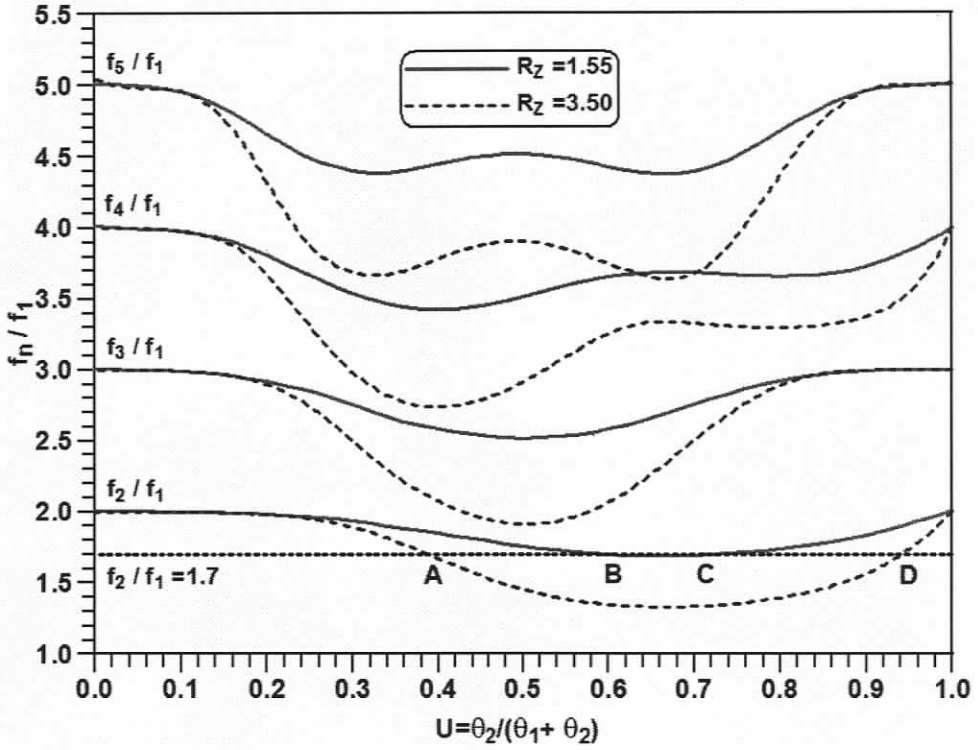

Fig. 5.2 Harmonic to fundamental mode ratios of a basic SIR as functions of length and impedance ratios.

The structural parameters of the coupled sections can be obtained by using the well-known even- and odd-mode characteristic impedances of coupled line sections. In addition, based on specifications of the two center frequencies, the impedance ratio R_Z and the electrical lengths of the SIR are estimated using equations (5.2a), (5.2b). Hence, the impedance characteristic of the un-coupled section of the SIR can be calculated through the impedance ratio and the impedance characteristic of coupled sections.

The next step in the design process is the determination of proper topologies to realize the coupling between step-impedance resonators, which is crucial for the bandwidth control of a dual-band performance. In other words, coupling coefficients control the bandwidth, and the coupling configuration assures the suppression performance of a synthesized step-impedance dual-band filter.

5.3 Dual-Band Coupling Configurations

In the design of dual-band filters, the inter-resonator coupling coefficients in both bands play an essential role and are distinctly different from those in classical single passband filters. Therefore, many traditional dual-band coupling schemes (e.g. Fig. 5.3) are limited when operated at two separated passbands and produce spurious and/or harmonic resonances close to the passbands. At the fundamental resonance frequency, the step-impedance resonator has strong electric and magnetic couplings at both ends and at the center of the transmission lines, respectively. At the first harmonic resonance frequency, the magnetic coupling at the center converts to electrical coupling due to the reduction in wavelength, thus changing the coupling coefficient for the second passband completely and making independent tuning impossible.

Therefore, an appropriate choice for dual-band filters is to utilize the inter-coupled open ends of transmission-line resonators (c.f. Figs. 5.4a-e). Fig. 5.3a shows a new comb-line configuration comparable to Fig. 5.3a. However, the feed structure is changed, and input/output positions are used to control additional attenuation poles. Figs. 5.4b-d show three different dual-band filter configurations with folded rectangular, triangular and circular step-impedance resonators, respectively. These structures are similar to that in Fig. 5.3b but achieve smaller size, larger bandwidth and broad out-of-band rejection. Fig. 5.4e is a complement of Fig. 5.3c with electric coupling at the end rather than magnetic coupling at the center. Moreover, it has smaller dimensions, more flexible bandwidth control and a wider stop-band region than that in Fig. 5.3c.

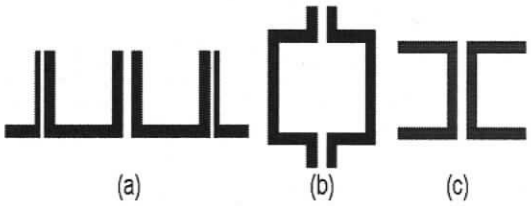

Fig. 5.3 Some traditional dual-band coupling schemes: (a) comb-line, (b) end-coupled, (c) transmission-line coupler.

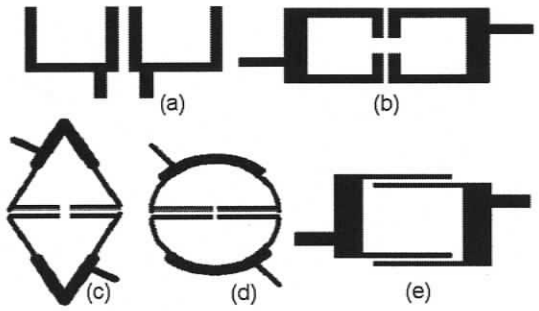

Fig. 5.4 Dual-band step-impedance resonators coupling configurations for wider stop bands: (a) modified comb-line, (b) modified end-coupled, (c) triangular, (d) circular, (e) modified hairpin.

For a half wavelength resonator, there are two proper feed points at opposite locations slightly off the center of the resonator. Fig. 5.5 shows two electric coupling structures constructed by hairpin resonators with different input feed points.

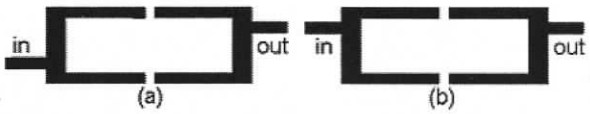

Fig. 5.5 In-phase (a) and out-of-phase (b) feed structures.

In Fig. 5.5a, the feed points are in phase when the circuit resonates at its fundamental frequency, whereas in Fig. 5.5b they are out of phase due to the different path lengths between input and output. Both arrangements can be used to design a filter. However, the configuration in Fig. 5.5a generates two more attenuation poles [112]. By slightly adjusting the actual feed locations and couplings in Fig. 5.5a, one attenuation pole can be allocated in the lower and one in the upper suppression region. In a folded arrangement of two hairpin step-impedance resonators (similar to Fig. 5.3a), possible cross coupling between input and output provides the potential for two additional poles in the stopband. In summary, a number of additional attenuation poles increase the out-of-band rejection and thus the applicable frequency range of these filters. Note that the new dual-band filter schemes are usually smaller in comparison with the traditional ones and that they do not require input/output impedance matching networks.

Fig. 5.6 shows the application of this simple theory using an example of a dual-band filter in the modified comb-line configuration of Fig. 5.4a on RT6006 substrate of height 635μm. The initial design is slightly tuned using Ansoft Designer and verified with IE3D. The slight differences between the two full-wave codes are in a range also observed in other applications [122]. Note that the outer arms of the SIRs are folded inward which contribute to smaller circuit size. The simulated results show that two passbands exist at center frequencies 2.6 GHz and 3.75 GHz with a bandwidth of almost 150 MHz in each passband. Three out of band transmission zeros are observed at 1.75, 2.25 and 3GHz. Moreover, two additional transmission zeros in the upper stop-band region form a complex zero pair at around 4.20 GHz. This is due to the harmonics of the zeros in the lower stop-band region and the phase displacement in this structure. This offers the potential for further out-of-band suppression as demonstrated in the next examples. Note that such a performance cannot be achieved with the conventional design of Fig. 5.3a [13].

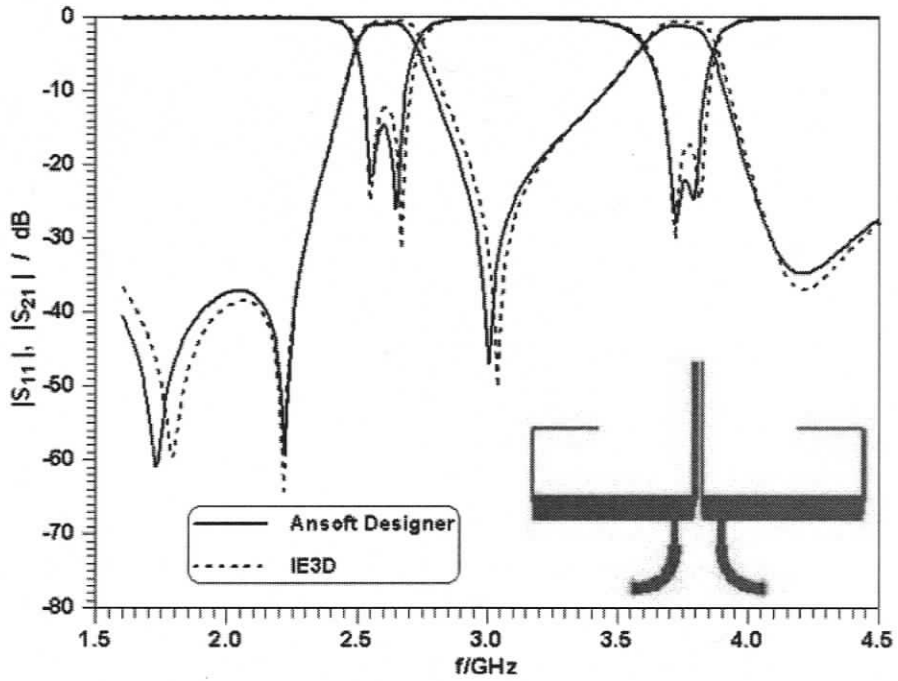

Fig. 5.6 Response of the modified dual-band comb-line configuration according to Fig. 5.4a.

Prototypes of four of the five filter structures shown in Fig. 5.4 have been fabricated on RT5880 using a substrate height of 508 μm.

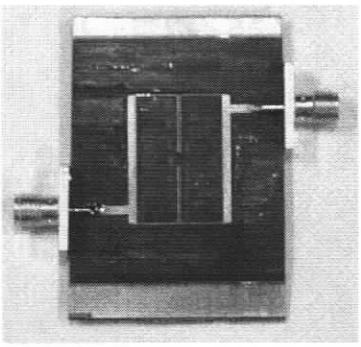

(a)

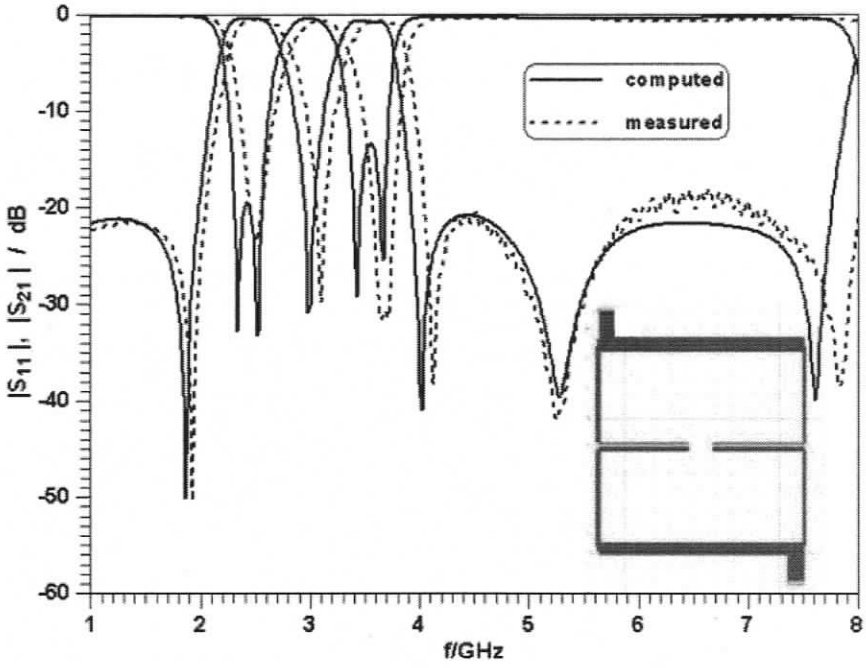

(b)

Fig. 5.7 Photograph (a) and computed (Ansoft Designer) and measured performances (b) of the modified end-coupled filter according to Fig. 5.4b.

Fig. 5.7a shows the prototype and Fig. 5.7b the computed and measured response of the modified end-coupled filter according to Fig. 5.4b. The design features relatively large bandwidths (250 MHz) in each passband, high selectivity and excellent out-of-band rejection up to 7.75 GHz. The five transmission zeros are located at 1.86, 3.0, 4.0, 5.28 and 7.6 GHz and are controlled by the shape of and coupling between the resonators as well as the positions of the input and output ports. Note that the two complex transmission zeros appearing in the example of Fig. 5.6 have been effectively separated. The measurements are in excellent agreement with

computations except for a small frequency shift towards higher frequencies, which has been already addressed in Section 4.3. Measured in-band insertion losses in Fig. 5.6b are 0.45 and 0.72 dB.

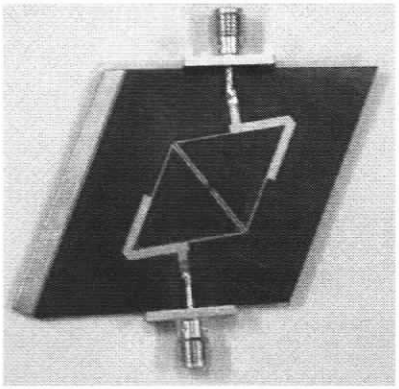

(a)

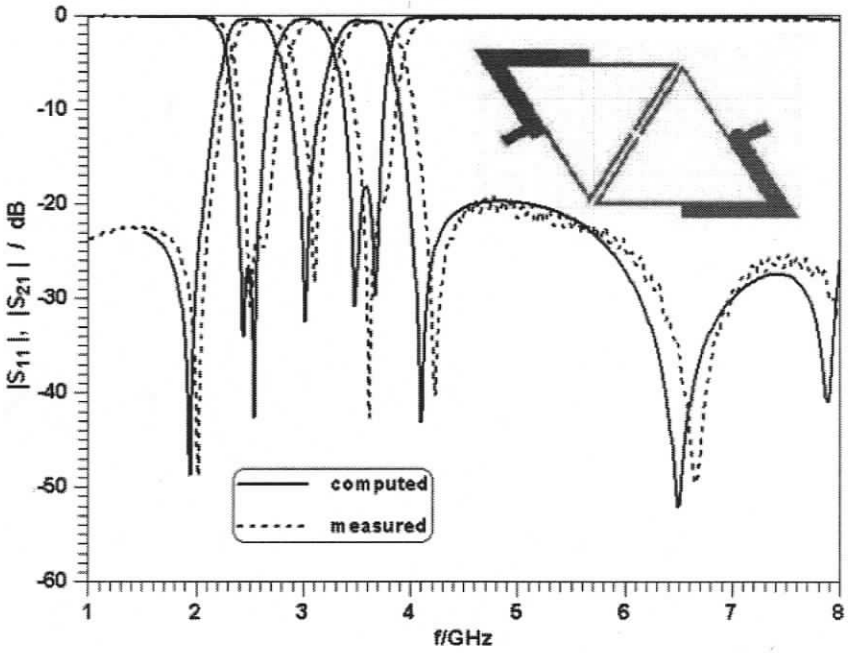

(b)

Fig. 5.8 Photograph (a), computed (Ansoft Designer) and measured performances (b) of the triangular end-coupled filter according to Fig. 5.4c.

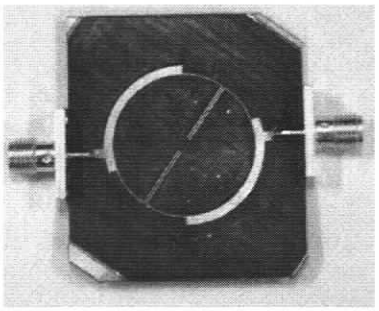

(a)

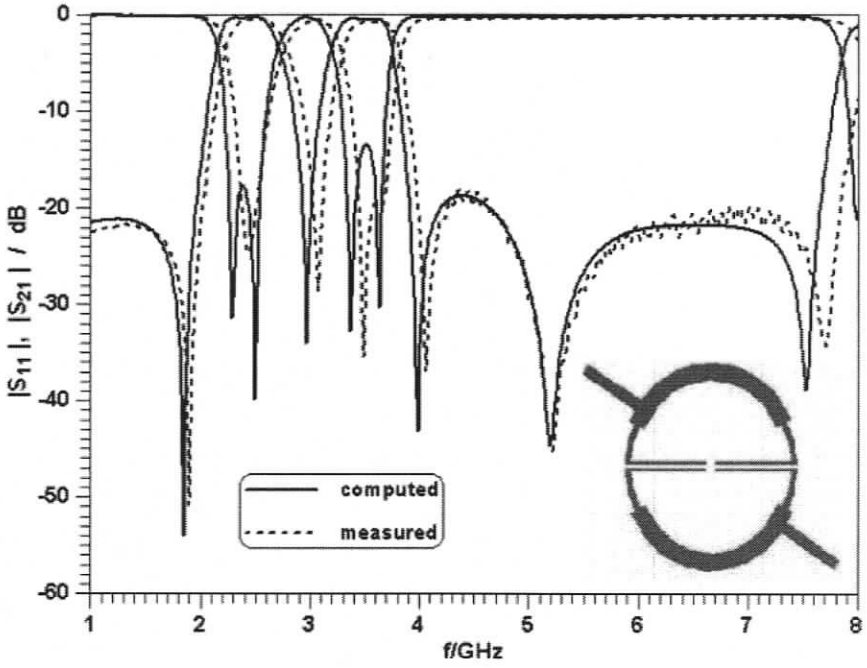

(b)

Fig. 5.9 Photograph (a), computed (IE3D) and measured performances (b) of the circular end-coupled filter according to Fig. 5.4d.

Fig. 5.8 and Fig. 5.9 show variations of this design in triangular and circular SIR arrangements according to Fig. 5.4c and Fig. 5.4d, respectively. The photographs give an excellent account of the actual size of the prototypes. While the bandwidths and locations of the lowest three transmission zeros are similar, the triangular structure in Fig. 5.8 is capable of moving the fourth transmission zero, which appears in Figs. 5.7 and 5.9 at around 5.3 GHz, upwards to 6.5 GHz. This structure thus achieves the widest stopband performance as validated by the measurements.

Note that all measurements in Fig. 5.7 to Fig. 5.9 achieve return losses and stop-band rejections close to or better than 20 dB and, therefore clearly outperform the initial designs on a different substrate presented in [147]. The measured in-band insertion losses for Fig. 5.8 and Fig. 5.9 are 0.65, 0.73, 0.5 and 0.76 dB.

The scheme of end-coupled hairpin SIRs (c.f. Fig. 5.4e) is used for the dual-band filter presented in Fig. 5.10a. The two passbands are centered at 2.45 and 3.6 GHz with bandwidths of 230 and 320 MHz, respectively. Transmission zeros are placed at 2.0, 3.0 and 4.2 GHz. We refrained from specifying other transmission zeros in this design in favor of a minimum return-loss of 20 dB in both passbands. Very good agreement with measurements is observed in Fig. 5.10b. The stop-band extends to above 8 GHz, as the measured attenuation value is 29 dB at 8 GHz. However, compared with Fig. 5.7 to Fig. 5.9, this comes at the expense of a reduced attenuation of 10 dB in the 5 GHz range. The measured in-band insertion losses in Fig. 5.10b are 0.52 dB in both bands.

So far, all designs presented show dual-band filters with two SIRs. This is due to the fact that capacitive end coupling is used to effectively control both passbands. In a multi-resonator arrangement, this scenario cannot be maintained and would result in resonator coupling such as displayed in Fig. 5.3c, which, as mentioned earlier, would result in opposite coupling coefficients for the two bands.

Another scenario of creating dual-band filters of higher order consists of cascading two-resonator dual-band structures. Such examples are presented in Fig. 5.11 and Fig. 5.12, which depict two cascaded configurations similar to those of Fig. 5.10 and Fig. 5.7, respectively. The spurious response in the upper frequency range at 6 GHz for the filter performance in Fig. 5.11 is due to the magnetic coupled segments, but it is eliminated by attenuation poles from the open-ended electric coupling configuration for the filter in Fig. 5.12. As shown in Fig. 5.12b, bandwidths, selectivity and out-of-band attenuation levels increase compared to the performance in Fig. 5.7b. However, since the coupling between the two dual-band filters is the only parameter varied in this design, the performance – as verified by the measurements – is not perfect. On the other hand, the measured stop-band peaks are well below 30 dB, which gives rise to the

possibility of broadening both bandwidths of such a dual-band filter design without compromising the good out-of band rejection of the filters presented in this chapter.

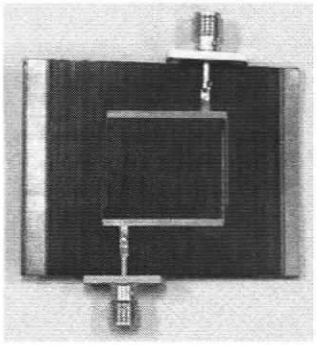

(a)

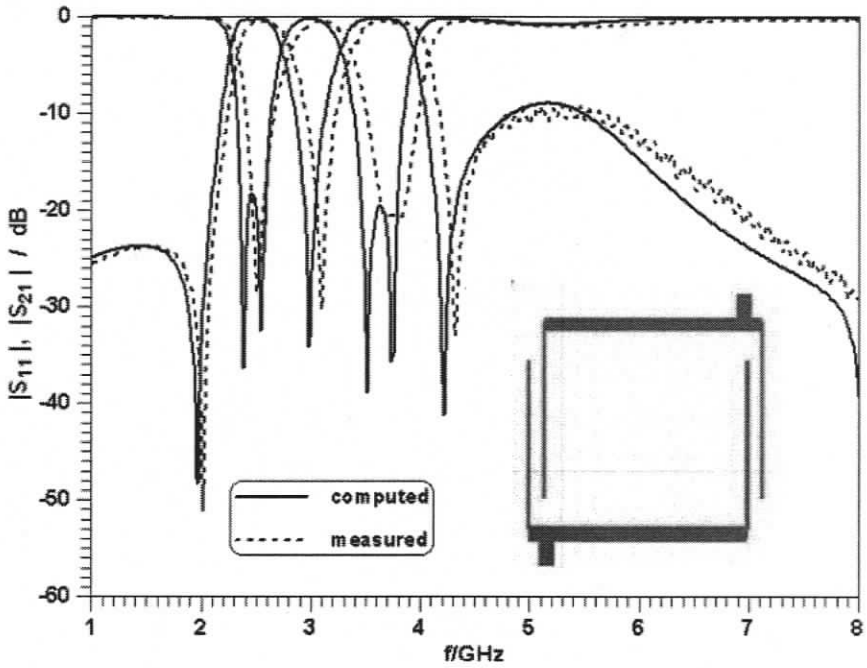

(b)

Fig. 5.10 Photograph (a), computed (IE3D) and measured performances (b) of the modified hairpin filter according to Fig. 5.4e.

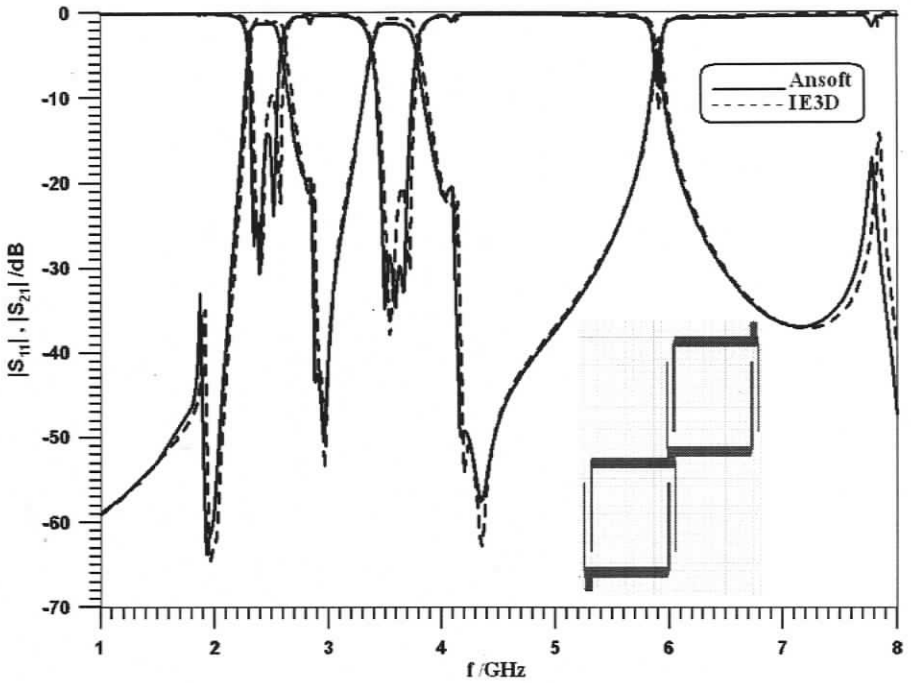

Fig. 5.11 Computed (IE3D and Ansoft Designer) performances of two-cascaded hairpin filters according to Fig. 5.4e.

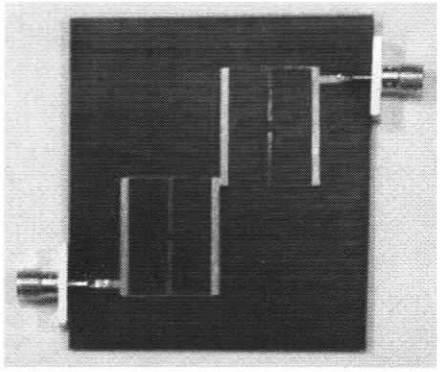

(a)

Fig. 5.12 Photograph (a), computed (IE3D) and measured performances (b) of two cascaded two-resonator filters according to Fig. 5.4b.

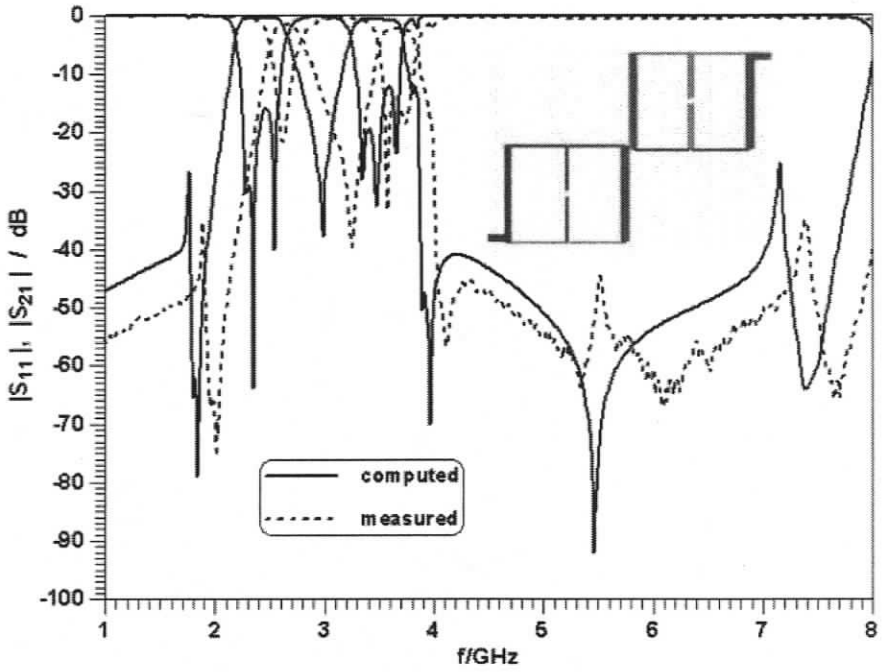

(b)

Fig. 5.12 Continued.

5.4 Multi-Band Filter Configurations

In order to create more attenuation poles and retain bandwidth flexibility in the passbands, new dual-band filter structures based on the classical comb-line topology but with different input/output coupling sections were proposed in Fig. 5.4. The structures in Fig. 5.13a is simplified in comparison to that in Fig. 5.4a but has folded outer high-impedance sections as in Fig. 5.6. The filters in Fig. 5.13b and 5.13c also involve cross coupling between the inputs and outputs of the dual-band filters. Compared to Fig. 5.6, this creates additional transmission zeros, which are located between the passbands for the configuration with inductive source/load coupling (Fig. 5.13b) and in the upper stop-band region for the structure with capacitive source/load coupling (Fig. 5.13c).

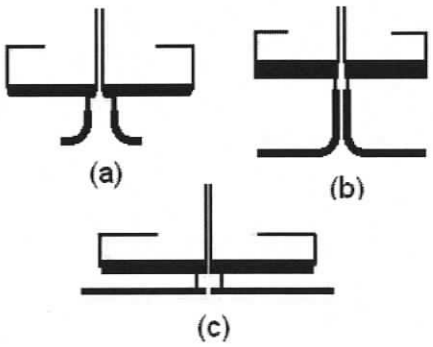

Fig. 5.13 Dual-band filters based on the classical comb-line coupling configuration: (a) without source/load coupling; (b) with inductive source/load coupling; (c) with capacitive source/load coupling.

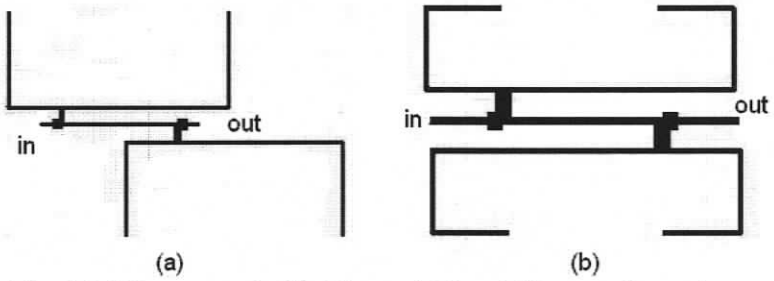

Fig. 5.14 New cascaded/ladder multi-band filter configurations.

Other configurations of dual- to multi-band filters are shown in Fig. 5.14. They form cascaded sections of SIRs similar to a ladder configuration with coupling through an out-of phase feed structure. The coupling between resonators at fundamental and harmonic resonances is adjusted through the location of feeds on the SIRs and the length and characteristic impedance between the feed points. These new configurations generate two transmission zeros from the feed structure, one in the lower stop-band region and one between the passbands. The positions of the input and the output are used to control the transmission zeros. Furthermore, additional passbands are created due to harmonics and the extra transmission line between the feed locations of the SIRs. Therefore, the new schemes are capable of generating multiband filter responses, which are suitable for wireless applications.

This section presents typical performance characteristics of the proposed dual- to multi-band filters. The designs use RT6006 and RT6010 with 17μm metal thickness, 0.635mm and 1.27mm substrate heights, respectively, and are verified by the commercial packages IE3D and

Ansoft Designer. Note that slight differences between Ansoft Designer and IE3D results have been observed previously in Chapter 4.

Fig. 5.15 shows the results for the filter configuration in Fig. 5.13b on RT6010 substrate with two 200 MHz passbands centered at 2.4 GHz and 3.5 GHz. Compared to Fig. 5.6, additional transmission zeros are placed between the two passbands by allocating inductive (positive) cross coupling between the source and the load. This cross coupling also compensates the phase displacement in Fig. 5.4a (c.f. Fig. 5.6) and generates a zero in the upper suppression region. Fig. 5.16 presents the performance of the filter scheme in Fig. 5.13c on RT6006 substrate. This structure is similar to that in Fig. 5.15, but it uses capacitive cross coupling between the source and the load. Capacitive source/load cross coupling compensates the phase displacement that causes the complex pair of zeros in Fig. 5.6. Consequently, we observe the appearance of the two transmission zeros on the upper side of the second passband.

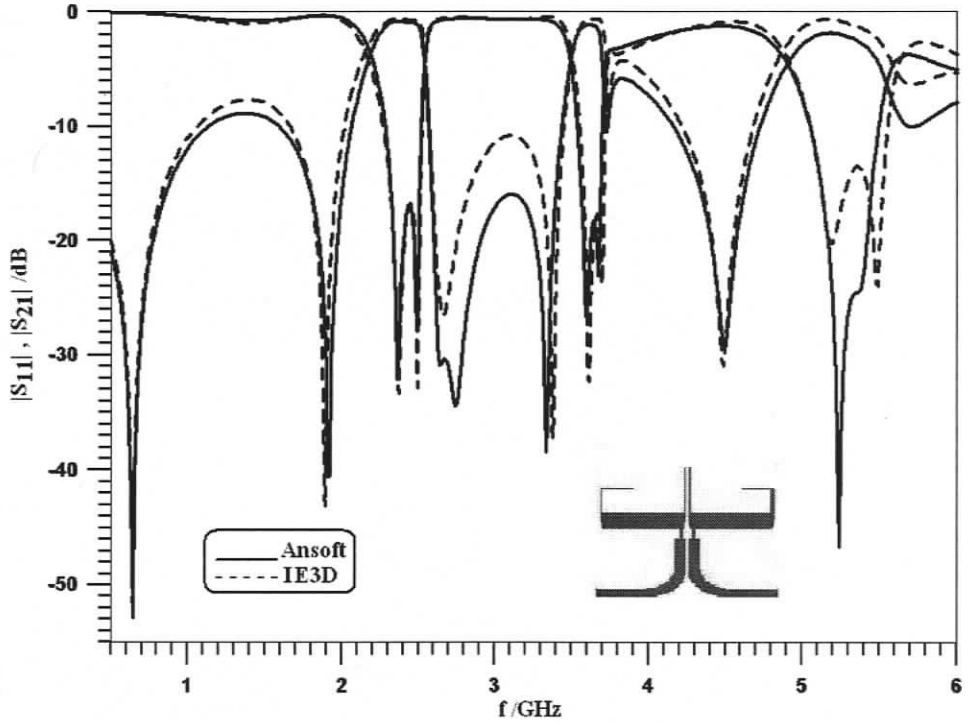

Fig. 5.15 Performance of the new dual-band comb-line filter with inductive source/load coupling according to Fig. 5.13b.

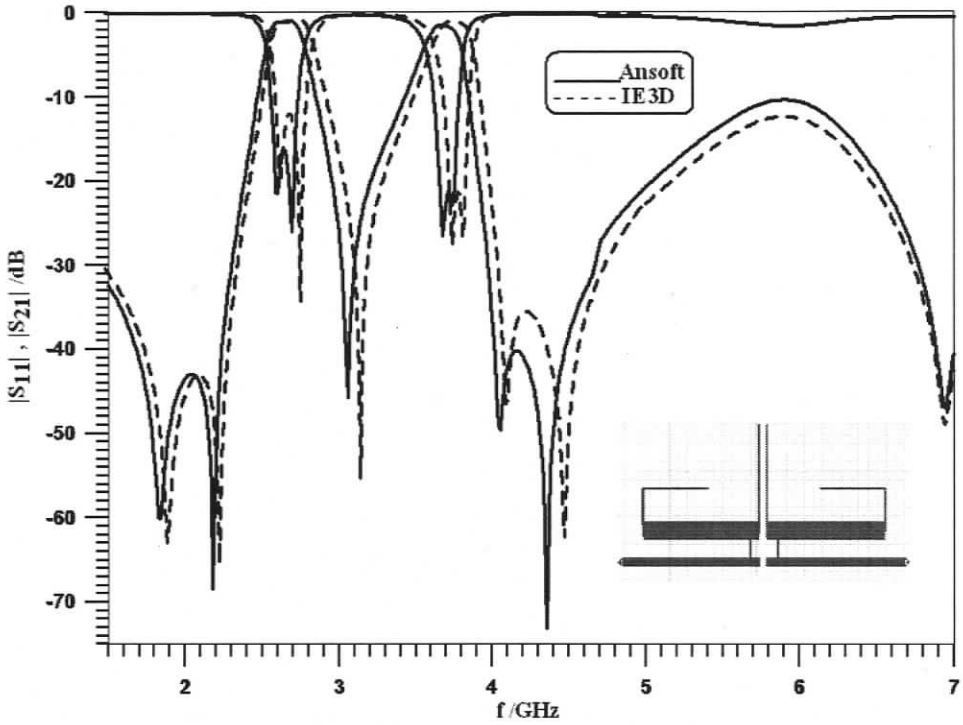

Fig. 5.16 Response of the new dual-band comb-line filter with capacitive source/load coupling according to Fig. 5.13c.

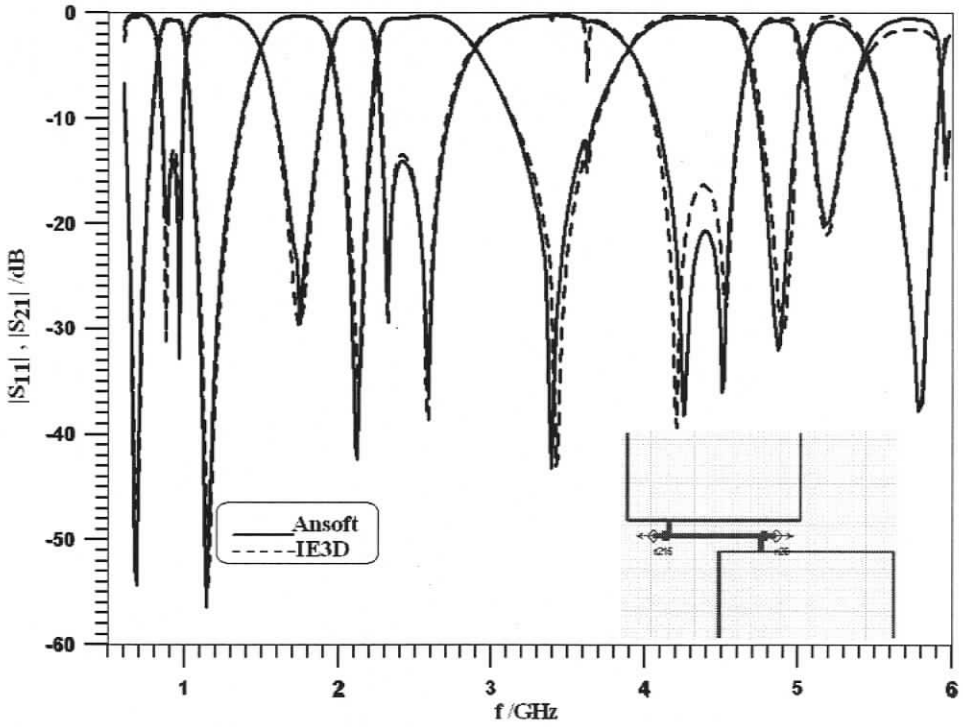

Fig. 5.17 Response of the new cascaded/ladder multi-band filter configuration according to Fig. 5.14a.

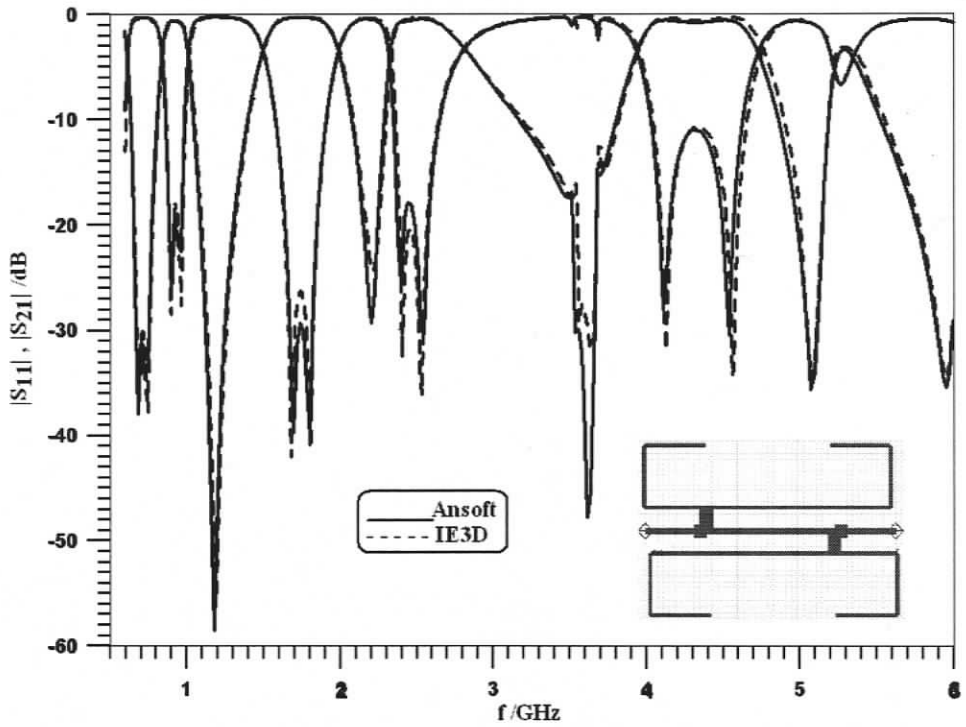

Fig. 5.18 Response of the new cascaded/ladder multi-band filter configuration according to Fig. 5.14b.

The examples in Fig. 5.17 and Fig. 5.18 show the performances of multiple-band filters with the cascaded ladder configurations in Fig. 5.14 on RT6006 substrate. The center frequencies are located at 0.925 GHz, 1.8 GHz and 2.4 GHz with 100 MHz, 100 MHz and 250 MHz bandwidths (-20dB), respectively.

The main advantage of these configurations is that they are capable of creating multiple passbands at desired center frequencies, which are suitable for wireless applications. Other advantages include small size, low cost and high efficiency. Note that both structures create four passbands between 0.5 GHz and 5 GHz. Compared to the dual-band filters in Figs. 5.6, 5.15, 5.16, the third passband is determined by the main line spacing between the feed points to the individual filters and, therefore, can be controlled. The fourth and fifth passbands appear as harmonics of the first and second ones, respectively.

5.5 Advanced Quasi-Elliptic Dual-Band Stepped-Impedance Filters

This section discusses advanced quasi-elliptic dual-band step-impedance filters. The number and location of attenuation poles as well as bandwidths of such quasi-elliptic dual-band filters are determined according to new compact SIR structures and coupling schemes, which vary in topology for narrowband to wideband applications. Moreover, implementation of source-load coupling generates additional transmission zeros.

5.5.1 Design Strategy

Fig. 5.19 depicts the progressive conversion of a conventional step-impedance resonator. In the folded SIR version (Fig. 5.19b), both high- and low-impedance segments are converted into two parallel sections, whose impedances are twice of those in Fig. 5.19a. The open-ended high-impedance segments on the sides in Fig. 5.19b attain tighter coupling between adjacent coupled resonators in order to approach extended bandwidth. Moreover, they contribute to a size reduction of the final filter structure.

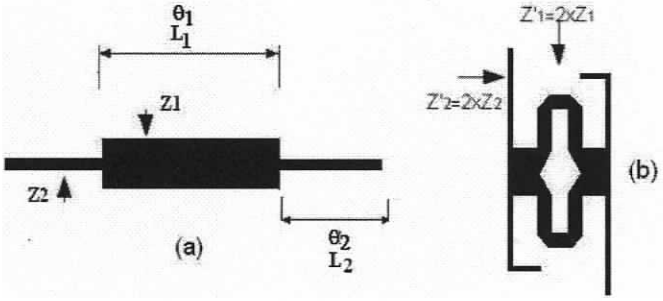

Fig. 5.19 Progressive conversion of SIR configuration.

Fig. 5.20 shows proposed open-ended coupling configurations between resonators and input/ouput and the equivalent impedance inverter circuit. Figs. 5.20a and 5.20b-c illustrate the coupling schemes implemented in narrow- to wide-bandwidth dual-band filters, respectively. Figs. 5.20b-c are similar to the coupled segments employed in ultra-wideband (UWB) filter design, e.g. [138], [140], and are capable of producing an additional reflection zero (pole) within the band. Note that the UWB designs in [138], [140] use two coupling sections, one each to the input and output, and, therefore, create two reflection zeros. The coupling configurations in Fig. 5.20b – Fig. 5.20e show a coupling section linking two step-impedance resonators. Hence they generate one reflection zero, and the open-ended stubs in Fig. 5.20c-d produce one transmission

zero each between passbands.

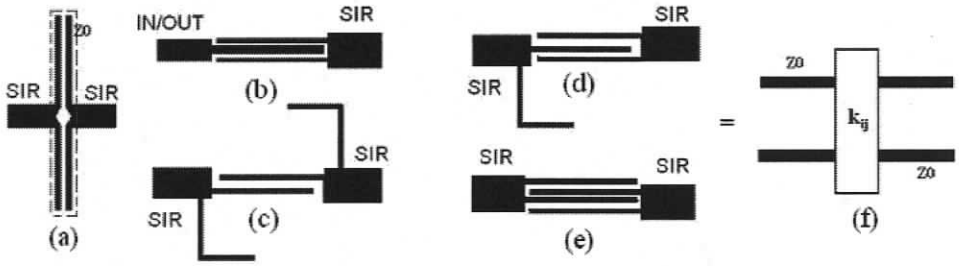

Fig. 5.20 Proposed open-ended coupling configurations of SIRs: (a) narrow bandwidth employment; (b,c,d,e) wide bandwidth employment; (f) equivalent impedance inverter circuit.

Narrow dual-band filters are generally synthesized via a coupling matrix at the center frequency of the first passband (f_1) and the desired bandwidth (Δf). Due to the capacitive coupling characteristics of the open-ended high-impedance coupling topology in Fig. 5.20a and the theoretically frequency-independent feature of the coupling matrix elements for narrow bandwidth, the achieved coupling coefficients are assumed approximately constant for the second passband as well. In other words, the same coupling matrix is utilized to represent both passbands.

On the other hand, the aforementioned feature of frequency independence varies for the coupling configurations in Figs. 5.20b-e due to the inductive coupling characteristics. In this case, dual-band filters are synthesized in the same procedures as UWB designs. In general, coupling is frequency dependent over a wide frequency range. Therefore, the coupling matrix concept cannot be applied to wide dual-band filter designs. Furthermore, the coupling segments in Figs. 5.20c-e represent not only a coupling component but also an additional resonator within the passband. Hence, the number of coupled-line segments shown in Figs. 5.20c-e increases the order of the filter due to the additional generation of reflection zero in each passband, which provides extended bandwidth.

To isolate both bands, at least one attenuation pole must be produced and located between passbands. The coupled-line section in Fig. 5.20a and the folded open-ended high-impedance transmission line in Figs. 5.20c-d can generate attenuation poles between passbands if the

electrical length θ_2 is selected as a quarter-wavelength at the overall center frequency, which is the arithmetic mean of the center frequencies of both passbands. The length of the low-impedance segment θ_1 in a basic SIR and the appropriate impedance ratio R_Z can then be read from the graph in Fig. 5.2.

Fig. 5.21 shows three dual-band filter structures using three cascaded SIRs for narrow bandwidth applications. Fig. 5.21a depicts the standard center section of an SIR (c.f. Fig. 5.19a) whereas in Fig. 5.21b and Fig. 5.21c, the folded resonator in Fig. 5.19b is utilized which reduces the sizes of those filters to about 60 percent of that in Fig. 5.20a. Fig. 5.21c also shows source/load (input-output) coupling to introduce attenuation poles in the leftmost and rightmost stopbands of the dual-band filter.

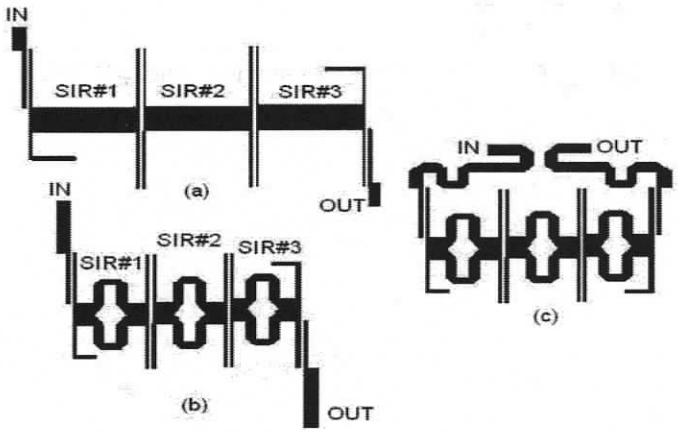

Fig. 5.21 Dual-band filter structures with three cascaded SIRs for narrow bandwidth applications; coupling according to Fig. 5.20a; (a) parallel open-ended high-impedance sections only; (b) additional parallel low-impedance sections; (c) including source-load coupling.

As an example, consider the SIRs shown in Fig. 5.21a and Fig. 5.21b. Let us assume a design example of a dual-band filter design with center frequencies at f_1=2.3 GHz and f_2=3.9 GHz so that f_2/f_1=1.7. The graph in Fig. 5.2 demonstrates that several length ratios, indicated as A to D, can be extracted in terms of two different impedance ratios (R_z=1.55 and R_z=3.5). The higher impedance ratio requires either wider low-impedance or narrower high-impedance segments, which means a larger structure of an SIR as well as rough and intricate fabrication. Therefore, the length ratios indicated as A and D in Fig. 5.2 are eliminated. The frequency ratios

of the second and third higher resonance frequencies to the fundamental mode (f_3/f_1 and f_4/f_1) are the key components to select an appropriate solution for the length ratio (U), since they ultimately lead to a filter response with extended upper rejection band.

As indicated in Fig. 5.2, the ratio of the second harmonic frequency to the fundamental mode (f_3/f_1) is 2.1 and 2.6 and the ratio of the third harmonic frequency (f_4/f_1) is equal to 3.25 and 3.5 for points B and C, respectively. Consequently, point C (U=0.67, R_Z=1.55) in Fig. 5.2 is the best solution. The substrate is selected as RT6010 with relative permittivity ε_r=10.2 and substrate thickness h=0.635mm. The length of the high-impedance coupling segment is a quarter-wavelength (≈ 9.2 mm) at $f_0 = \sqrt{f_1 f_2} = 3.0\,\text{GHz}$. Therefore, the length of the low-impedance segment of the SIR can be calculated through the specified length ratio (U=0.67) in Fig. 5.2. The impedance characteristic of the high-impedance segment (Z_2) of the basic SIR is selected as 40 Ω for all filter structures so that parallel high-impedance segments in Fig. 5.19b are at 80 Ω. The respective value of the low-impedance segment (Z_1) of the SIR is calculated by the specified impedance ratio (R_Z=1.55) such that Z_1=26 Ω.

Let us further assume that the 10dB bandwidths of the dual-band filter be 300 MHz in each passband. Three-cascaded single-element SIRs depicted in Fig. 5.21a and Fig. 5.21b are used to cover the dual-band filter specifications, including the desired bandwidth in each passband and a high isolation between bands. The normalized coupling matrix of the three-pole filter is

$$M = \begin{bmatrix} 0 & 1.035 & 0 & 0 & 0 \\ 1.035 & 0 & 0.947 & 0 & 0 \\ 0 & 0.947 & 0 & 0.947 & 0 \\ 0 & 0 & 0.947 & 0 & 1.035 \\ 0 & 0 & 0 & 1.035 & 0 \end{bmatrix} \tag{5.10}$$

Finally, the gaps between the open-ended coupled-line sections and the input/output paths are determined by matching the actual coupling elements with those of the coupling matrix for the desired bandwidth and center frequency according to equations (5.8) and (5.9). The gap between individual coupled line sections is varied using the closed-form expressions in, equations (4.3)-

(4.5) until a coupling value is obtained which equals the respective entry in the coupling matrix.

In our experience, fine-tuning of about five to ten percent of the synthesized dimensions might have to be applied to adjust all interactions between the elements involved. Thus the initial design is sufficient to employ standard optimization techniques or trial-and-error procedures on the coupled-line sections. Note that as long as the individual passbands are narrow, this design approach (in terms of coupling matrix and appropriate selection of impedance ratios) can be employed for any dual-band filter and is not limited to applications where the two passbands are close to each other. For wide-bandwidth applications, however, the design is approximately restricted to dual-band filters with nearby passbands. This is due to the coupling segments and the equal-length open stubs, which sufficiently represent reflection, and transmission zeros only near the center frequency.

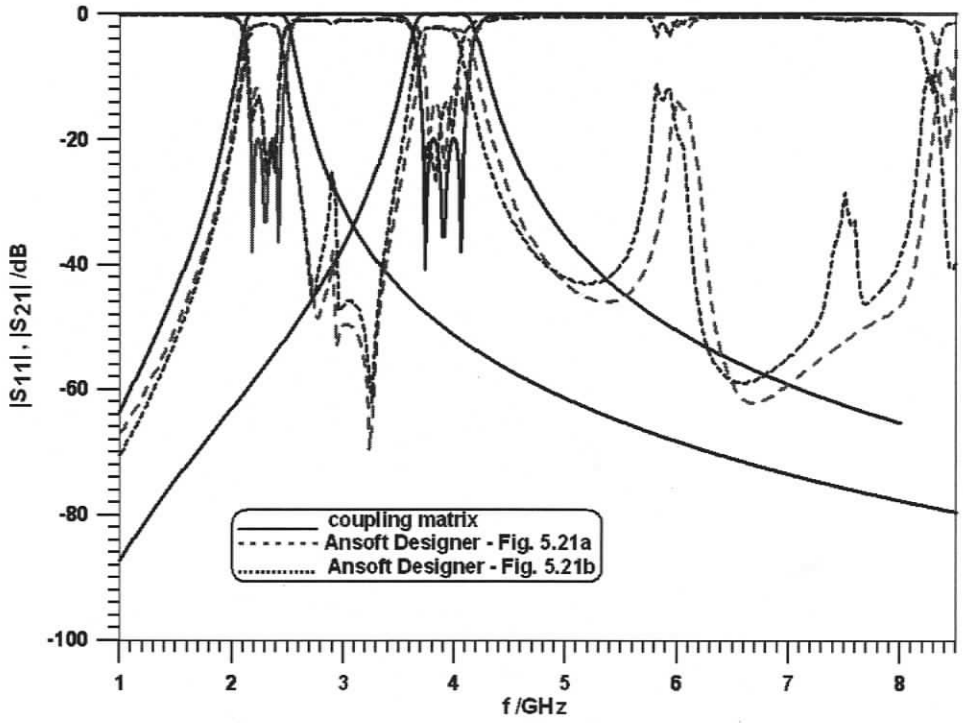

Fig. 5.22 Performance of the dual-band filter structures of Fig. 5.21a (dashed lines) and Fig. 5.21b (dotted lines) with those obtained from the individual coupling matrices (solid lines).

Fig. 5.22 shows the comparison of the performances of the actual dual-band filters in Fig. 5.21a and Fig. 5.21b with the performance of the coupling matrix of equation (5.10) in each passband. The simulation results agree with the theoretical response of the coupling matrix within each passband. The computed insertion loss is less than 2dB, and the return loss is better than 10dB in each passband. The simulated 10dB bandwidths are 300MHz and 350 MHz for the first and second passbands, respectively. The additional bandwidth on the second passband is due to the frequency-dependence of the coupled-line sections in the filter structure, which is ignored in the dual-band filter synthesis. Three transmission zeros at 2.75 GHz, 3 GHz and 3.25 GHz are generated between the passbands due to the coupled quarter-wavelength open-ended high-impedance segments. The resonance peaks at 6 GHz and 8.4 GHz are due to the second and third harmonics of the folded SIR (f_3 and f_4) as indicated in Fig. 5.2. The spurious passband at 7.6 GHz of the filter structure in Fig. 5.21b, which is below -27dB, exists for all filter structures designed by the new folded low-impedance SIR configuration (see also next section) and is attributed to coupling between the high-impedance and the folded low-impedance segments in the structure shown in Fig. 5.19b. This is evidenced, e.g., by comparing Fig. 5.23 with Fig. 5.24a. The filter in Fig. 5.23 uses straight, instead of folded low-impedance sections and, therefore, the peak at 7.6 GHz disappears. Hence, this peak appears to be a direct consequence of miniaturization.

5.5.2 Design Performance

This section presents some examples of dual-band filters, which have been synthesized, fabricated and measured. The results of both narrowband and wideband prototypes verify the design process described above.

5.5.2.1 Dual-Band Filters for Narrowband Applications

Fig. 5.23 and Fig. 5.24a confirm the performance of the dual-band filter configurations in Fig. 5.21a and Fig. 5.21b, respectively. General agreement is observed between simulations and measurements. However, in both figures (as well as all following ones), a shift of the measured response towards lower frequencies occurs. Fig. 5.23b displays the comparison and good agreement between measurements and Ansoft simulation performance upon inspection of the

actual dimensions of the filter prototype in the inset of Fig. 5.23a by a precision microscope.

A tolerance analysis in Fig. 5.24b shows that the aformentioned shift is mainly attributed to the fabrication of the coupling slots. With slot widths on the order of 100 μm and fabrication tolerances of up to +/-25μm, under-etching significantly moves the measured filter response towards lower frequencies. In addition, the dielectric constant tolerance on the order of +5 percent of the utilized substrate is considered in the tolerance analysis in Fig. 24b, which demonstrates better performance matching with measurement data. This is a disadvantage of the proposed coupling schemes but is common to most planar filter structures requiring tight coupling for UWB or multi-band operation.

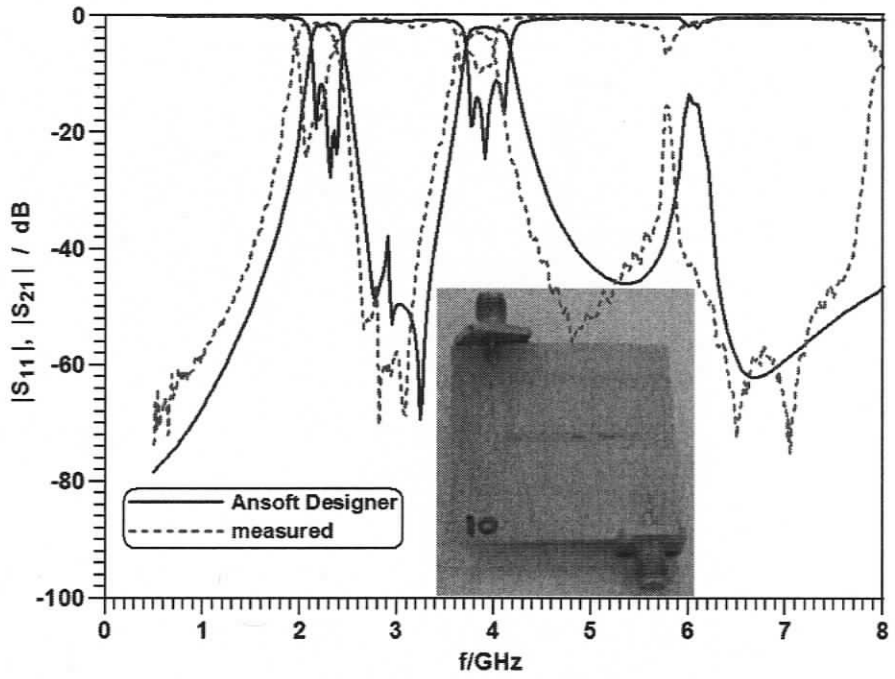

(a)

Fig. 5.23 (a) Simulated and measured performances of a dual-band filter using a three-cascaded SIR configuration according to Fig. 5.21a and (b) comparison between measurement data and simulation of the actual dimensions of the filter prototype.

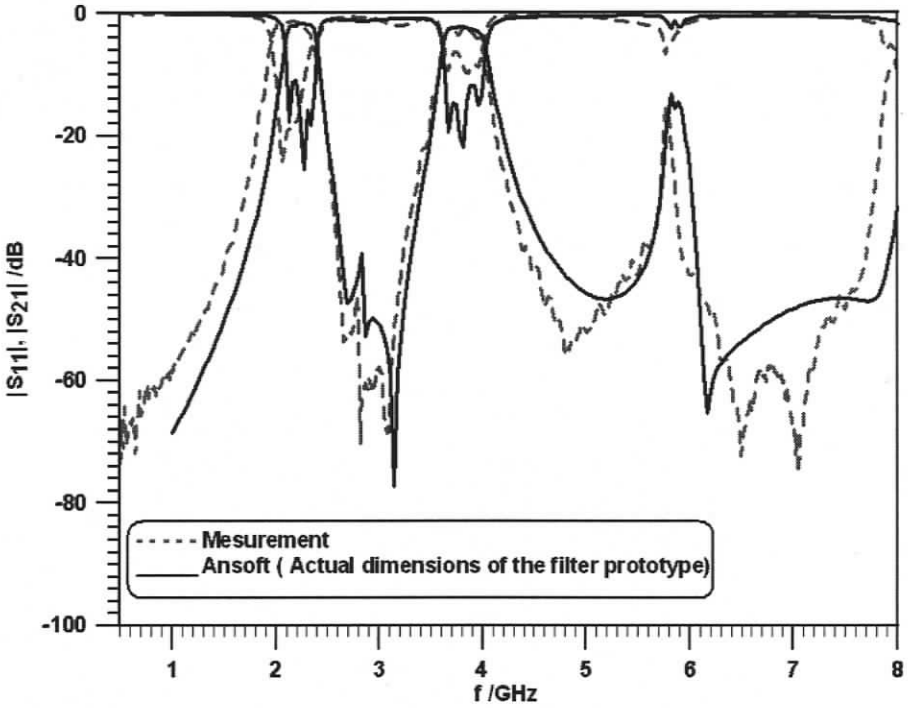

(b)

Fig. 5.23 Continued.

Moreover, in cascaded arrangements, where the high-impedance lines branch off as shown in Fig. 5.20a, two wider-line sections are fairly close to each other and produce small but unwanted coupling. This is the main cause for the spurious response between the two passbands in Fig. 5.23 and Fig. 5.24a. To a lesser degree, this coupling is also present in Fig. 5.25, but it vanishes for the structures in Fig. 5.26 to Fig. 5.31, which employ different coupling schemes between the SIRs. A size comparison between the two filters in Fig. 5.23 and Fig. 5.24a shows that the structure in Fig. 5.24a (19 x 20 mm^2) occupies only 60 percent of the substrate area compared to that of Fig. 5.23.

The dual-band filters in these examples exhibit multiple attenuation poles between the two passbands. With respect to the design theory, however, attenuation poles in the lower and/or upper rejection bands are not considered (although a number of attenuation poles appear in the upper bands of the measurements and are attributed to the measurement setup). Source-load coupling is capable of generating additional attenuation poles in the upper and lower stopband

regions. The location of such poles is primarily dependent on the value and type (capacitive or inductive) of the source-load coupling. Due to unavailable coupling topologies for multi-harmonics elements such as step-impedance resonators, the number of poles generated by source-load coupling is as yet unpredictable.

Fig. 5.25 shows the performance of the dual-band filter of Fig. 5.24 when source-load coupling is employed (c.f. Fig. 5.21c). Two transmission zeros on the left side of the first passband (at 0.7 GHz and 1.65 GHz) and seven transmission zeros on the right side of the second passband - at 4.25 GHz, 5.2 GHz, 5.9 GHz, 6.1 GHz, 6.6 GHz, 7.5 GHz and 7.6 GHz - are apparently generated by the source-load coupling. The number of attenuation poles appearing in the lower rejection band does not necessarily change with additional resonators; however, source-load coupling eventually increases the number of attenuation poles in the upper stopband and thus significantly improves the rejection in this frequency range. Although the dimensions of the dual-band filter in Fig. 5.24 remain unchanged in Fig. 5.25, except for the additional source-load coupling, the latter has also a minor impact on the locations of the multiple poles between the passbands.

A comparison between Fig. 5.25 and Fig. 5.24 confirms the sharp selectivity of each passband by allocating attenuation poles in the lower/upper stopbands through source-load coupling. The source/load coupling also adjusts the poles between the bands and moves them slightly outwards, which increases the selectivity of each passband. Due to the additional path between source and load, the general (across the frequency range) attenuation level in Fig. 5.25 is lower than that in Fig. 5.24.

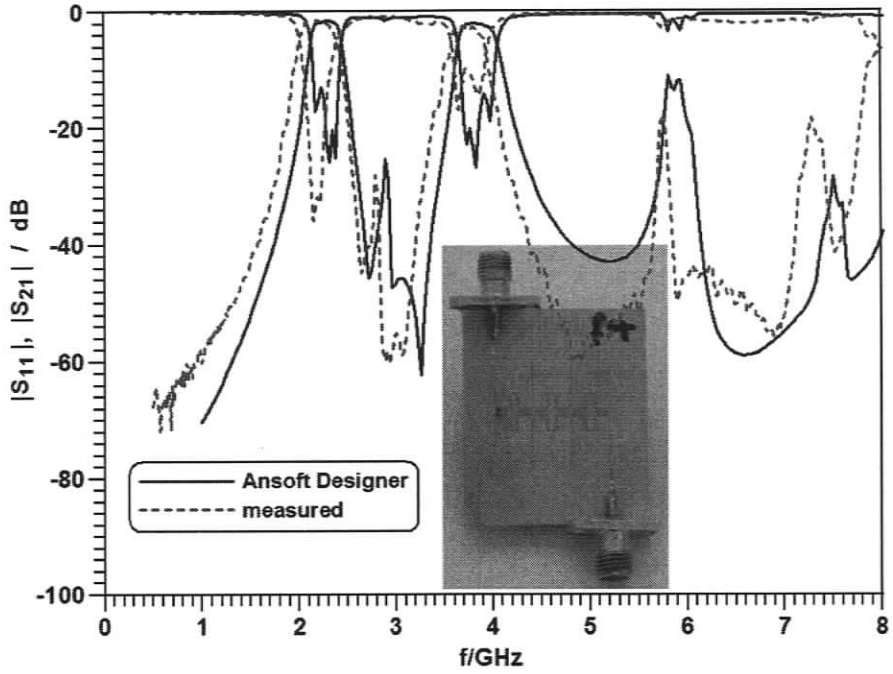

(a)

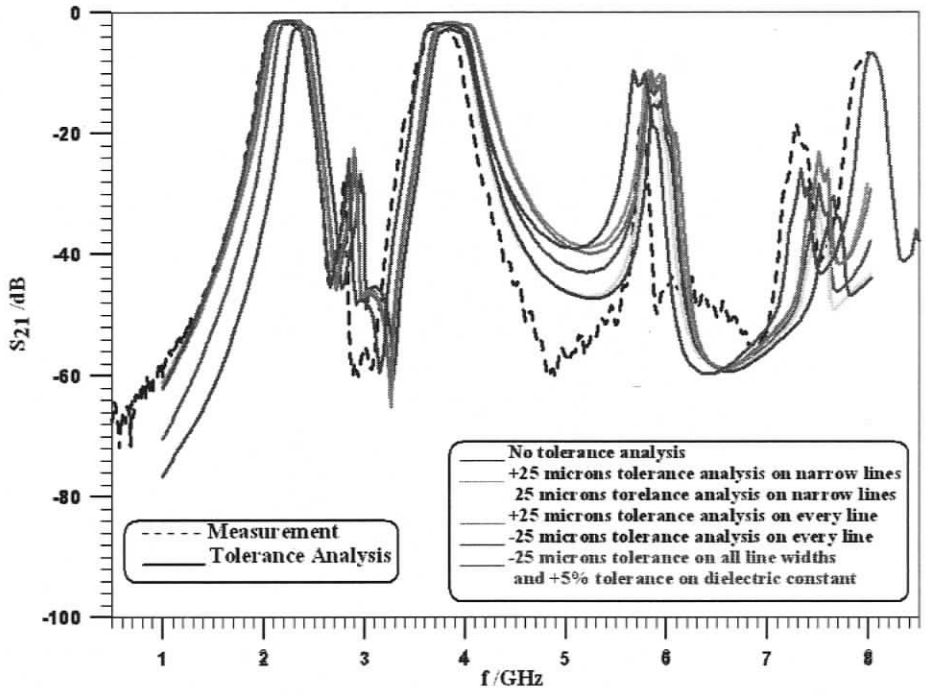

(b)

Fig. 5.24 (a) Simulated and measured performances of a dual-band filter using a three-cascaded SIR configuration according to Fig. 5.21b and (b) tolerance analysis on coupling slots and transmission line widths up to +/- 25 μm and +5% dielectric constant of the utilized substrate.

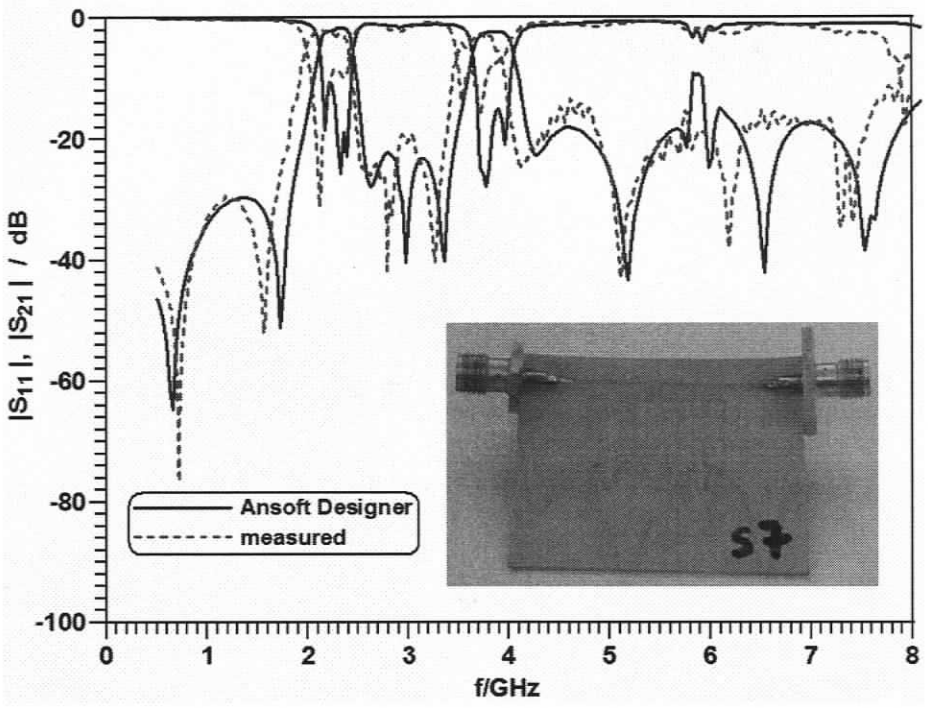

Fig. 5.25 Simulated and measured performances of the source-load coupled version of the dual-band filter in Fig. 5.24.

5.5.2.2 Dual-Band Filters for Wideband Applications

The dual-band filter design for wideband applications is mainly based on the design of UWB filters [138], [140]. The coupling configuration in Fig. 5.20c can generate two attenuation poles within an ultra-wide bandwidth due to the folded high-impedance segments, whose lengths are a quarter-wavelength at center frequency f_0. The design procedure is the same as that demonstrated in the previous section for narrow dual-band filters, but it considers the additional reflection zero in each band due to the fact that the quarter-wavelength coupled-line section acts as an extra resonator [138]. Thus the filter shown in the inset of Fig. 5.26 creates one reflection zero in each passband, which are due to the center coupled line section (one reflection zero) and those at the input and output (one double reflection zero). Since these sections must be similar in length in order to operate in both frequency bands, the two passbands for such designs must be close together - as already mentioned in the previous section. The proposed input/output-coupling segment in Fig. 5.20b also eliminates the required tight coupling in traditional UWB filters and reduces high-precision fabrication requirements due to wider coupling slots.

Fig. 5.26 shows the simulated and measured performances of a three-pole dual-band filter using two SIRs and quarter-wavelength coupled-line sections as resonators. The circuit depicted in the inset of Fig. 5.26 is fabricated on RT6010 substrate material of height h=0.635mm. The center frequencies of the first and second passbands are assumed to be f_1=2.2 GHz, f_2=3.5 GHz (f_2/f_1=1.6) with a 10 dB bandwidth of 600 MHz. However, as mentioned earlier the bandwidth in the upper band is increased to 700 MHz by the frequency dependence of the coupling coefficients. The center frequency of the entire filter is located at f_0=2.78 GHz, which specifies the physical lengths of the high-impedance coupling segment to be a quarter-wavelength. The length and impedance ratios of the resonators employed in the filter structure are determined based on the graphs in Fig. 5.2.

Good agreement is observed between simulations and measurement. The insertion loss is less than 2 dB and the return loss is better than 10 dB in both bands. The slight frequency shift in the measured results is due to fabrication tolerances as explained earlier in this section. The spurious bands at 5.8 GHz and 7.8 GHz represent the second and third harmonic modes of the employed SIRs, respectively, which - for this design - is the maximum possible distance from the second band due to the length and impedance ratios in Fig. 5.2.

For the wide dual-band filter in the previous example, the rejection beyond the second passband is relatively low due to the third harmonic resonances. Therefore, attenuation poles are required in this frequency range in order to create a sharp skirt. This can be achieved through source-load coupling which is capable of generating such poles in both the lower and upper rejection bands. The locations of the attenuation poles can be changed by the source-load coupling coefficient.

Fig. 5.27 shows the performance of the dual-band filter in Fig. 5.26 with added magnetic source-load coupling. A number of attenuation poles are produced at 1 GHz, 1.5 GHz, 4.5 GHz, 5 GHz and 6.5 GHz, which contribute to sharper selectivity in both bands. Moreover, source-load coupling separates the double attenuation pole at 3 GHz in Fig. 5.26 and moves them slightly outward such that two attenuation poles appear between the passbands in Fig. 5.27.

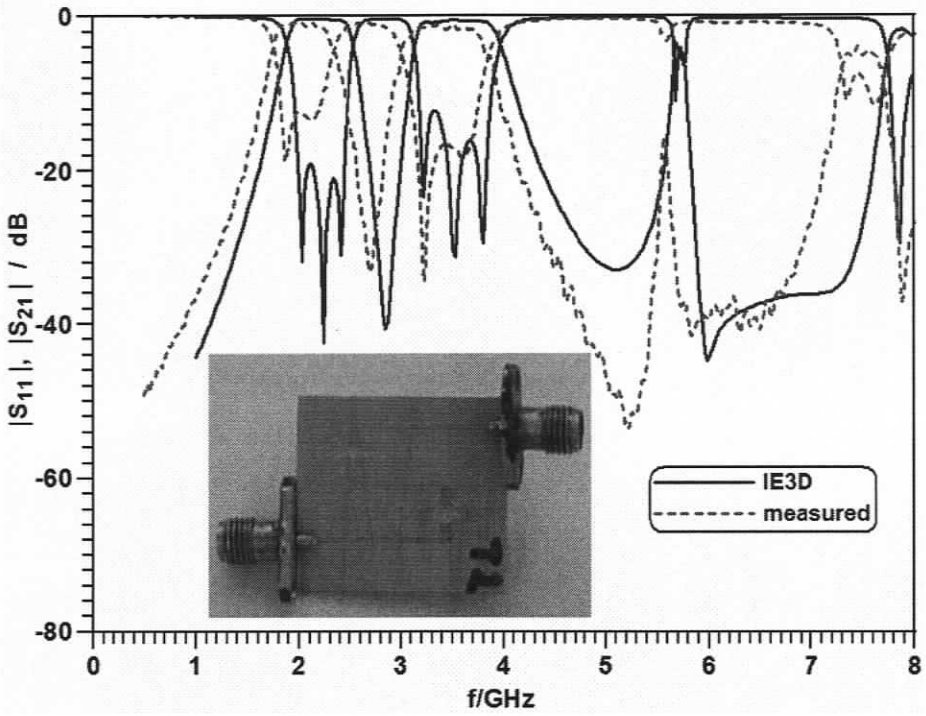

Fig. 5.26 Simulated and measured performances of a three-pole dual-band filter using the two cascaded SIRs from Fig. 5.19b and a coupled-line segment from Fig. 5.20b.

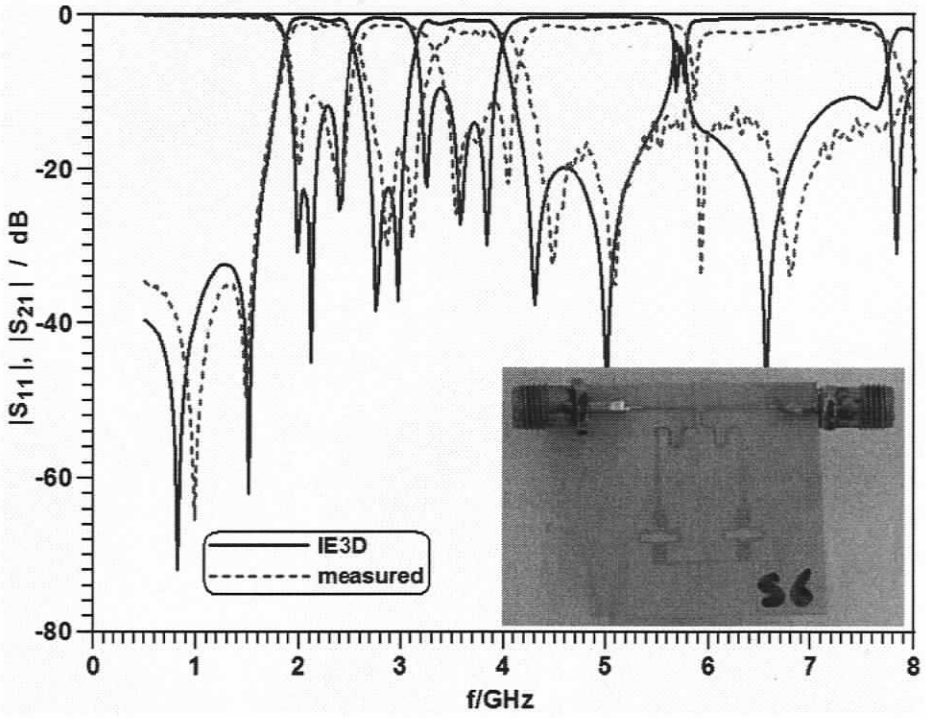

Fig. 5.27 Simulated and measured performances of the source-load-coupled version of the dual-band filter in Fig. 5.26.

In order to demonstrate the flexibility of the wide dual-band filter design approach, another dual-band filter on a different substrate material (RT6010) and the same height as the former examples is designed at a higher midband frequency (f_0=7 GHz). The filter structure as well as the performance obtained from measurements and simulations are depicted in Fig. 5.28. The centre frequencies of the first and second bands were specified as f_1=5.25 GHz and f_2=8.85 GHz ($f_2/f_1 \approx 1.7$) with 22 percent (1.5 GHz) bandwidth in each band. Note that two attenuation poles at 6.8 GHz and 7 GHz in the measurement replace the double attenuation pole between the passbands in the computations. This is due to the areas between the low-impedance segments of the SIRs (c.f. Fig. 5.19b), which have been manually enlarged due to an error in the prototyping process.

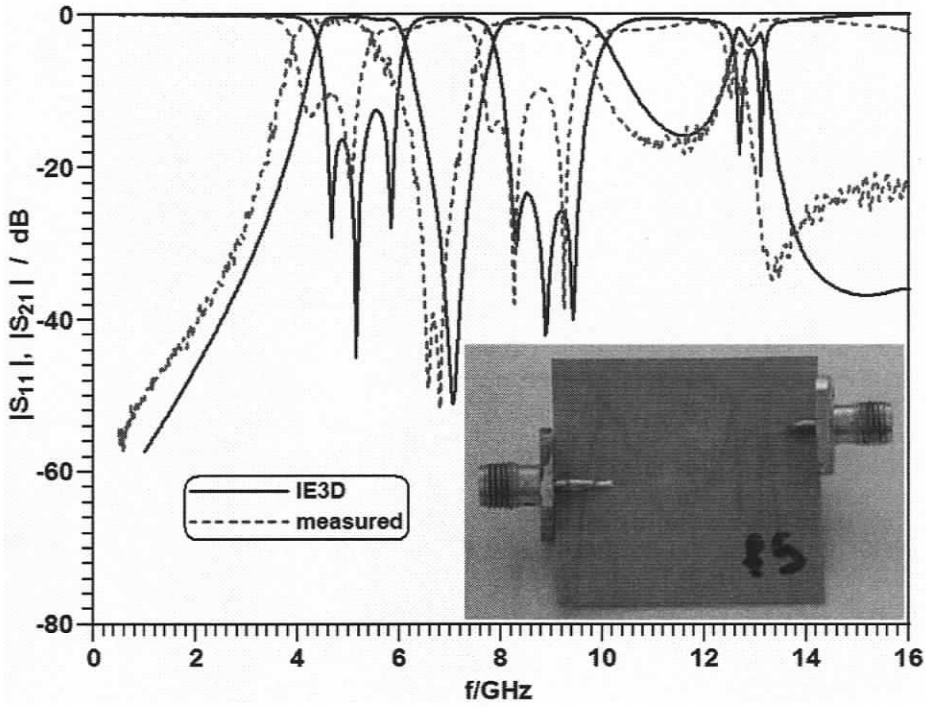

Fig. 5.28 Simulated and measured performances of a three-pole dual-band filter using two cascaded SIRs of Fig. 5.19b and coupled-line sections of Fig. 5.20c for f_0=7 GHz.

In order to extend the fractional bandwidth in each passband, more resonators are required. A four-pole dual band filter prototype with three cascaded SIRs is shown in the inset of Fig. 5.29. It uses RT6006 substrate with h=0.635mm. The design specifications are: f_1=4.86 GHz, f_2=9.15 GHz ($f_2/f_1 \approx 1.9$), and a 3 dB bandwidth of 2 GHz (42 percent). Fig. 5.29 shows the simulated performance. To allocate the two resonances of the third (middle) SIR within the two

passbands, different impedance and length ratios are selected for this resonator. Otherwise, the use of the same SIR as the first and last resonators would create reflection zeros too close to the rejection band between the passbands.

Source-load coupling is also implemented for the dual-band filter topology in Fig. 5.29. In comparison, Fig. 5.30 confirms additional attenuation poles at 1.2 GHz, 3.2 GHz, 11.4 GHz and 12.6 GHz. It is again observed that source-load coupling moves the attenuation poles between the bands slightly outward to 6.6 GHz and 7.5GHz compared to 6.8 GHz and 7.2 GHz in Fig. 5.29, which leads to higher selectivity for each passband. Source-load coupling improves selectivity for each passband and creates sharp skirts in both the lower and upper suppression regions.

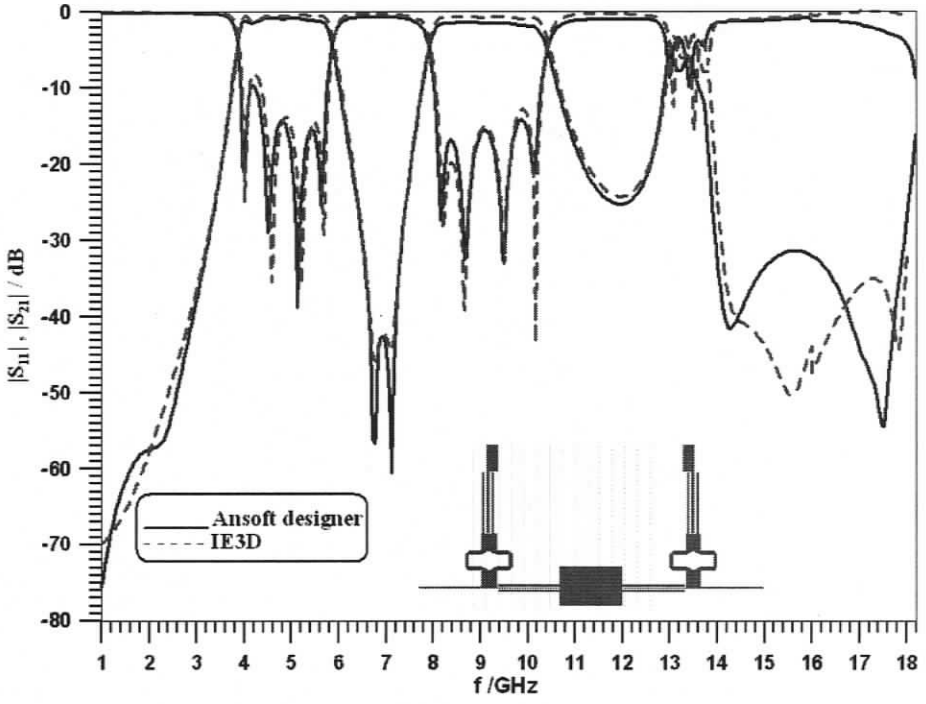

Fig. 5.29 Simulated performances of a four-pole, three-SIR dual-band filter (f_0=7 GHz) using SIRs of Fig. 5.19 and coupled-line segments of Figs. 5.20b, d.

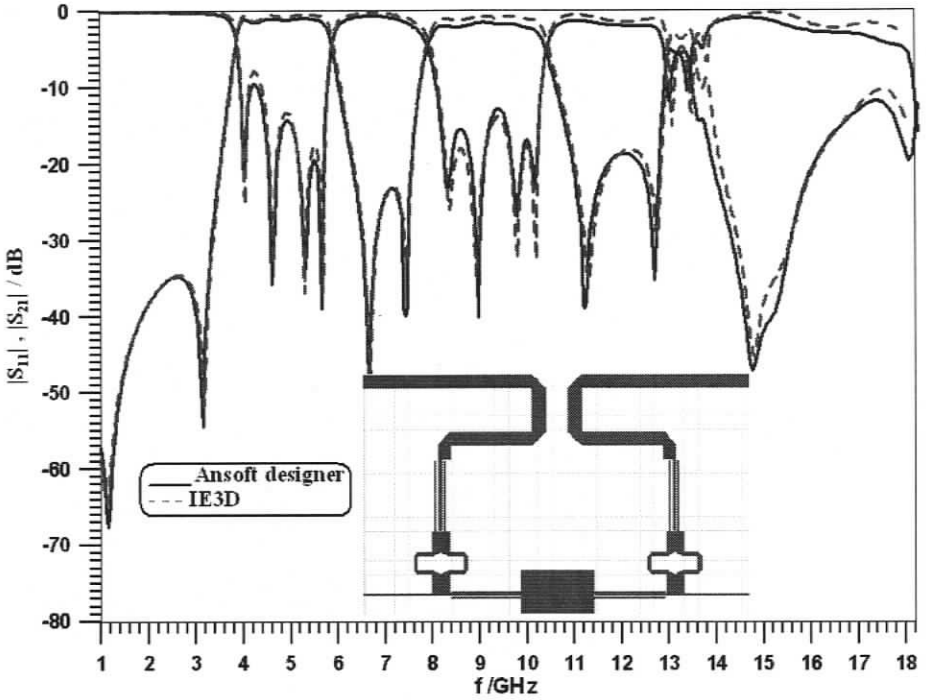

Fig. 5.30 Response of the source-load-coupled version of the dual-band filter presented in Fig. 5.29.

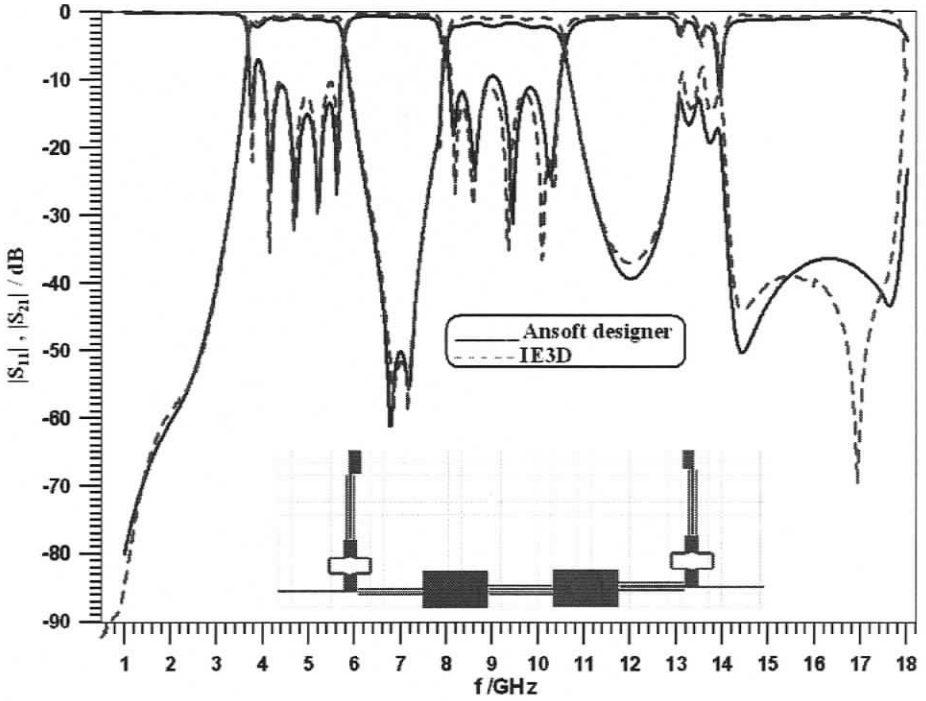

Fig. 5.31 Simulated performance of a five-pole, four-SIR dual-band filter (f_0=7GHz,) using SIRs of Fig. 5.19, and coupled-line sections of Figs. 5.20b, d, e.

A five-pole dual-band filter approaching 48 percent fractional bandwidth including four cascaded SIRs can be set up as shown in the inset of Fig. 5.31. The center frequencies are

selected at f_1=4.7 GHz and f_2=9.2 GHz ($f_2/f_1 \approx 1.95$). The simulated performances, as depicted in Fig. 5.31, confirm 3 dB bandwidths of 2.1 GHz and 2.3 GHz. The insertion loss is less than 2 dB, and the return loss is better than 10 dB. The substrate used for this filter prototype is RT6006 with h=0.635mm.

5.6 Summary

The proposed compact configurations of step-impedance resonators (SIRs) with or without folded high- and low-impedance segments and open-ended coupled-line section are excellent candidates for narrow and wide dual-band filter applications in wireless communication systems. The wideband design approach is primarily based on UWB filter designs, but folded quarter-wavelength open-ended high-impedance segments generate attenuation poles in the UWB passband to create two highly isolated bands. Enhanced coupling elements provide larger bandwidths, and resonator folding reduces occupied substrate area.

The narrow dual-band filter design is based on the synthesis of the coupling matrix, which is assumed to be valid for both bands. Parallel quarter-wavelength open-ended electric-coupling segments provide not only the required couplings for both bands but also produce the attenuation poles to isolate the two passbands.

In all design approaches, the next (spurious) resonances of the SIRs should be moved as far as possible towards higher frequencies in order to widen the stopband between the upper passband and the next harmonic band or to generate multi-passband performance. Moreover, source-load coupling can be applied to both dual-band design approaches. Its effect is to distribute a number of attenuation poles in the lower/upper rejection bands and, additionally, move the attenuation poles between the passbands slightly outwards. This is reflected in sharp passband skirts as well as extended upper stopbands. The simplicity and flexibility of the design approaches are demonstrated at various examples covering different substrate materials and frequency bands. The main advantages of the proposed dual-band filter design approaches are the ease of fabrication, compact size, low cost and advanced performance. The measured results of six prototyped dual-band filters show good agreement with simulations and thus verify the design approach.

CHAPTER 6

Compact Ultra-Wideband Filters in Microstrip Technology

6.1 Introduction

Since the introduction of unlicensed use of ultra-wideband (UWB) technology in the 3.1 - 10.6 GHz range, the realization of low cost UWB wireless systems has been considered a fundamental research topic for both military and commercial applications [36]. In this context, the characterization, design and fabrication of passband filters covering the entire UWB frequency range are challenging tasks [38]. Their specifications include high-performance electrical responses but, at the same time, they must be mass-producible at low cost and small size. In order to avoid distortions of the signal, it is essential to maintain filter linearity (amplitude and group delay) within the passband and good selectivity and suppression in the stopband.

Parallel-coupled transmission lines for ultra-broadband microstrip passband filters with bandwidths up to 70 percent are presented in [148], [149]. However, the filter size is not compact, and the design lacks transmission zeros to increase selectivity. A similar technique is used in [150], [138] and includes impedance steps and coupled-line sections as inverter circuits. The bandwidths of these structures are around 50 and 110 percent, respectively. A similar version in coplanar waveguide technology [151] achieves 104 percent bandwidth. While these latest results are excellent, the number of possible transmission zeros, as required for high selectivity filters, is very limited as is the stopband attenuation towards higher frequencies. Ring resonators with additional stubs are introduced in [39]. Control of the attenuation pole frequency is achieved by adjusting both the ring and stub impedances. In order to increase the bandwidth and number of transmission zeros, multi-stage resonator arrangements are required, which increases component

size. Dual-mode stopband ring resonators with two tuning stubs are used in [152] to construct a wide passband with two sharp stopbands. Due to the characteristics of the bandstop resonators, however, this filter has additional passbands to the left and right of the stopbands. A compact ultra-wideband LTCC filter employing four resonators and 1-to-4 cross coupling is introduced in [45]. However, the bandwidth is only 50 percent. Other ultra-wideband filters with similar characteristics and smaller bandwidths have been designed in coplanar waveguide [43], [153], substrate integrated waveguide [154] and microstrip technology [155]. A new ultra-wide band filter structure with more than 100 percent bandwidth and wide stop-band regions is introduced in [47]. It uses cascaded broadside-coupled microstrip-coplanar waveguide structures but requires an additional low-pass filter to suppress the spurious passband in the upper band region.

Recent UWB filter designs tend to focus on compactness for reasons of fabrication, cost and integration with other system boards [46], [47], [138], [140], [150], [151], [156]. Conventional configurations of the step-impedance resonator (SIR) require very small gaps between the coupled segments, hence high manufacturing accuracy and higher expenses [46], [47], [150], [151]. In addition, based on all investigations it is clear that the typical microstrip SIR, which is tightly coupled to the input/output lines, is capable of producing an UWB filter covering the 3.1-10.6 GHz frequency range; however, the attenuation on both sides of the passband is rather poor [138], [150]. Cascading multiple SIRs also features good performance in both passband and stopband regions, but the designs are rather long and spacious [139].

In the past few years, several planar filter configurations have been reported for UWB applications. However, few efforts have been made to reduce size, manufacturing cost and simultaneously enhance performance.

The first part of this Chapter focuses on modified approaches of the impedance-step, additional-stub and parallel coupled microstrip-line concept for the design of very compact broadband filters. Cross coupling is introduced to generate additional transmission zeros. Wide out-of-band rejection is obtained by controlling the number and positions of transmission zeros close to the lower and upper skirt of the passband. Ultra-wideband filter structures with improved

filter characteristics such as sharp selectivity and enhanced bandwidth are presented subsequently.

The fundamental purpose of this Chapter is to introduce SIRs, which facilitate stronger coupling between coupled segments. Thus the requirement of relatively small gaps in coupled-line sections is significantly reduced. Moreover, a new and compact SIR composed of parallel high-impedance and folded low impedance segments, which differs from those in [145], [146], is presented and applied to the design of UWB filters with and without source/load coupling. Measurements and/or commercially available field solvers verify all designs.

6.2 Theory

Fig. 6.1a shows a schematic view of the SIRs used for our practical designs. They include a structure with folded low-impedance (Z_1) and parallel high-impedance segments (Z_2). The main task in using a SIR is to control the harmonic resonance frequencies in terms of the impedance ratio (R_Z=Z_2/Z_1) as well as the electrical lengths, θ_1 and θ_2, of the low- and high-impedance segments, respectively. This usually done by solving two transcendental equations for the alternating odd- and even-mode resonances, e.g. equations (5.2) [140]. Fig. 6.1b shows the ratio of the higher-order resonance frequencies to that of the fundamental mode versus the ratio U of electrical lengths (c.f. Fig. 6.1a)

$$U = \frac{\theta_2}{\theta_1 + \theta_2} \tag{6.1}$$

and with impedance ratio R_Z as parameter.

In the synthesis of an ultra-wideband filter, the fundamental resonance and a proper number of harmonic resonances are required to be allocated within the passband. For instance, an ultra-wideband filter utilizing triple-mode SIRs is designed such that the center frequency of the filter is selected to be the first harmonic frequency, which is the arithmetic mean of the fundamental and second harmonic resonances, which are properly defined close to the edges of the passband. In order to cover a specific bandwidth, a number of SIRs should be cascaded and

the input/output connected by quarter-wavelength coupled-line sections at the center frequency (θ_2). Note that such sections act as inverters and can increase the order of the UWB filter by two, e.g. [138].The concept for UWB filter design is to match the resonant frequencies of the SIRs with the reflection zeros generated from a Chebyshev polynomial.

The other parameters of the SIRs can be determined by using the graph in Fig. 6.1b. The value of the electrical length and impedance ratios are selected such that other higher-order modes, which are not utilized in the passband of a UWB filter, are located as far as possible from the upper edge of the passband. For instance, the points labeled A_1, B_1, C_1 and D_1 in Fig. 1b show the locations of different electrical length ratios in terms of various impedance ratios for a specific passband filter design. If the first harmonic ratio placed within the passband is 1.7 for U=0.42 and R_Z=2.4 (A_1), points A_2, A_3 and A_4 represent the locations of the next harmonic frequencies. This procedure is identical to that presented in Chapter 5. However, more harmonics are considered here.

Using the first two higher-order modes in addition to the fundamental mode, the locations of points A_3 and A_4 for the fourth and fifth harmonic frequency ratios should have maximum distance from points A_1 and A_2 in order to create the largest band gap from the main passband. The larger this band gap, the broader is the upper-band suppression region and the fewer are the effects of those higher-order modes on the main passband performance.

6.3 Design Procedure

Let us first consider in Fig. 6.2a the layout of an ultra-wideband filter (similar to the one in [138]) including the centered transmission-line (TL) resonator with impedance steps and two sections of parallel-coupled microstrip lines (PCMLs), which act as admittance inverters (J). Fig. 6.2b depicts the equivalent circuit topology.

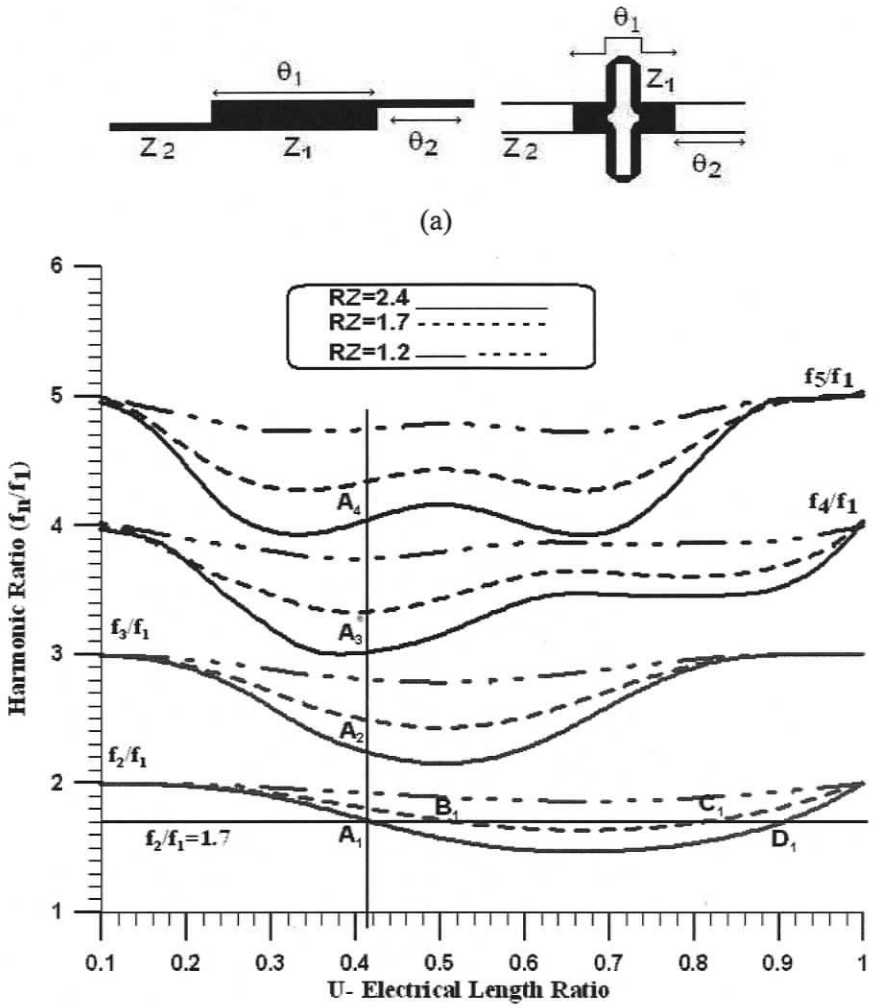

Fig. 6.1 Step-impedance resonator (SIRs) used in this chapter (a); and harmonic ratios of the SIRs in terms of electrical length and impedance ratios (b).

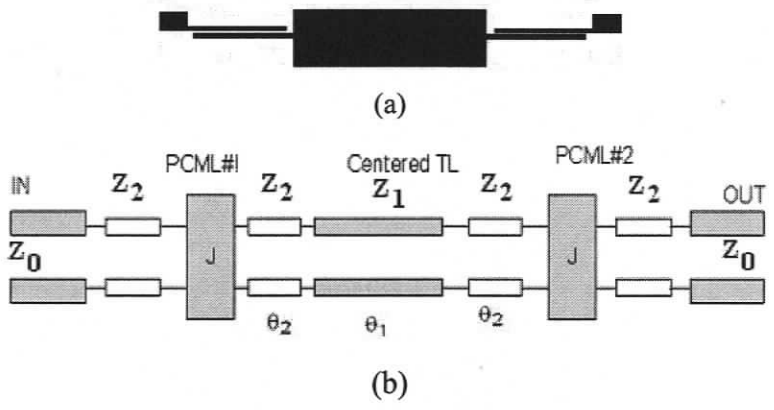

Fig. 6.2 Layout (a) of an ultra-wideband filter (similar to [138]) and equivalent circuit topology (b).

Using transmission-line theory, and under the simplified assumption that the impedance of the centered TL equals that of the input/output lines, the reflection coefficient can be formulated as a closed-form function

$$S_{11} = \frac{j(1-\bar{J}^4)\tan(\Phi)}{2\bar{J}^2 + j(1+\bar{J}^4)\tan(\Phi)} \tag{6.2}$$

where $\bar{J} = \frac{J}{Y_0}$ is the normalized inverter, and the total electrical length is

$$\Phi = \frac{\theta_2}{2} + \theta_1 + \frac{\theta_2}{2} \tag{6.3}$$

For a broadband filter design, we use the fundamental and the next two harmonic resonances of the stepped impedance resonator. The two PCMLs create two more in-band reflection zeros. Thus a broadband five-pole bandpass filter is created with a single line resonator.

The lengths of the PCML sections are a quarter wavelengths at center frequency with very tight coupling to create a broad passband. The centered transmission line is half a wavelength long with low characteristic impedance. After obtaining initial dimensions for given substrate height and permittivity, the design proceeds by adjusting the characteristic impedances and gaps in the PCMLs - towards tight coupling - and the characteristic impedance of the middle transmission line towards a low impedance profile. The resonant length is adjusted to compensate for the phase deviations introduced by the inverters.

In order to increase the bandwidth of this filter configuration, a new high impedance resonator is added according to Fig. 6.3. The additional resonator increases the bandwidth by up to ten percent and, at the same time, bypasses the triple-resonance stepped impedance resonator to generate up to three transmission zeros above the passband. The location of these transmission zeros can be used to improve the upper skirt of the filter and/or the suppression band towards higher frequencies. The length and impedance characteristic of the new resonator may be defined such that it is tightly coupled and adds a reflection zero in the lower passband.

Fig. 6.3 Modified ultra-wideband filter configuration with cross coupling/additional resonator.

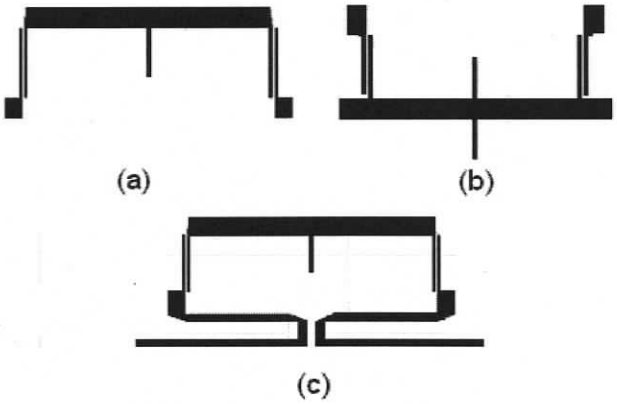

Fig. 6.4 Folded ultra-wideband filter configurations with a single stub (a), dual stubs (b), and source-load coupling with added single stub (c).

In order to obtain a more compact filter design, the structure in Fig. 6.2a can be folded. Moreover, parallel open-ended stubs can be added to the centered transmission line. This is shown in Fig. 6.4. The stub creates a strong reflection zero at the upper edge of the passband and a sharp attenuation pole in the upper rejection band. It also attenuates the second harmonic of the passband and broadens the stopband region up to the third passband harmonic. The stubs should have resonance lengths close to a quarter-wavelength at the upper passband frequency as well as high impedance characteristics to reduce their impact on the passband operation.

Moreover, to place transmission zeros in the lower/upper rejection band, a direct source-load cross coupling can be applied to the folded structures. This is shown in Fig. 6.4c and includes an additional stub. Four extra transmission zeros, two on each side of the passband, are created and controlled by the source/load coupling coefficient.

Typically, sharp transitions from the passband to the stopbands can be accomplished by allocating attenuation poles on both sides of the passband. The implementation of source/load supports such an approach for the proposed cascaded/folded UWB configurations. The locations

of the attenuation poles are defined in terms of the sign and the strength of the source/load coupling. A strong and positive source/load coupling can typically generate two attenuation poles on each side of the passband and a number of other poles in the upper stopband region.

6.4 Performances

6.4.1 Simulation Results

The design guidelines presented in the previous section are applied to the various filter configurations introduced in Fig. 6.3 and Fig. 6.4. All filters are designed on RT6006 substrate with a height of h=635μm and are verified by the two commercial field solvers Ansoft Designer and IE3D. Note that we refrained from using any aperture compensation in the ground plane of the circuits such as [43], [48], which ease the fabrication process.

Fig. 6.5 depicts the results obtained with the ultra-wideband filter configuration in Fig. 6.3. As predicted, up to three transmission zeros can be placed in the upper rejection band (Fig. 6.5b) by controlling the length of the new resonator and the bypass source/load coupling (as compared to Fig. 6.5a). This creates a wide suppression band and a sharp roll-off skirt on the upper side of the passband. The return loss is better than 12 dB from 3.2 to 7 GHz. The 3dB bandwidth is around 80 percent (3-7.1 GHz), and the predicted passband insertion loss is less than 1 dB. The slight peak at around 3.5 GHz believed to be caused by a weak coupling between the center section of the stepped impedance resonator and the bridging resonator (c.f. insets in Fig. 6.5).

The results of configurations with additional stubs (Fig. 6.4a-b) are shown in Fig. 6.6. Apparently, the additional stubs increase the bandwidth for a single resonator up to eight percent and insert a strong attenuation pole at the upper edge of the passband. It also has a dramatic attenuation impact on the second harmonic of the passband due to the lowpass characteristics. In Fig. 6.6a, the reflection coefficient is better than -13 dB from 4.2 to 9.5 GHz with a predicted insertion loss less than 0.65 dB. The corresponding values in Fig. 6.6b are: 15 dB from 3.2 to 7.3 GHz, and less than 0.5 dB. The configuration in Fig. 6.6b is slightly more compact and has better upper stop-band rejection up to the third passband harmonic.

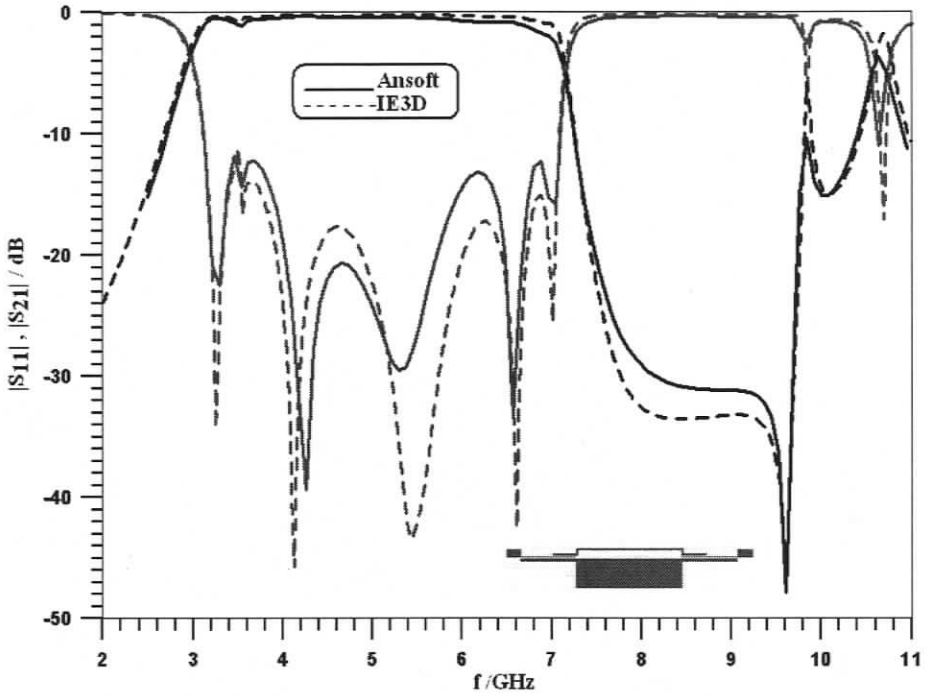

(a)

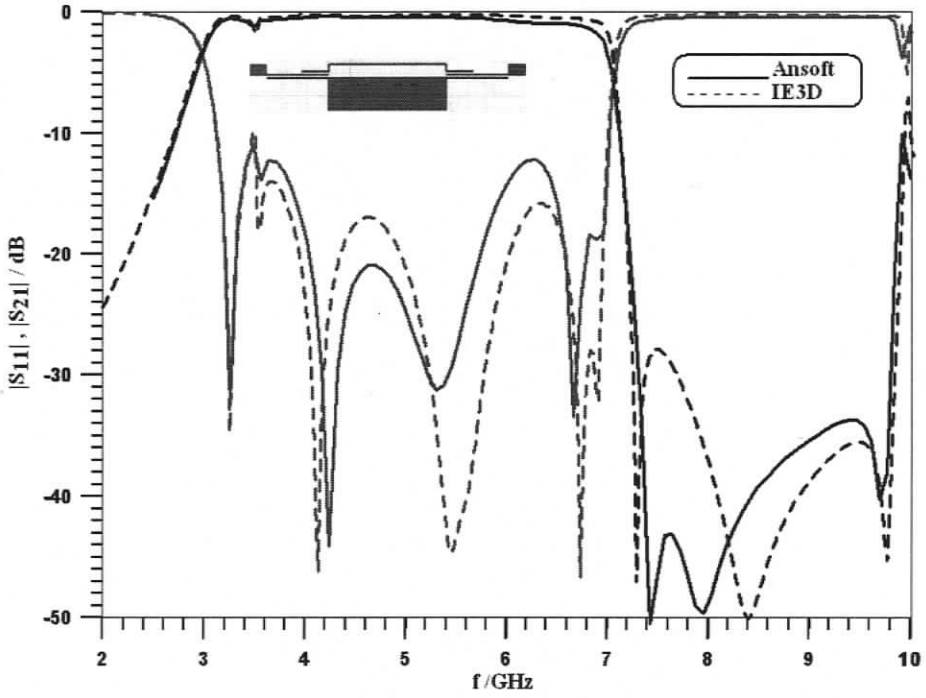

(b)

Fig. 6.5 Simulated performances of the modified ultra-wideband filter configuration according to Fig. 6.3 with a short additional resonator and weak cross coupling (a), and longer resonator and strong cross coupling (b).

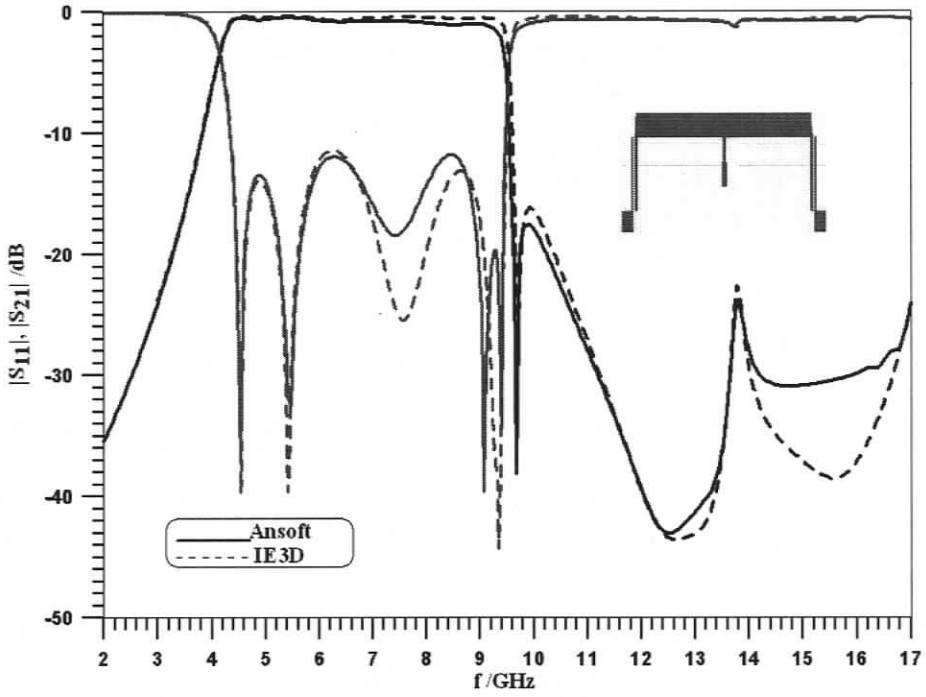

(a)

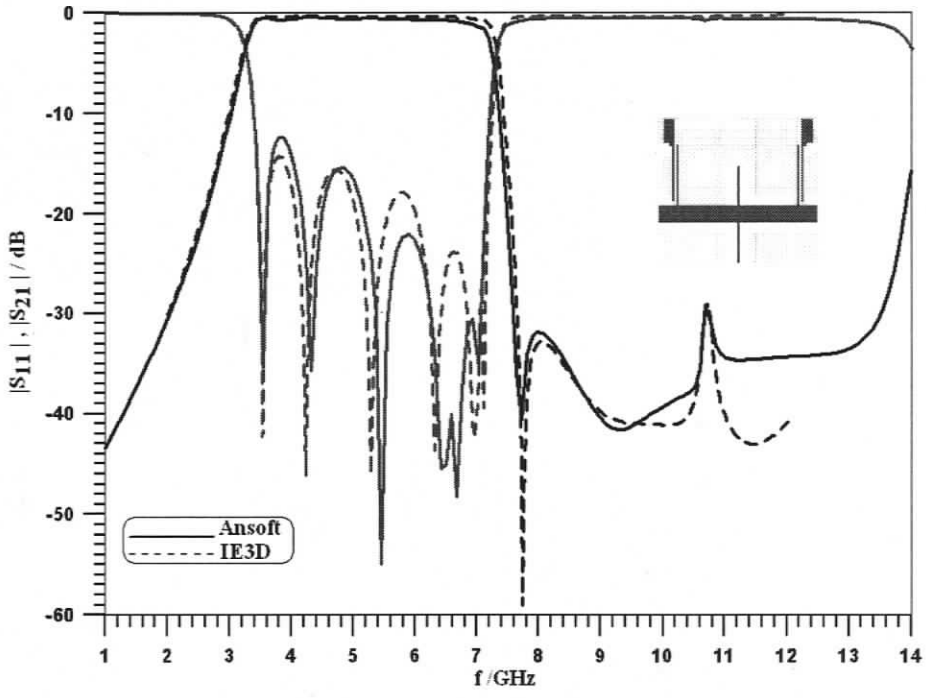

(b)

Fig. 6.6 Simulated responses of ultra-wideband filter configurations according to Fig. 6.4a-b; bandwidth of 4.2 - 9.5 GHz (a), 3.2 - 7.3 GHz (b).

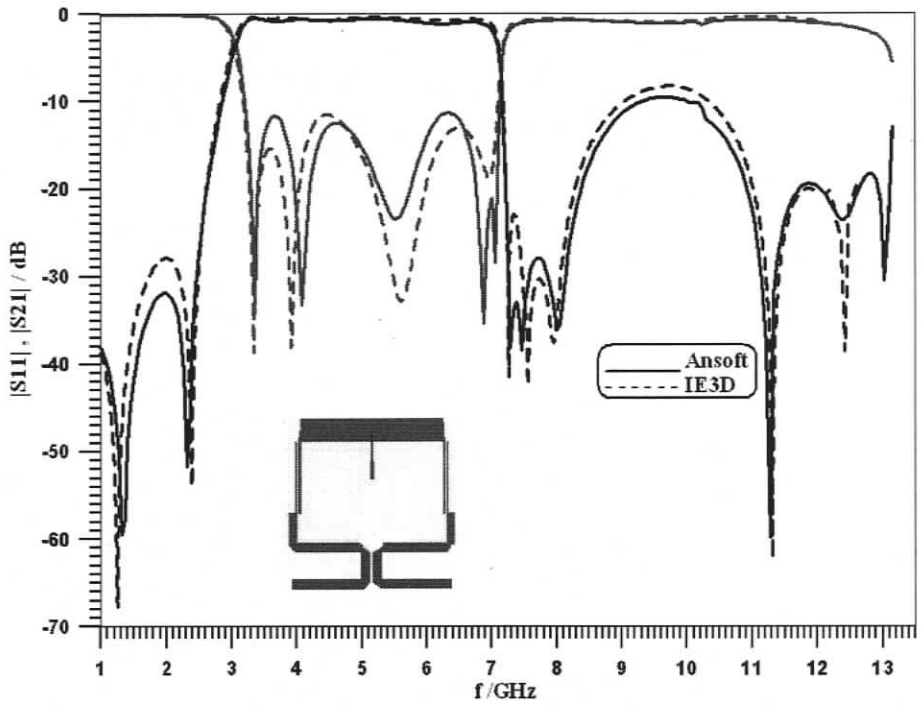

Fig. 6.7 Performances of ultra-wideband filter configuration with direct source-load coupling according to Fig. 6.4c.

Direct source-load coupling can be easily implemented to the ultra-wideband filter structure to create transmission zeros on both sides of the passband. Fig. 6.7 shows the performance of a UWB filter according to Fig. 6.4c. Two extra zeros are located on each side of the passband due to the cross coupling; their locations can be adjusted by the source-load coupling coefficient (length). Fig. 6.7 also shows one of the additional transmission zeros generated by the stub. The 3dB bandwidth is from 3 to 7.1 GHz with a return loss of 11 dB.

6.4.2 Measurement Results

This section presents microstrip design examples of compact ultra-wideband filters using different types and numbers of SIRs. They are designed for fabrication on RT6006 substrate with thickness of h=635 μm and conductor layers of 35 μm. The relative permittivity of the substrate is taken as 6.15 for all designs. The numerical designs have been carried out with Ansoft Designer, verified by IE3D, then prototyped and measured.

Three cascaded SIRs in a folded configuration are used to design an UWB filter to cover 3.1-9.6 GHz band. Fig. 6.8a shows the filter structure with simulated and measured performances. The 3 dB fractional bandwidth is 102 percent. The upper stopband extends from 10 GHz to 15 GHz with better than 20 dB measured suppression. The simulated insertion loss is less than 2 dB.

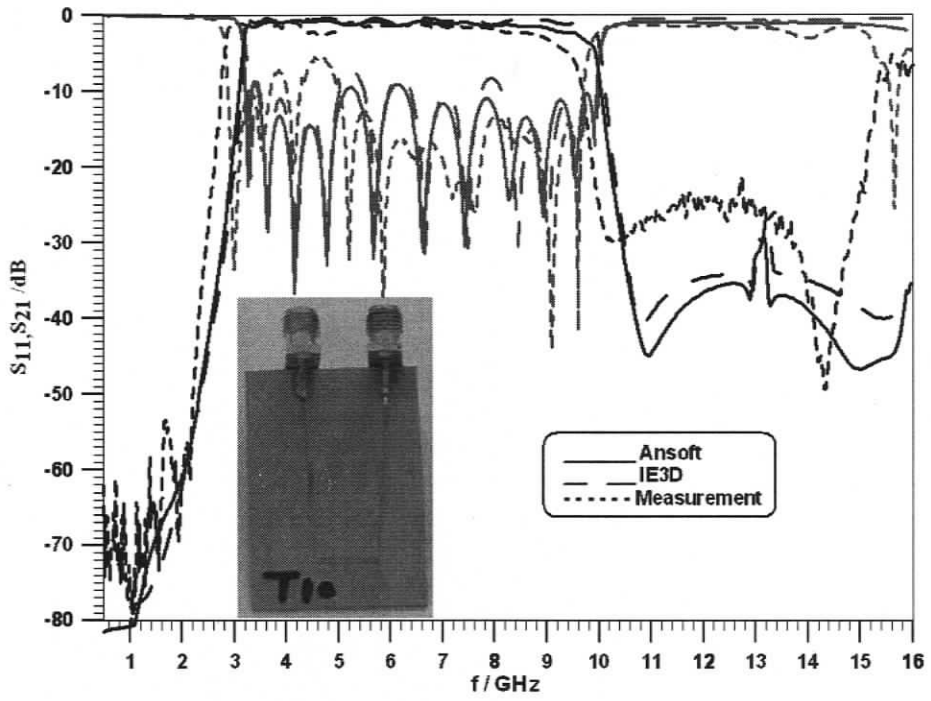

(a)

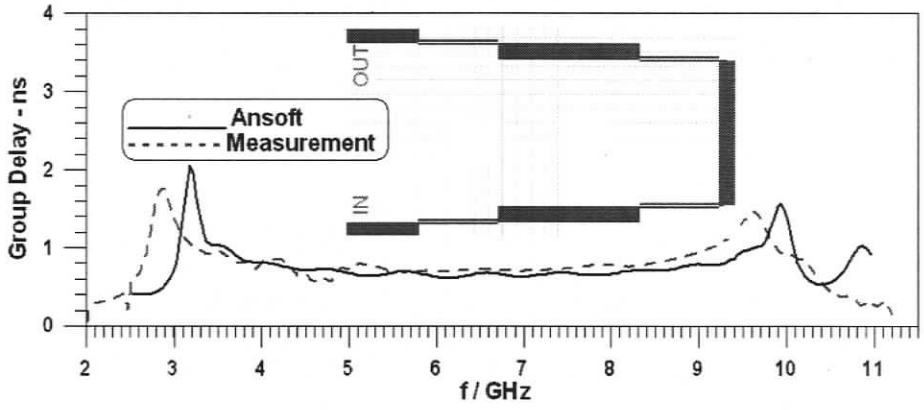

(b)

Fig. 6.8 Measured and computed performances of a folded UWB filter with three cascaded SIRs; transmission and reflection coefficients in dB (a) and group delay (b).

Agreement between measurements and simulations is generally good, thus verifying the design procedure. However, a slight downward frequency shift is observed in the measurements (and in those of the following examples). This is attributed to a slightly higher substrate permittivity and metal-etching tolerances (c.f. Results in Chapter 5). The appearance of the transmission minima in the upper stopband is due to the inter-coupling between the harmonic and fundamental resonances. Due to the complexity of the SIR for triple-mode resonance operation, a direct coupling-matrix-type model (as used for narrowband filters in Chapter 4) has limited validity in UWB applications. The size of the entire structure in Fig. 6.8a is 14mm in width and 25mm in length.

Fig. 6.8b shows the measured and computed group delay performance of the filter, which is extracted from the transmission phase measurements in the passband as

$$\tau = -\frac{\partial \varphi_{21}}{\partial \omega} \tag{6.4}$$

The group delay can also be extracted in the stopbands. However, the output signal is diminished in the suppression region due to the existence of attenuation poles. Therefore, the group delay at frequencies out of the passband is expressed through the reflection phase

$$\tau = -\frac{\partial \varphi_{11}}{\partial \omega} = -\frac{\partial \varphi_{22}}{\partial \omega} \tag{6.5a}$$

which is derived from the properties of an assumed lossless symmetric two-port device.

$$|S_{11}|^2 + |S_{22}|^2 = 1 \tag{6.5b}$$

$$(<S_{11} + <S_{22}) - (<S_{21} + <S_{12}) = +/- k\pi \quad k = 1,2,... \tag{6.5c}$$

The results demonstrate that the group delay variation in the passband is less than 0.4 ns and that good agreement between experimental and numerical results is obtained.

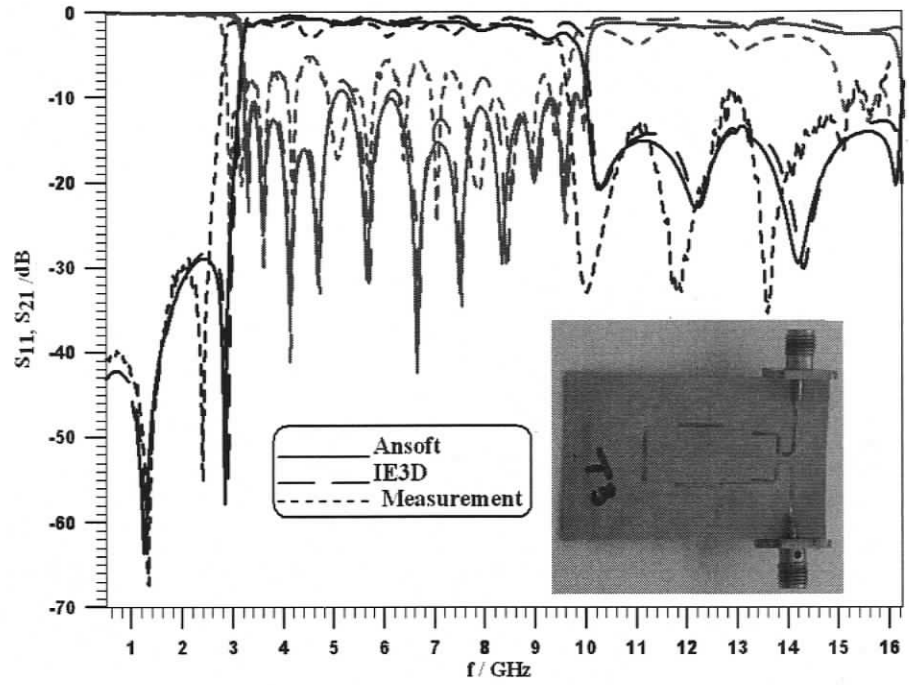

(a)

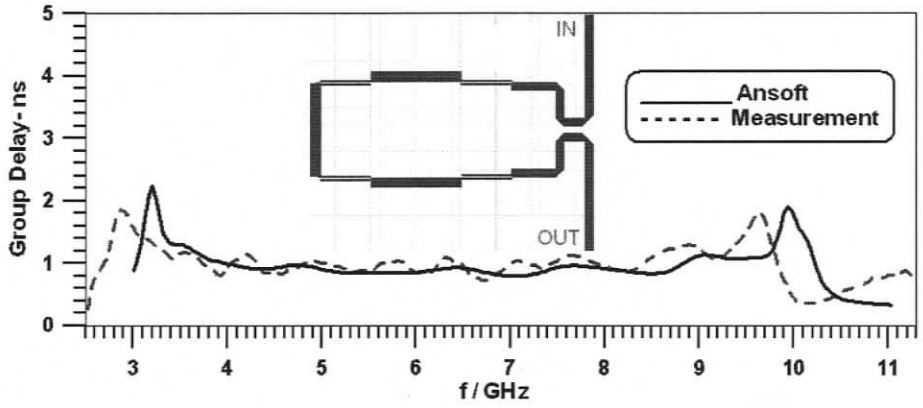

(b)

Fig. 6.9 Measured and computed performances of the folded UWB filter in Fig. 6.8, but with added source/load coupling; transmission and reflection coefficients in dB (a) and group delay (b).

The performance of the UWB filter of Fig. 6.8, but with added source/load coupling, is depicted in Fig. 6.9. Six attenuation poles at 1.4 GHz, 3 GHz, 10.2 GHz, 12 GHz, 14 GHz and 16 GHz are generated through the positive source/load coupling (Fig. 6.9a). Except for the frequency shift mentioned earlier, these poles are well represented in the measurements, and overall agreement is good. This example demonstrates that not necessarily all of the theoretical maximum number of transmission zeros can be independently placed. This is due to the fact that

the coupling between resonances in individual SIRs does not follow the traditional coupling scheme, which assume constant coupling between resonators. Fig. 6.9b reports the numerical and experimental group delay results. Compared to Fig. 6.8b, the variation is only slightly increased to 0.6 ns. Note that the size of the filter structure in the inset of Fig. 6.9a is 30mm x 15 mm.

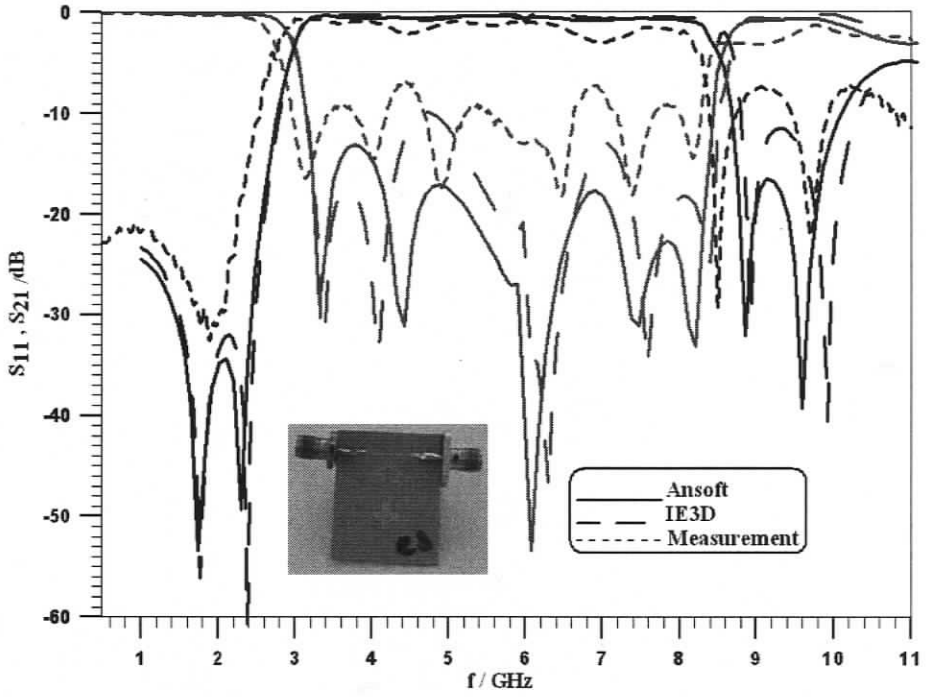

(a)

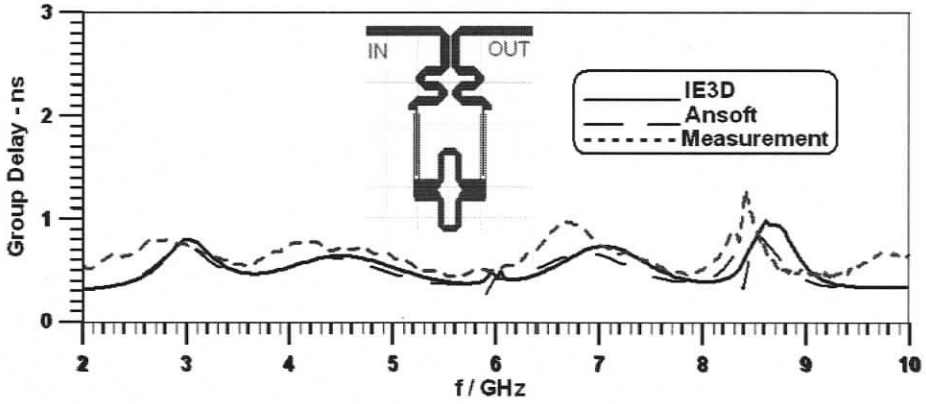

(b)

Fig. 6.10 Measured and computed performances of a five-pole UWB filter with a single triple-mode SIR with folded low-impedance and parallel high-impedance segments and added source/load coupling; transmission and reflection coefficients in dB (a) and group delay (b).

Fig. 6.10a shows the layout and performance of a five-pole UWB filter using a single triple-mode SIR with folded low-impedance and parallel high-impedance segments (c.f. Fig. 6.1a, right). Input and output ports of the SIR are folded to permit source/load-coupling implementation. The inductive source/load coupling generates two attenuation poles on each side of the passband at 1.8 GHz, 2.4 GHz, 8.8 GHz and 9.6 Ghz.

The measured insertion loss is less than 3 dB within the passband. The 3 dB fractional bandwidth is 97 percent, which is 15 percent higher than the single UWB filter structure presented in [140]. This is due to the high-impedance coupling segments of this SIR, which contribute to stronger coupling while maintaining a manageable gap width. The measured dip instead of the two computed attenuation poles in the lower stopband is due to a fabrication error of the folded low-impedance segment, which necessitated that the SIR be modified by hand. In addition, the previously mentioned frequency shift appears in the experimental performance.

The filter structure in Fig. 6.10 is more compact with source/load coupling (8 mm x 20 mm) than other UWB filters with a single SIR scheme proposed in [140]. The measured group delay depicted in Fig. 6.10b exhibits good agreement with the computations within the frequency range of interest. The group delay variation is 0.6 ns.

Three cascaded triple-mode SIRs with folded low-impedance and parallel high-impedance segments are utilized to design an eleven-pole UWB filter. Fig. 6.11a shows both the filter structure as well as the numerical and experimental performances. (Note that the two wider dips in the simulated S_{11} performance at 5.7 GHz and 8.3 GHz resemble two reflection zeros each, but the theoretical fine tuning of the filter was terminated once a return loss of 10 dB achieved). The filter covers the bandwidth from 3 GHz to 10.7 GHz. Good agreement is observed for the numerical and experimental results. Especially, the steep slope between 11 GHz and 12 GHz is reproduced by the measurements. However, the peak in the S_{21} performance at 14 GHz is not. This is attributed to slightly stronger coupling (slightly narrower gap in the prototype) between the cascaded SIRs. Note that the bandwidth is also slightly increased due this effect. Fig. 6.11b depicts the group delay performance of both simulation and experiment. The measured group delay variation is approximately 0.7 ns within the band of interest. The dimension of the

entire filter structure in Fig. 6.11 is 42mm x 6 mm.

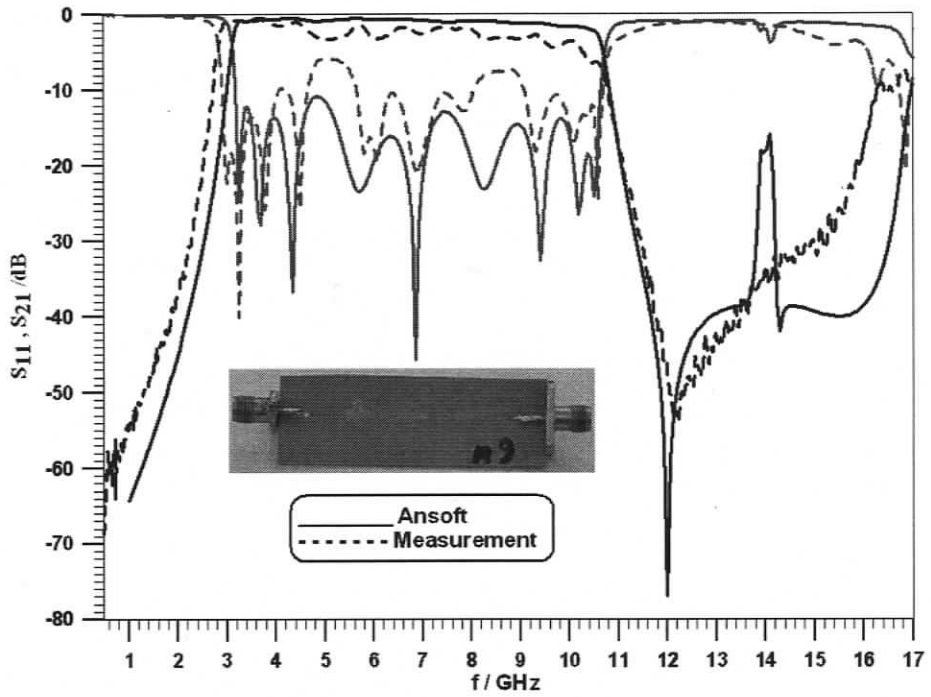

(a)

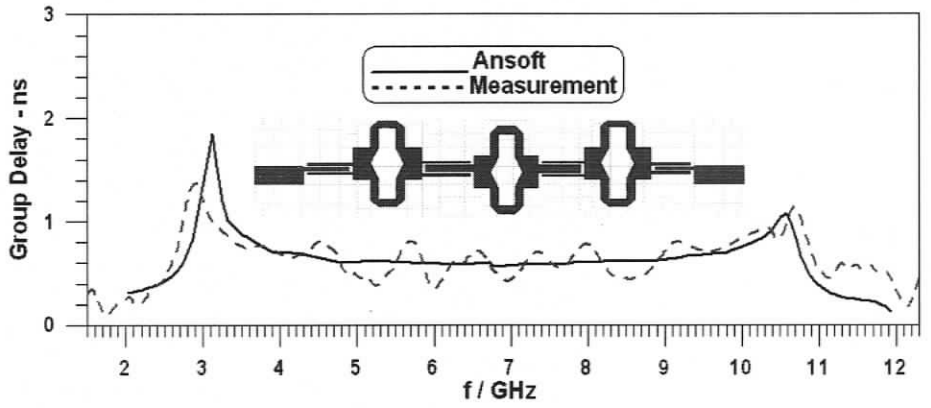

(b)

Fig. 6.11 Measured and computed performances of an eleven-pole UWB filter with three cascaded triple-mode SIRs with folded low-impedance and parallel high-impedance segments; transmission and reflection coefficients in dB (a) and group delay (b).

Structural folding and source/load coupling is added on the example in Fig. 6.11 to generate attenuation poles in the stopband regions. Fig. 6.12 shows the numerical and experimental performances for comparison with Fig. 6.11. Due to fabrication errors on the folded

low-impedance segments (the respective segments have been altered by hand), the agreement between theoretical and experimental results in Figs. 6.12a is far from expectation. Moreover, when comparing the theoretical results of Fig. 6.12b with those in Fig. 6.11b, the influences of source/load coupling and structural folding on the group delay becomes apparent. The variation in the passband increases significantly which is corroborated by the measurements. The total size of the filter structure is 18 mm x 22 mm.

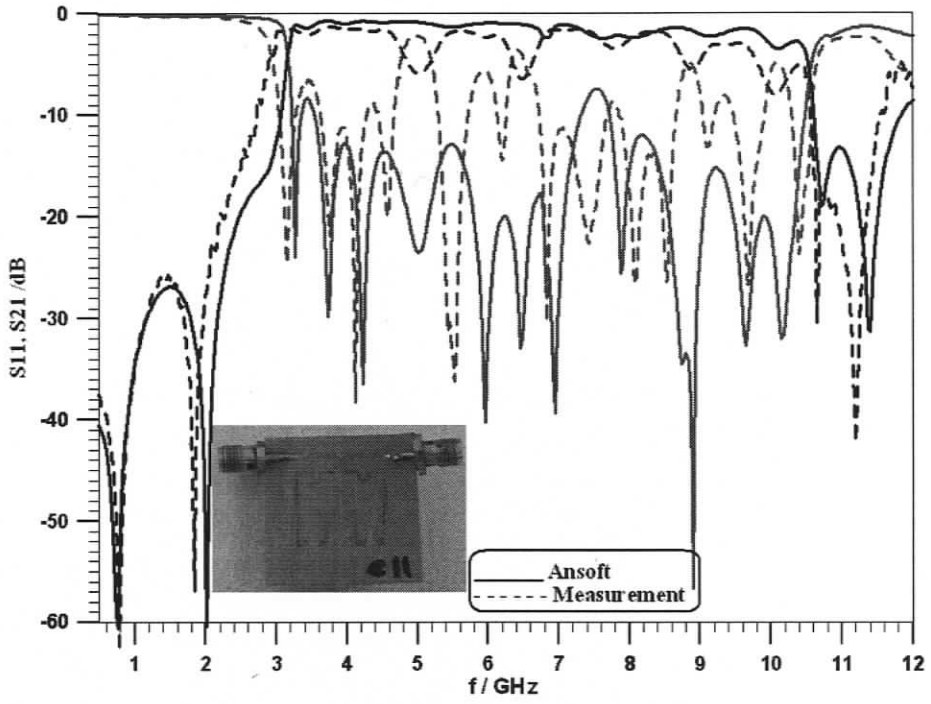

(a)

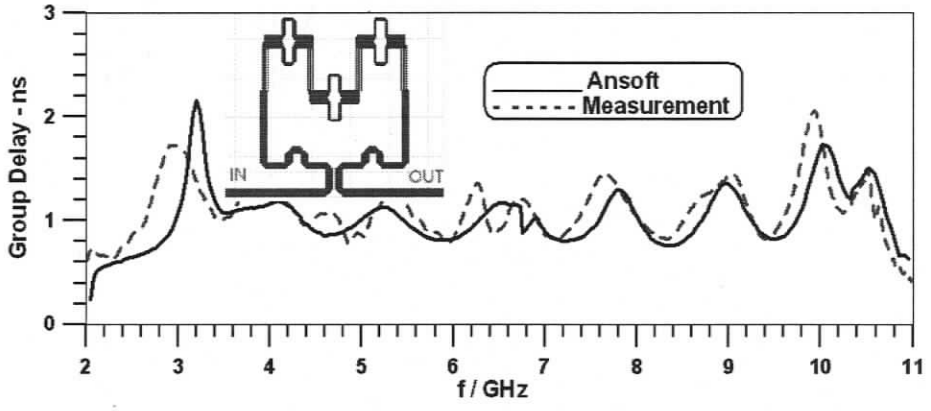

(b)

Fig. 6.12 Measured and computed performances of the UWB filter in Fig. 6.11, but in a folded arrangement with added source/load coupling; transmission and reflection coefficients in dB (a) and group delay (b).

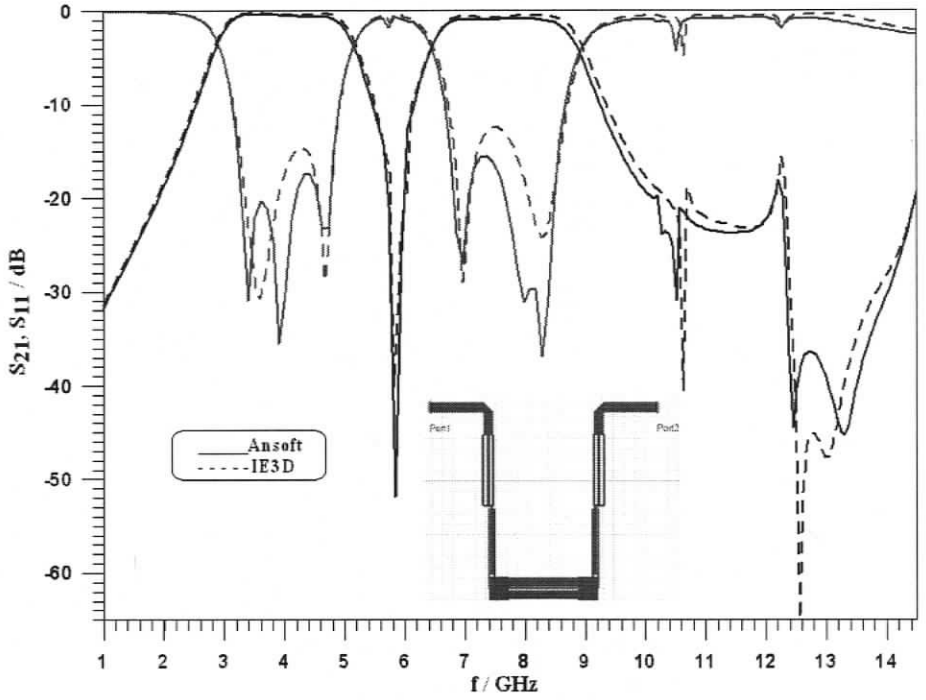

(a)

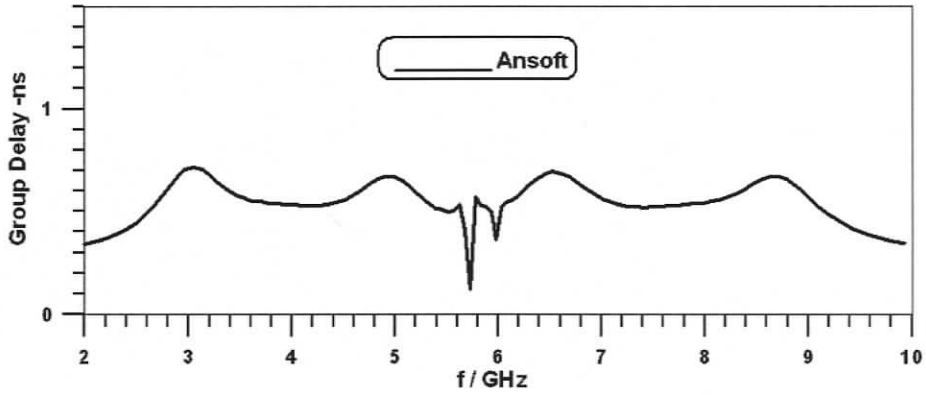

(b)

Fig. 6.13 Simulated performances of the proposed UWB/notch filter design; transmission and reflection coefficients in dB (a) and group delay (b) from Ansoft Designer.

The last example is on the design of a notch within the ultra-wide passband as depicted in Fig. 6.13. The filter is similar to that in Fig. 6.10 but refrains from folding the low-impedance segment and from using source/load coupling. In order to create a transmission zero within the band of interest, three quarter-wavelength open-stubs within the input/output coupling sections as well as in the low-impedance segment of the SIR (c.f. inset in Fig. 6.13a) are employed at the specified frequency. However, the utilization of a single stub is not enough to produce significant

attenuation. Therefore, three open quarter-wavelength stubs operating at 5.8 GHz are used in this design. This makes it possible to control the notch bandwidth with the coupling gap on the side of the open-stub and the transmission lines

Furthermore, the utilized stub can operate as an additional resonator due to its quarter-wave length and ultimately increases the number of reflection zeros within passband. In addition, due to the low-impedance segment length of the SIR, the location of the notch frequency is limited towards the lower part of the passband.

Fig. 6.13 exhibits the simulated performance of the proposed UWB filter with notch characteristic. The lengths of the open stubs are a quarter-wavelength at the center frequency (f_0=5.8 GHz) of the UWB filter. A dual-band filter with three reflection zeros in each band is created and separated by an attenuation pole. The attenuation poles in the upper stopband region are generated due to the harmonics of the utilized open stubs and the additional coupling between elements. Good agreement between the results of the two field solvers is observed in Fig. 6.13a. The group-delay performance obtained from one of the simulators is shown in Fig. 6.13b. The variations are 0.1 ns within the two passbands. The size of the entire structure is 12 mm x 18 mm.

6.5 Summary

Guidelines for the design of compact planar ultra-wide passband filters are presented. The core section is based on three resonances of a stepped-impedance resonator and coupled mirostrip segments. Adding cross coupling or folding the filter to create source-load coupling presents viable options for increasing the bandwidth and improving the selectivity. Additional impedance stubs can be used to create transmission zeros close to the upper band edge and in the upper stopband.

The properties of different compact UWB filters using two different microstrip stepped-impedance resonator configurations are also investigated in single and cascaded arrangements. Source/load coupling has been added to create attenuation poles left and right of the passband. However, this measure has proven to be a disadvantage when low group-delay variations are envisaged. The reported numerical and experimental results demonstrate the feasibility of the

design process. Moreover, the used stepped-impedance resonators permit to achieve stronger inter-resonator coupling, thus exhibiting good properties in terms of wide bandwidth and reasonable group delay variation. They also contribute to size reduction and retain simple structural features for low-cost fabrication with typical accuracy requirements. In other words, the designs refrain from using ground plane apertures and, therefore, do not complicate fabrication. It is also demonstrated that the employed coupling schemes between SIRs can be modified to create a narrow notch within the UWB frequency range.

CHAPTER 7

Conclusions and Recommendations for Future Work

7.1 Summary

The main objective of this thesis is to address the challenging issues of advanced microwave dual- to multi- and ultra-wide-band filter design in the context of wireless and telecommunication systems. The size of the filters, as well as any other resonant components, is highly dependent upon the physical dimensions of the structure. In order to establish standing electromagnetic waves, the dimensions of resonant structures need to be at least a quarter of a wavelength, which imposes size limitation. Furthermore, the type and size of these components critically affect the power efficiency and ohmic losses. The aforementioned issues have so far precluded microwave dual-, multi- and ultra-wide-band filters from being integrated monolithically into transceiver circuitry.

In response to the above needs, novel approaches and topologies for the synthesis and design of high-performance filters are proposed. In addition to performance, matching networks for proposed filters are eliminated. The implementation of highly folded resonators in the filter structures is investigated as it is another important requirement that must be fulfilled before integrating filters into electronic circuits and microsystems becomes a reality.

7.2 Contributions

The major contributions of this thesis fall into three different categories:

7.2.1 Broad-Band Coupling Matrix

The concept of a new class of coupling matrix integrated with potential lower/higher-order modes through the cavities of microwave filters is demonstrated. This approach takes advantage of the filter topology to achieve improved performance in a wide frequency range. Using this concept enables designers to consider lower/higher-order propagating modes in order to eliminate or take advantage of unwanted pass/stop-bands. Several examples of waveguide single- to multi-mode filters operating in various frequency ranges are demonstrated to verify this concept. The proposed approach can also be applied to any other microwave structure in either waveguide or planar technologies.

7.2.2 Advanced Dual- to Multi-Band Filters

Another aspect of this research focuses on a new generation of dual- to multi-band filter design. One approach is to implement cross coupling between proper resonance components in a coupling matrix to generate attenuation poles within and out of a passband, thus, producing two or more separated bands at desired frequencies with quasi-elliptic response. The use of higher-order modes within this approach in waveguide technology can additionally enhance stopband performance by introducing multiple transmission zeros. The method is achieved for any planar or cavity resonators and is demonstrated in this research through various examples in microstrip and waveguide technologies.

The bandwidth of the new generation of cross-coupled dual- to multi-band filters is rather small and highly dependent on the number of employed resonators. On the other hand, the physical dimension of these filters inherently increases with larger bandwidths or better performances. Therefore, as part of filter miniaturization and bandwidth enhancement effort, a new class of step-impedance resonators based on harmonic-tuning properties is proposed. Using these new resonators, advanced coupling configurations are realized and; therefore, both narrow- to ultra-wide dual-band filters up to 50 percent bandwidth in each passband are realizable. Furthermore, standard coupled-line to cross-coupled techniques enable excellent quasi-elliptic performances of the new filters, specifically with respect to sharp roll-off passband, perfect isolation and broad bandstop regions. Multi-band filters applicable in wireless communications may be realized with either positive or negative source-load coupling in distinctive topologies.

The filters that have been introduced are about an order of magnitude smaller than their standard counterparts, while still achieving higher-quality performance.

7.2.3 New Generation of Ultra-Wideband Filters

An approach similar to the one used for designing ultra-wide dual-band filters can be applied to ultra-wideband filters. Due to new folded step-impedance resonator structure, stronger coupling elements between coupled segments as well as compact size can be achieved. Multiple cascaded resonators contribute to a larger number of reflection zeros within the passband and therefore extend bandwidth. In addition, spurious passbands due to the third harmonic property of SIRs can be suppressed through open stubs, which also act as resonators and generate one reflection and one transmission zero each on the upper edge of the passband. Source/load cross-coupling can be applied either to new ultra-wideband filters, similar to dual-band filters, or those with open-ended transmission lines that act as additional resonator. The aforementioned techniques enhance the passband and stopband performances of new ultra-wideband filters and can contribute to integration in planar circuits due to their compact size and low cost.

7.3 Future Work

In addition to basic wireless/telecommunication systems, there are three distinct features in this research that can be applied to other related technologies. First, the need for miniaturized RF and electromagnetic passive components is inevitable. Secondly, multi-band requirements of microwave multi-port devices demand a high effort to keep the losses of miniature structures as low as possible, especially at higher frequencies, and to achieve perfect matching between ports. Thirdly, the tunable multi-harmonic nature of step-impedance resonators calls for high-impedance miniature multi-band to ultra-wideband antennas for integration. The high-impedance characteristic ensures that the power consumption of the system will be at minimum. The following discussion, more specifically, outlines some of the interesting venues in which this research can be pursued in the future.

7.3.1 Fabrication of Filters on Advanced Substrates

Engineering new materials with both negative permiability and permittivity has created a new avenue for RF engineering research. This new generation of meta-materials has great potential to be used as substrates for microwave circuits such as filters. Suppressing surface waves, controlling near field couplings, manipulating the permittivity and permeability of substrates, etc. are among the advantages of this class of materials, which can uniquely address antenna and filter needs such as further miniaturization and bandwidth enhancement. In addition, the application of multi-layer and LTCC substrates can significantly help further miniaturization through aperture coupling and wavelength reduction, respectively.

7.3.2 Fabrication of Dual- to Multi-Band Microwave Multi-Port Structures

Multi-port microwave structures play an essential role in communication systems. These devices, such as hybrids, circulators, etc. can work in specific frequency ranges or in various frequency ranges depending on the number of output ports, e.g. diplexers and multiplexers. The main course of this research can be applied on each channel to address dual- to multi-band channels. This can excessively reduce not only the entire size of communication systems but also losses, specifically in higher frequencies.

7.3.3 Miniature Antennas for Biomedical and Wireless Applications

The highly efficient folded components proposed in this research can find numerous applications in biomedical and wireless fields. Having a low-loss miniature electromagnetic probe, capable of transmitting and receiving narrow dual-band data, is critical in the design of sensors for implantable devices. Moreover, the implementation of a tunable multi-harmonic stepped-impedance resonator can particularly address miniaturized dual- to multi- and ultra-wideband antennas for wireless applications. The idea of miniaturized resonators capable of demonstrating both electric and magnetic field couplings with minimal loss can particularly be explored for this class of applications.

Bibliography

[1] V. Belevitch, "Recent development in filter theory", IRE Trans. Circuit Theory, Vol. 5, No. 4, pp. 236-252, Dec. 1958.

[2] G.L. Matthaei, L. Young, E.M.T. Jones, Microwave Filters, Impedance Matching Networks and Coupling Structures, New York: McGraw-Hill, 1964.

[3] A.E. Atia and A.E. Williams, "New type of waveguide band pass filters for satellite transponders", COMSAT Tech. Rev., Vol. 1, no. 1, pp. 21-43, 1971.

[4] R.R. Mansour, S. Ye, S.F. Peik, V. Dokas, B. Fitzpatrick, "Quasi-dual-mode resonators", IEEE Trans. Microwave Theory Tech., Vol. 48, pp. 2476-2480, Dec. 2000.

[5] R.R. Mansour, S. Ye, S. Peik, V. Dokas, B. Fitzpatrick, "Quasi-dual-mode resonators", IEEE MTT-S Int. Microwave Symp. Dig., pp. 183-185, Boston, USA, June 2000.

[6] S. Avrillon, A. Chousseaud, S. Toutain, "Dividing and filtering function integration for the development of a band-pass filtering power amplifier", IEEE MTT-S Int. Microwave Symp. Dig., pp. 1173-1176, Seattle, USA, June 2002.

[7] H. Miyake, S. Kitazawa, T. Ishizaki, T. Yamanda, Y. Nagatomi, "A miniaturized monolithic dual-band filter using ceramic lamination technique for dual-mode portable telephones", IEEE MTT-S Int. Microwave Symp. Dig., pp. 789-792, Denver, USA, June 1997.

[8] C. Quendo, E. Ruis, C. Person, "An original topology of dual-band filter with transmission zeros", IEEE MTT-S Int. Microwave Symp. Dig., pp. 1093-1096, Philadelphia, USA, June 2003.

[9] C.H. Chang, H.S. Wu, H.J. Yang, C.K. Tzuang, "Coalescend single-input single output dual-band filter", IEEE MTT-S Int. Microwave Symp. Dig., pp. 511-514, Philadelphia,

USA, June 2003.

[10] C. Quendo, E. Rius, C. Person, "Narrow bandpass filters using dual-behavior resonators based on stepped-impedance stubs and different-length stubs", IEEE Trans. Microwave Theory Tech., Vol. 52, pp. 1034-1044, Mar. 2004.

[11] C. Quendo, E. Rius, C. Person, "Narrow bandpass filters using dual-behavior resonators", IEEE Trans. Microwave Theory Tech., Vol. 51, pp. 734-743, Mar. 2003.

[12] C.C. Chen, "Dual-band bandpass filter using coupled resonator pairs", IEEE Microwave Wireless Comp. Lett., Vol. 15, pp. 259-261, Apr. 2005.

[13] S.F. Chang, Y.H. Jeng, J.L. Chen, "Dual-band step-impedance bandpass filter for multimode wireless LANs", IEE Electronics Lett., Vol. 40, pp. 38-39, Jan. 2004.

[14] W. Ma, Q-X. Chu, "A novel dual-band step-impedance filter with tunable transmission zeros", Proc. Asia Pacific Microwave Conf. , Vol. 1, 4p. , Suzhou, China, Dec. 2005.

[15] H.M. Lee, C.R. Chen, C.C. Tsai, C.M. Tsai, "Dual-band coupling and feed structure for microstrip filter design", IEEE MTT-S Int. Microwave Symp. Dig., pp. 1971-1974, Fort Worth, USA, June 2004.

[16] A.A.A. Apriayana, Z.Y. Ping, "A dual-band BPF for concurrent dual-band wireless transceiver", *Proc.* 5th Electronics Packaging Tech. Conf. , pp. 145-149, Singapore, Dec. 2003.

[17] L.C. Tsai, C.W. Hsue, "Dual band pass-band filters using equal length coupled serial shunted lines and Z-transform technique", IEEE Trans. Microwave Theory Tech., Vol. 54, pp. 1111-1117, Apr. 2004.

[18] M. Makimoto, S. Yamashita, Microwave Resonators and Filters for Wireless Communication: Theory, Design and Application. Berlin: Springer Verlag, pp. 66-80, 2000.

[19] J. Kocbach, K. Folgero, "Design procedure for waveguide filters with cross-couplings",

IEEE MTT-S Int. Microwave Symp. Dig., pp. 1449-1452, Seattle, USA, June 2002.

[20] R.J. Cameron, J.D. Rhodes, "Asymmetric realization for dual-mode bandpass filters", IEEE Trans. Microwave Theory Tech., Vol. 29, pp. 51-58, Jan. 1981.

[21] D.R. Jachowski, "Alternative designs for dual-mode filters", IEEE MTT-S Int. Microwave Symp. Dig., pp. 1087-1090, Denver, USA, June 1997.

[22] S. Amari, U. Rosenberg, J. Bornemann, "A novel approach to dual and triple-mode pseudo-elliptic filter design", Proc. 34th European Microwave Conf., pp. 993-996, Amsterdam, The Netherlands, Oct. 2004.

[23] S.C. Holme," A 12 GHz channel contiguous multiplexer for satellite applications", IEEE MTT-S Int. Microwave Symp. Dig., San Francisco, USA, June 1984.

[24] J. Lee, M.S. Uhm, I.B. Yom, "A dual-passband filter of canonical structure for satellite applications", IEEE Microwave Wireless Comp. Lett.,, Vol. 14, pp. 271-273, June 2004.

[25] J.S. Hong, M.J. Lancaster, R.B. Greed, D. Jedamzik, "Highly selective microstrip bandpass filters for HTS and other application", Proc. 28th European Microwave Conf., pp. 1-6, Amsterdam, The Netherlands, Oct. 1998.

[26] S. Amari, "Synthesis of cross-coupled resonator filters using an analytical gradient-based optimization technique", IEEE Trans. Microwave Theory Tech., Vol. 48, pp. 1559-1564, Sep. 2000.

[27] K.S.K. Yeo, M.J. Lancaster, J.S. Hong, "The design of microstrip six-pole quasi-elliptic filter with linear phase response using extracted-pole technique", IEEE Trans. Microwave Theory Tech., Vol. 49, pp. 321-327, Feb. 2001.

[28] J. Bornemann, U. Rosenberg, S. Amari, R. Vahldieck, "Edge-conditioned vector basis functions for the analysis and optimization of rectangular waveguide dual-mode filters", IEEE MTT-S Int. Microwave Symp. Dig., pp. 1695-1698, Anaheim, USA, June 1999.

[29] S. Amari, U. Rosenberg. J. Bornemann, "Singlets, cascaded singlets, and the non-

resonating node model for advanced modular design of elliptic filters", IEEE Microwave Wireless Comp. Lett., Vol. 14, pp. 237-239, May 2004.

[30] G. Tudosie, E. Ogli, R. Vahldieck, "Hybrid EM-simulator based optimization of microwave and millimeter wave diplexers and multiplexers", IEEE MTT-S Int. Microwave Symp. Dig., pp. 1219-1222, Philadelphia, USA, June 2003.

[31] J. Bornemann, J. Uher, "H-plane waveguide filters with E-plane dispersive inverters for high power application", Proc. ANTEM 2002/URSI, pp. 197-200, Ottawa, Canada, July 2004.

[32] J.S. Hong, M.J. Lancaster, "Aperture-coupled microstrip open-loop resonators and their applications to the design of novel microstrip band-pass filters", IEEE Trans. Microwave Theory Tech., Vol. 47, pp. 1848-1855, Sep. 1999.

[33] J.S. Hong, M.J. Lancaster, "Canonical microstrip filter using square open-loop resonators", IEE Electronics Lett., Vol. 31, pp. 2020-2022, Nov. 1995.

[34] U. Rosenberg, S. Amari, J. Bornemann, R. Vahldieck, "Compact pseudo highpass filters formed by cavity and iris resonators", Proc 34th European Microwave Conf., pp. 985-989, Amsterdam, The Netherlands, Oct. 2004.

[35] A.G. Lamperez, M. Salazar-Palma, T.K. Sarkar, "Analytical synthesis of microwave multiport network", IEEE MTT-S Int. Microwave Symp. Dig., pp. 455-458, Fort Worth, USA, June 2004.

[36] Federal Communications Commission (FCC), Revision of Part 15 of the Commission's Rules Regarding Ultra-Wideband Transmission Systems, First Report and Order, FCC 02-48, 2002.

[37] R. Clarke, R. Karunarante, C. Scharader, "Ultra-wideband antenna" Technical Report, EE198B, San Jose State University, Fall 2004.

[38] Z.N. Chen, X.H. Wu, H.F. Li, N. Yang, M.Y.W. Chia, "Considerations for source pulses and antennas in UWB radio systems", IEEE Trans. Antennas Propag., Vol. 52, pp. 1739-

1748, July 2004.

[39] H. Ishida, K. Araki, "Design and analysis of UWB bandpass filter with ring filter", IEEE MTT-S Int. Microwave Symp. Dig., pp. 1307-1310, Fort Worth, USA, June 2004.

[40] H. Ishida, K. Araki, "A design of tunable UWB filters", International Workshop on Ultra-wideband Systems and Technologies, pp. 424-428, Kyoto, Japan, May 2004.

[41] K. Hashimoto, H. Asano, K. Matsuda, N. Yokoyama, T. Omori, M. Yamaguchi, "Wideband love wave filters operating in GHz range on Cu-grating/rotated-YX LiNbO3-substrate structure" IEEE Ultrasonic Symp., pp. 1330-1334, Montreal, Canada, Aug. 2004.

[42] W. Menzel, M.S. Rahman Tito, L. Zhu, "Low-loss ultra-wideband (UWB) filters using suspended stripline", Proc. Asia Pacific Microwave Conf. , 4p , Suzhou, China, Dec. 2005.

[43] B.-S. Kwon, S.-S. Myoung, Y.-H. Kim, J.-G. Yook, "Co-planar waveguide filter with ground perforation for ultra-wideband system", Proc. Asia Pacific Microwave Conf., Vol. 3 4p, Suzhou, China, Dec. 2005.

[44] A. Saitou, H. Aoki, N. Satomi, K. Honjo, K. Sato, T. Koyama, K. Watanabe, "Ultra-wideband differential mode bandpass filters embedded in self-complementary antennas", IEEE MTT-S Microwave Symp. Dig., pp. 717-720, Long Beach, USA, June 2005.

[45] C.-W. Tang, C.-C. Tseng, H.-H. Liang, S.-F. You, "Development of ultra-wideband LTCC filter", Proc. IEEE Int. Conf. Ultra-Wideband, pp.320-322, Zurich, Switzerland, Sep. 2005.

[46] H. Wang, L. Zhu, W. Menzel," Ultra-wideband bandpass filter with hybrid microstrip /CPW structure", IEEE Microwave Wireless Comp. Lett., Vol. 15, No. 12, pp. 844-846, Dec. 2005.

[47] K. Li, "UWB bandpass filter: structure, performance and application to UWB pulse generation", Proc. Asia Pacific Microwave Conf., Vol. 1, 4p, Suzhou, China, Dec. 2005.

[48] H. Wang, L. Zhu, "Aperture-backed microstrip line multiple-mode resonator for design of a novel UWB bandpass filter", Proc. Asia Pacific Microwave Conf., Vol. 1, 4p , Suzhou,

China, Dec. 2005.

[49] P. Cai, Z. Ma, X. Guan, X. Yang, Y. Kobayashi, T. Anada, G. Hagiwara, "A compact UWB bandpass filter using two-section open-circuited stubs to realize transmission zeros", Proc. Asia Pacific Microwave Conf., Vol. 1, 4p , Suzhou, China, Dec. 2005.

[50] K. Li, D. Kurita, T. Matsui, "UWB bandpass filters with multi notched bands", Proc. 36th European Microwave Conf., pp. 591-594, Manchester, UK, Sep. 2006.

[51] W. Menzel, P. Feil, "Ultra-wideband (UWB) filter with WLAN notch", Proc. 36th European Microwave Conf., pp. 595-598, Manchester, UK, Sep. 2006.

[52] R. Gómez-García, J.I. Alonso, "Systematic method for the exact synthesis of ultra-wideband filtering responses using high-pass and low-pass sections", IEEE Trans. Microwave Theory and Tech., Vol. 54, pp. 3751-3764, Oct. 2006.

[53] T. -N. Kuo, S. -C. Lin, C. H. Chen, "Compact ultra-wideband bandpass filters using composite microstrip–coplanar-waveguide structure", IEEE Trans. Microwave Theory and Tech., Vol. 54, pp. 3772-3778, Oct. 2006.

[54] S. Sun, L. Zhu, "Capacitive-ended interdigital coupled lines for UWB bandpass filters with improved out-of-band performances", IEEE Microwave and Wireless Comp. Lett., Vol. 16, No. 8, pp. 440-442, Aug. 2006.

[55] P. Cai, Z. Ma, X. Guan, G. Zheng, T. Anada, "A novel sub-millimeter-wave UWB filter", Proc. 14th International Conf. Terahertz Electronics, pp. 240-243, Shanghai, China, Sep. 2006.

[56] D. Packiaraj, M. Ramesh, A. T. Kalghatgi, "Broad band filter for UWB communications", Proc. 36th European Microwave Conf., pp. 606-608, Manchester, UK, Sep. 2006.

[57] Y. Liu, C.W. Chow1, H.K. Tsang, "Silicon waveguides based ultra-wide-band filter for Raman amplification", Proc. IEEE Laser and Electro-Optics Society, pp. 609-610, Montreal, Canada, Oct. 2006.

[58] G.M. Yang, R. Jin, J. Geng, X. Huang, G. Xiao, "Ultra-wideband bandpass filter with hybrid quasi-lumped elements and defected ground structure", IET Microwave Antennas Propag., Vol. 1, No. 3, pp. 733-736, June 2007.

[59] R. Li, L. Zhu, "Compact UWB bandpass filter using stub-loaded multiple-mode resonator", IEEE Microwave Wireless Comp. Lett., Vol. 17, pp. 40-42, Jan. 2007.

[60] J.A. Ruiz-Cruz, Y. Zhang, K.A. Zaki, A.J. Piloto, J. Tallo, "Ultra-wideband LTCC ridge waveguide filters", IEEE Microwave Wireless Comp. Lett., Vol. 17, pp. 115-117, Feb. 2007.

[61] H. Shaman, J.-S. Hong, "A novel ultra-wideband (UWB) bandpass filter (BPF) with pairs of transmission zeros", IEEE Microwave Wireless Comp. Lett., Vol. 17, pp. 121-123, Feb. 2007.

[62] N. Thomson, J. -S. Hong, "Compact ultra-wideband microstrip/coplanar waveguide bandpass filter", IEEE Microwave Wireless Comp. Lett., Vol. 17, pp. 184-86, Mar. 2007.

[63] C.-H. Wu, Y.-S. Lin, C.-H. Wang, C.H. Chen, "A compact LTCC ultra-wideband bandpass filter using semi-lumped parallel-resonance circuits for spurious suppression", Proc. 37th European Microwave Conf., 4p, Munich, Germany, Oct. 2007.

[64] M. Nedil, T.A. Denidni, A. Djaiz, "Ultra-wideband microstrip to CB-CPW transition applied to broadband filter", IEEE Electronics Lett., Vol. 43, pp. 464-466, Ap. 2007.

[65] J.-S. Hong, K. Li, "Recent development of ultra-wideband (UWB) filters", Proc. IEEE Int. Symp. Microwave, Antenna, Propagation, and EMC Technologies for Wireless Communications, pp. 442-445, Hangzhou, China, Aug. 2007.

[66] T.-N. Kuo, C.-H. Wang, C.H. Chen, "A compact ultra-wideband bandpass filter based on split-mode resonator", IEEE Microwave Wireless Comp. Lett., Vol. 17, pp. 852-854, Dec. 2007.

[67] B. Pham, A. Dinh, "A Q-enhanced transformer coupling dynamic dual-mode 5GHz bandpass NB / interference rejection UWB filter", Proc. IEEE Custom Integrated Circuits

Conf., pp. 20-3-1-20-3-4, San Jose, USA, Sep. 2007.

[68] I. Pele, M. Crespin, Y. Mahe, S. Toutain, "Association of a UWB filter with a UWB antenna: Control of antenna characteristics", *I*EEE AP-S Int. Symp., pp. 1425-1428, Honolulu, USA, June 2007.

[69] X. Gong, J. Wang, W. Wang, "An improved design method for UWB filter using two-section open-circuited stubs", Proc. Int. Conf. Microwave Millimeter Wave Technology, pp. 18-21, Guilin, China, Ap. 2007.

[70] H. Shaman, J.-S. Hong, "Ultra-wideband (UWB) bandpass filter with embedded band notch structures", IEEE Microwave Wireless Comp. Lett., Vol. 17, pp. 193-195, Mar. 2007.

[71] A. Balalem, W. Menzel, J. Machac, A. Omar, "A simple ultra-wideband suspended stripline bandpass filter with very wide stop-band", IEEE Microwave Wireless Comp. Lett., Vol. 18, pp. 170-172, Mar. 2008.

[72] G.-M. Yang, R. Jin, C. Vittoria, V. G. Harris, N. X. Sun, "Small ultra-wideband (UWB) bandpass filter with notched band", IEEE Microwave Wireless Components Lett., Vol. 18, pp. 176-178, Mar. 2008.

[73] W.M. Fathelbab, F. Khoury, J.J. Kellar, K.W. White, "Ultra-wideband (UWB) hairpin-comb filters with broad stopband performances", IEEE Radio Wireless Symp. Dig., pp. 451-454, San Diego, USA, Jan. 2008.

[74] R.J. Cameron, "Fast generation of Chebyshev filter prototypes with a-symmetrically prescribed transmission zeros", ESA Journal, Vol. 6, pp. 83-95, 1982.

[75] R.J. Cameron, "General prototype network synthesis methods for microwave filter", ESA Journal, Vol. 6, pp. 193-206, 1982.

[76] R.J. Cameron, "Advanced coupling matrix synthesis techniques for microwave filters", IEEE Trans. Microwave Theory Tech., Vol. 51, pp. 1-10, Jan. 2003.

[77] S. Amari, U. Rosenberg and J. Bornemann, "Adaptive synthesis and design of resonator filters with source/load-multiresonator coupling", IEEE Trans. Microwave Theory Tech., Vol. 50, pp. 1969-1978, Aug. 2002.

[78] R.M. Kurzrok, "General three-resonator filters in waveguide", IEEE Trans. Microwave Theory Tech., Vol. 14, pp. 46-47, Jan. 1966.

[79] W.A. Atia, K.A. Zaki, A.E. Atia, "Synthesis of general topology multiple coupled resonator filters by optimization", IEEE MTT-S International Microwave Symp. Dig., pp. 821-824, Baltimore, USA, June 1998.

[80] A.G. Lamperez, M. Salazar-Palma, M.J.P. Cruz, I.H. Carpintero, "Synthesis of cross-coupled lossy resonator filters with multiple input/output couplings by gradient optimization", IEEE AP-S Int. Symp. Dig., pp. 52-55, Columbus, USA, July 2003.

[81] S. Amari, U. Rosenberg, "Direct synthesis of a new class of bandstop filters", IEEE Trans. Microwave Theory Tech., Vol. 52, pp. 607-616, Feb. 2004.

[82] A. Lamecki, P. Kozakowski, M. Mrozowski, "Fast synthesis of coupled-resonator filters", IEEE Microwave Wireless Comp. Lett., Vol. 14, pp. 174-176, Apr. 2004.

[83] A.E. Atia, A.E. Williams, "Narrow bandpass waveguide filters", IEEE Trans. Microwave Theory Tech., Vol. 20, pp. 258-265, Apr. 1972.

[84] A.E. Atia, A.E. Williams, R.W. Newcomb, "Narrow band multiple coupled cavity synthesis", IEEE Trans. Circuits Systems, Vol. 21, pp. 649-655, Sep. 1974.

[85] A.E. Williams, "A four cavity elliptic waveguide filter", IEEE Trans. Microwave Theory Tech., Vol. 18, pp. 1109-1114, Dec. 1970.

[86] R.J. Cameron, "General coupling matrix synthesis methods for Chebyshev filtering functions", IEEE Trans. Microwave Theory Tech., Vol. 47, pp. 433-442, Apr. 1999.

[87] R.J. Cameron, J.D. Rhodes, "Asymmetric realization for dual-mode bandpass filters", IEEE Trans. Microwave Theory Tech., Vol. 29, pp. 51-58, Jan. 1981.

[88] R.M. Kurzrok, "General four resonator filters at microwave frequencies", IEEE Trans. Microwave Theory Tech., Vol. 14, pp. 295-296, June 1966.

[89] D. Chambers, J.D. Rhodes, "A low pass prototype allowing the placing of integrated poles at real frequencies", IEEE Trans. Microwave Theory Tech., Vol. 31, pp. 40-45, Jan. 1993.

[90] J.D. Rhodes, S.A. Alseyab, "The generalized chevyshev low pass prototype filter", Int. J. Circuit Theory Applications, Vol. 8, pp. 113-125, 1980.

[91] R. Levy, "Direct synthesis of cascaded quadruplet (CQ) filters", IEEE Trans. Microwave Theory Tech., Vol. 43, pp. 2940-2944, Dec. 1995.

[92] R. Levy, "Filter with single transmission zeros at real and imaginary frequencies", IEEE Trans. Microwave Theory Tech., Vol. 24, pp. 172-181, Apr. 1976.

[93] P. Kozakowski, A. Lamecki, M. Mrozowski, "Eigenvalue approach to synthesis of prototype filters with source/load coupling", IEEE Microwave Wireless Comp. Lett., Vol. 15, pp. 98-100, Feb. 2005.

[94] G. Macchiarella, "Synthesis of prototype filters with triplet sections starting from sources and loads", IEEE Microwave Wireless Comp. Lett., Vol. 12, pp. 42-44, Feb. 2002.

[95] G. Macchiarella, "A powerful tool for the synthesis of prototype filters with arbitrary topology", IEEE MTT-S International Microwave Symp. Dig., pp. 1467-1470, Philadelphia, USA, June 2003.

[96] R.N. Gajaweera, L.F. Lind, "Rapid coupling matrix reduction for longitudinal and cascaded-quadruplet microwave filters", IEEE Trans. Microwave Theory Tech., Vol. 51, pp. 1578-1583, May 2003.

[97] K.C. Gupta, R. Garg, R. Chadha, Computer Aided Design of Microwave Circuits, Norwood, MA: Artech House, 1981.

[98] S. Amari, P. Harscher, R. Vahldieck, J. Bornemann, "Novel analytic gradient evaluation techniques for optimization of microwave structures", IEEE MTT-S International Microwave Symp. Dig., pp. 31-34, Anaheim, USA, June 1999.

[99] J.D. Rhodes, R. Levy, "Generalized multiplexer theory", IEEE Trans. Microwave Theory Tech., Vol. 27, pp. 99-111, Feb. 1979.

[100] J.D. Rhodes, R. Levy, "Design of general manifold multiplexers", IEEE Trans. Microwave Theory Tech., Vol. 27, pp. 111-123, Feb. 1979.

[101] A.G. Lamperez, T.K. Sarkar, M. Salazar-Palma, "Filter model generation from scattering parameters using the Cauchy method", Proc. 32nd European Microwave Conf., pp. 413-416, Milano, Italy, Sep. 2002.

[102] Y.-X. Guo, L. C. Ong, M. Y. W. Chia, B. Luo, "Dual-band bandpass filter in LTCC," IEEE MTT-S Int. Microwave Symp. Dig., pp. 2219-2222, Long Beach, USA, June 2005.

[103] M.-L. Chuang, "Concurrent dual band filter using single set of microstrip open-loop resonators," IEE Electronics Lett., Vol. 41, pp. 1013–1014, Sep. 2005.

[104] G. Macchiarella, S. Tamiazzo, "Design techniques for dual-passband filters," IEEE Trans. Microwave Theory Tech., Vol. 53, pp. 3265–3271, Nov. 2005.

[105] R.J. Cameron, M. Yu, Y.Wang, "Direct-coupled microwave filters with single and dual stopbands," IEEE Trans. Microwave Theory Tech., Vol. 53, pp. 3288–3297, Nov. 2005.

[106] M. Mokhtaari, J. Bornemann, S. Amari, "Coupling-matrix design of dual/triple-band uni-planar filters," IEEE MTT-S Int. Microwave Symp. Dig., pp. 515–518, San Francisco, USA, June 2006.

[107] E. G. Cristal, S. Frankel, "Hair-pin line and hybrid hair-pin line/ half-wave parallel-coupled-line filters," IEEE Trans. Microwave Theory Tech., Vol. 20, pp. 719–728, Nov. 1972.

[108] J. Bornemann, S. Amari, R. Vahldieck, "A flexible S-matrix algorithm for the design of folded waveguide filters," Proc. 35th European Microwave Conf., pp. 405-408, Paris, France, Oct. 2005.

[109] U. Rosenberg, "Multiplexing and double band filtering with common multimode cavities," IEEE Trans. Microwave Theory Tech., Vol. 38, pp. 1862–1871, Dec. 1990.

[110] M. Mokhtaari, J. Bornemann, S. Amari, "Advanced filter design using cross-coupled networks with higher-order resonances," Proc. 35th European Microwave Conf., pp. 1423-1426, Paris, France, Oct. 2005.

[111] J.S. Hong, M.J. Lancaster, "Coupling of microstrip square openloop resonators for cross-coupled planar microwave filters", IEEE Trans. Microwave Theory Tech., Vol. 44, pp. 2099-2109, Nov. 1996.

[112] S.Y. Lee, C.M. Tsai, "New cross-coupled filter design using improved hairpin resonators", IEEE Trans. Microwave Theory Tech., Vol. 48, pp. 2482-2490, Dec. 2000.

[113] J.S. Hong, M.J. Lancaster, "Design of highly selective microstrip bandpass filters with a single pair of attenuation poles at finite frequency", IEEE Trans. Microwave Theory Tech., Vol. 48, pp. 1098-1107, July 2000.

[114] J.S. Hong, M.J. Lancaster, "Microstrip cross-coupled trisection bandpass filters with asymmetric frequency characteristics", IEE Proc. Microwave Antennas Propag., Vol. 146, pp. 84-90, Feb. 1999.

[115] W. Wang, J.S. Fu, Y.Z. Xiong, Y. Lu, "A compact bandpass filter using folded λ/4 coupled-line resonators", Proc. 4th Int. Conf. Microwave Millimeter Wave Technology, pp. 260-263, Beijing, China, Aug. 2004.

[116] M.G. Banciu, R. Ramer, A. Ioachim, "Microstrip filters using new compact resonators", IEE Electronics Lett., Vol. 38, pp. 228-229, Feb. 2002.

[117] S.J. Yao, R. Bonetti, A.E. Wiliams, "Generalized dual-plane multicoupled line filters", IEEE Trans. Microwave Theory Tech., Vol. 41, pp. 2182-2189, Dec. 1993.

[118] E.G. Cristal, S. Frankel, "Hair-pin line and hybrid hair-pin line/half-wave parallel-coupled-line filters", IEEE Trans. Microwave Theory Tech.., Vol. 20, pp. 719-728, Nov. 1972.

[119] B.C. Wadell, Transmission Line Design Handbook, Boston: Artech House, 1991.

[120] R.R. Mansour, "Design of superconductive multiplexer using single mode and dual mode filters", IEEE Trans. Microwave Theory Tech., Vol. 42, pp. 1411-1418, July 1994.

[121] J.A. Curtis, J.F. Fiedziuszko, "Miniature dual-mode microstrip filters", IEEE MTT-S Int. Microwave Symp. Dig., pp.443-446, June 1991.

[122] K. Rambabu, J. Bornemann, "Simplified analysis technique for the initial design of a class of LTCC filters," IEEE Trans. Microwave Theory Tech., Vol. 53, pp. 1787–1791, May 2005.

[123] J. Uher, J. Bornemann, U. Rosenberg, Waveguide Components for Antenna Feed Systems—Theory and CAD. Norwood, MA: Artech House, 1993.

[124] H.-Y.A. Yim, K.-K.M. Cheng, "Novel dual-band planar resonator and admittance inverter for filter design and applications", IEEE MTT-S Int. Microwave Symp. Dig., pp. 2187-2190, Fort Worth, USA, June 2004.

[125] C.-M. Tsai, H.-M. Lee, C.-C. Tsai, "Planar filter design with fully controllable second passband", IEEE Trans. Microwave Theory Tech., Vol. 53, pp. 3429-3439, Nov. 2005.

[126] X. Guan, Z. Ma, P. Cai, Y. Kobayashi, T. Anada and G. Hagiwara, "Synthesis of dual-band bandpass filters using successive frequency transformations and circuit conversions", IEEE Microwave Wireless Comp. Lett., Vol. 16, pp.110-112, Mar. 2006.

[127] M.-I. Lai, S.-K. Jeng, "Compact microstrip dual-band bandpass filters design using genetic-algorithm techniques", IEEE Trans. Microwave Theory Tech., Vol. 54, pp. 160-167, Jan. 2006.

[128] M. Sagawa, M. Makimoto, S. Yamashita, "Geometrical structures and fundamental characteristics of microwave stepped-impedance resonators", IEEE Trans. Microwave Theory Tech., Vol. 45, pp. 1078-1085, July 1997.

[129] J.-T. Kuo, H.-S. Cheng, "Design of quasi-elliptic function filters with a dual-passband response", IEEE Microwave Wireless Comp. Lett., Vol. 14, pp. 472-474, Oct. 2004.

[130] J.-T. Kuo, T.-H. Yeh, C.-C. Yeh, "Design of microstrip bandpass filters with a dual-passband response", IEEE Trans. Microwave Theory Tech., Vol. 53, pp. 1331-1337, Apr. 2005.

[131] S. Sun, L. Zhu, "Coupling dispersion of parallel-coupled microstrip lines for dual-band filters with controllable fractional pass bandwidths", IEEE MTT-S Int. Microwave Symp. Dig., pp. 2195-2198, Long Beach, USA, June 2005.

[132] S. Sun, L. Zhu, "Novel design of dual-band microstrip bandpass filters with good in-between isolation", Proc. Asia Pacific Microwave Conf., 4p., Suzhou, China, Dec. 2005.

[133] T.-H. Huang, H.-J. Chen, C.-S. Chang, L.-S. Chen, Y.-H. Wang, M.-P. Houng, "A novel compact ring dual-mode filter with adjustable second-passband for dual-band applications", IEEE Microwave Wireless Comp. Lett., Vol. 16, pp. 360-362, June 2006.

[134] M. Mokhtaari, K. Rambabu, J. Bornemann, S. Amari, "Advanced stepped-impedance dual-band filters with wide second stopbands", Proc. Asia Pacific Microwave Conf., pp. 2285-2288, Bangkok, Thailand, Dec. 2007.

[135] J. Wang, Y.-X. Guo, B.Z. Wang, L.C. Ong, "Dual-band stepped-impedance band-pass filter", Proc. 36th European Microwave Conf., pp. 902-904, Manchester, UK, Oct. 2006.

[136] H. Zhang, K.J. Chen, "A tri-section stepped-impedance resonator for cross-coupled bandpass filters", IEEE Microwave Wireless Comp. Lett., Vol. 15, pp. 401-403, June 2005.

[137] C.-H. Lee, C.-I. G. Hsu, H.-K. Jhuang, "Design of a new tri-band microstrip BPF using combined quarter-wavelength SIRs", IEEE Microwave Wireless Comp. Lett., Vol. 16, pp. 494-596, Nov. 2006.

[138] L. Zhu, S. Sun, W. Menzel, "Ultra-wideband (UWB) bandpass filters using multiple-mode resonator", IEEE Microwave Wireless Comp. Lett., Vol. 15, pp. 796-798, Nov. 2005.

[139] Y.-C. Chiou, J.-T. Kuo, E. Cheng, "Broadband quasi-Chebyshev bandpass filters with multimode stepped-impedance resonators (SIRs)", IEEE Trans. Microwave Theory Tech., Vol. 54, pp. 3352-3358, Aug. 2006.

[140] M. Mokhtaari, J. Bornemann, S. Amari, "Folded compact ultra-wideband stepped-impedance resonator filters", IEEE MTT-S Int. Microwave Symp. Dig., pp. 747-750, Honolulu, USA, June 2007.

[141] P. Cai, Z. Ma, X. Guan, Y. Kobayashi, T. Anada, G. Hagiwara, "A novel compact ultra-wideband bandpass filter using a microstrip stepped-impedance four-modes resonator", IEEE MTT-S Int. Microwave Symp. Dig., pp. 751-754, Honolulu, USA, June 2007.

[142] A.A.A. Apriyana, Z.Y. Ping, "A dual-band BPF for concurrent dual-band wireless transceiver", Proc. 5th Electronics Packaging Technology Conf., pp. 145 – 149, Singapore, Dec. 2003.

[143] S. Sun, L. Zhu, "Compact dual-band microstrip band pass filters without external feeds", IEEE Microwave Wireless Comp. Lett., Vol. 15, pp. 644-646, Oct. 2005.

[144] S.-Y. Lee, "Optimum resonant conditions of stepped impedance resonators", Proc. 35th European Microwave Conf., pp. 417-420, Paris, France, Oct. 2005.

[145] M. Mokhtaari, J. Bornemann, S. Amari, "Dual-band stepped-impedance filters for ultra-wideband applications", Proc. 37th European Microwave Conf., pp. 779-782, Munich, Germany, Oct. 2007.

[146] M. Mokhtaari, J. Bornemann, S. Amari, "Quasi-elliptic dual-band stepped-impedance filters with folded parallel high-impedance segments", Proc. 37th European Microwave Conf., pp. 862-865, Munich, Germany, Oct. 2007.

[147] M. Mokhtaari, J. Bornemann, S. Amari, "New reduced-size step-impedance dual-band filters with enhanced bandwidth and stopband performance", IEEE MTT-S Int. Microwave Symp. Dig., San Francisco, USA, June 2006.

[148] L. Zhu, H. Bu, K. Wu, "Aperture compensation technique for innovative design of ultra-broadband microstrip bandpass filter", IEEE MTT-S Int. Microwave Symp. Dig., pp. 315-318, Boston, USA, June 2000.

[149] L. Zhu, H. Bu, K. Wu, "Aperture compensation and multipole generation techniques leading to the emergence of a new planar filter", Proc. Asia Pacific Microwave Conf., pp. 1310-1314, Sydney, Australia, Dec. 2000.

[150] W. Menzel, L. Zhu, K. Wu, F. Bögelsack, "On the design of novel compact broad-band planar filters", IEEE Trans. Microwave Theory Tech., Vol. 51, pp. 364-370, Feb. 2003.

[151] J. Gao, L. Zhu, W. Menzel, F. Bögelsack, "Short-circuited CPW multiple-mode resonator for ultra-wideband (UWB) bandpass filter", IEEE Microwave Wireless Comp. Lett., Vol. 16, pp. 104-106, Mar. 2006.

[152] L.-H. Hsieh, K. Chang, "Compact, low insertion-loss, sharp-rejection, and wide-band microstrip bandpass filters", IEEE Trans. Microwave Theory Tech., Vol. 51, pp. 1241-1246, Apr. 2003.

[153] Y.-K. Kuo, C.-H. Wang, C.H. Chen, "Novel reduced-size coplanar-waveguide bandpass filters", IEEE Microwave Wireless Comp. Lett., Vol. 11, pp. 65-67, Feb. 2001.

[154] Z.C. Hao, W. Hong, H. Li, H. Zhang, K. Wu, "A broadband substrate integrated waveguide (SIW) filter", IEEE AP-S Int. Symp. Dig., pp. 598-601, Washington, USA, July 2005.

[155] C. Nguyen, "Development of new miniaturized bandpass filter having ultra-wide bandwidth", IEE Electronics Lett., Vol. 30, pp. 767-768, May 1994.

[156] M. Mokhtaari, J. Bornemann, S. Amari, "Compact planar ultra-wide pass-band filters with source-load coupling and impedance stubs", Proc. Asia Pacific Microwave Conf., pp. 155-158, Yokohama, Japan, Dec. 2006.

Appendix – Matlab Codes

Matlab codes for cross-coupling matrix and electric and magnetic coupling coefficients

----------Filter Synthesis----------

```
%The program in order to find the proper coupling matrix for the filter
%structure
format short;
N=input('please enter the number of resonatores:');
Recognition=input('If you have the initial coupling matrix for optimization Enter 1, otherwise
Enter 0');
if Recognition==1
   M=input('please enter initial coupling matrix M :');
else
M=[];
M=eye(2+N,2+N);
for i=1:(N+1)
M(i,i)=0;
M(i,i+1)=0.5;
M(i+1,i)=0.5;
end
M(2+N,2+N)=0;
end
R1=input('please enter the normalized input resistor:');
R2=input('please enter the normalized output resistor:');
optR=input('Would you like to do optimization of the input/output resistor? Yes press 1, No press
0.');
%for k=1:N+2
%   for p=k:N+2
%     if abs(k-p)==1
%        M(k,p)=.75;
%       M(p,k)=M(k,p);
%     end
     %%%%if k==p & k~=1 & k~=(N+2)
     %%%%   if k==3 |k==5 |k==7
     %%%%      M(k,p)=-.45;
     %%%%   else
     %%%%   M(k,p)=-.8;
     %%%%   end
     %%%%end
     %   end
     %end

Mmin=[];
Mmax=[];

P(N+2,N+2)=0;
Control=input(' Do you want to enter the control elements of coupling matrix? Yes press "1", No
Press "0"');
```

```
i=0;
j=0;
formmin=[];
formmax=[];
while Control==1
   form=input(' Please enter the coupled elements to control in Optimization in the form of [i,j]');
   I=form(1);
   J=form(2);
   if I<=(N+2) & J<=(N+2)
      P(I,J)=1;
      P(J,I)=1;
         sign=input(' Is there any minimum value for this coupling element? Yes press 1, No press
0');
         if sign==1
         min=input('How much is the minimum value considered of this coupling element in the
optimization program? ');
         formmin=[formmin;form];
         Mmin=[Mmin;min];
         end
         sign=input('Is there any maximum value for this coupling element? Yes press 1, No press
0');
         if sign==1
         max=input('How much is the maximum value considered of this coupling element in the
optimization program? ');
         formmax=[formmax;form];
         Mmax=[Mmax;max];
         end

   else
      input('you have entered wrong connection, Please ENTER to Continue');
   end
   Control=input(' Do you want to enter more control elements of coupling matrix? Yes press "1",
No Press "0"');
end

%Entering the maximum and minimum value of coupling elemnts into the filter
%topology;

long=length(Mmin);
for i=1:long
   I=formmin(i,1);
   J=formmin(i,2);
   if M(I,J)<Mmin(i)
      M(I,J)=Mmin(i);
   end
end
long=length(Mmax);
for i=1:long
   I=formmax(i,1);
   J=formmax(i,2);
   if M(I,J)>Mmax(i)
      M(I,J)=Mmax(i);
   end
end
```

```
%P=input('please enter the P matrix:');
%returnloss=input('please enter the return loss:');
%[centerfreq,band]=bandwidth(returnloss);
centerfreq=input('Enter the center frequency of the filter:');
band=input('Enter the bandwidth of the filter:');
sign=1;
f=[];
S11p=[];
S21p=[];
weight1=[];
weight1=[];
weight2=[];
input('In the next step, please enter the important frequencies ( Poles and Zeros ) in the
optimization from min to max respectively and their scattering parameters : PRESS ENTER');
while sign==1
   fin=input('Please enter frequency :');
   f=[f;fin];
   Sin=input(' Please enter the magnitude of S11 of the frequency you entered :');
   weight=0;
   while weight==0
   wgt=input('How much is the weight on this element? Please enter a weight value between 1 to
10!');
      if wgt>=1 & wgt<=10
      weight1=[weight1;wgt];
      weight=1;
      else
      input('Error! Please Enter to go to input the right weight value!');
      end
   end
   S11p=[S11p;Sin];
   Sin=input('Please enter the magnitude of S21 of the frequency you entered :');
   weight=0;
   while weight==0
   wgt=input('How much is the weight on this element? Please enter a weight value between 1 to
10!');
      if wgt>=1 & wgt<=10
      weight2=[weight2;wgt];
      weight=1;
      else
      input('Error! Please Enter to go to input the right weight value!');
      end
   end

   S21p=[S21p;Sin];
   Yes=input('Do you want to add more frequency? Yes press 1 No press 0');
   if Yes==0
      sign=0;
   end
end
save testoffilter S11p, S21p, f;
w=f(:);
w0=centerfreq;
deltaw=band;
%load filey P;
```

```
P=abs(P);
eps=1e-28;
ep=1;
figure(1);
hold;
%%%%plot(w,20.*log10(abs(S21p(151:801))),'c');
%%%%plot(w,20.*log10(abs(S11p(151:801))),'g');
plot(w,20.*log10(abs(S21p(:))),'c');
plot(w,20.*log10(abs(S11p(:))),'g');
Yes=input('Is there any NON resonator node in the filter topology ? yes press 1 No press 0');
Node=[];

while Yes==1
   node=input('Please enter the Non-resonating node number :');
   Node=[Node;node];
   Yes=input('Is there any other NON resonator node in the filter topology ? yes press 1 No press
0');
end
i=sqrt(-1);
[fx,invtotal,S11t,S21t]=Fxx1(M,R1,R2,w,w0,deltaw, Node);
count=1;
F=[];
F(count)=(fx')*(fx);
leng=length(M);
number=0;
previous=[];
S=[];
lg=length(w);
while (ep)>eps
n=0;
K=[];
N=[];
lengK=[];
lengN=[];
test=[];
for k=1:leng%ceil(leng./2)
   for p=k:leng
      if P(k,p)==1
         n=n+1;
         test(leng,leng,n)=0;
         test(k,p,n)=1;
         test(p,k,n)=1;
         %test(leng-k+1,leng-p+1,n)=1;
         %test(leng-p+1,leng-k+1,n)=1;
         %lengK=[lengK;leng-k+1];
         %lengN=[lengN;leng-p+1];

         %if k==1 & p==2
         %   test(5,6,n)=1;
         %   test(6,5,n)=1;
         %   lengK=[lengK;5];
         %   lengN=[lengN;6];
         %else
         %   if k==1 & p==3
```

```
        %       test(3,6,n)=1;
        %       test(6,3,n)=1;
        %       lengK=[lengK;3];
        %       lengN=[lengN;6];
        %     else
        %       if k==2 & p==4
        %         test(4,5,n)=1;
        %         test(5,4,n)=1;
        %         lengK=[lengK;4];
        %         lengN=[lengN;5];
        %       else
        %         if k==1 & p==4
        %           test(4,6,n)=1;
        %           test(6,4,n)=1;
        %           lengK=[lengK;4];
        %           lengN=[lengN;6];
        %         else
  %                 if k==2 & p==2
  %                   test(6,6,n)=1;
  %                   lengK=[lengK;6];
  %                   lengN=[lengN;6];
  %                 else
  %                   lengK=[lengK;k];
  %                   lengN=[lengN;p];
  %                 end
  %               end
  %             end
  %           end
  %       end
        %test(leng-k+1,leng-p+1,n)=1;
        %test(leng-p+1,leng-k+1,n)=1;
        K=[K;k];
        N=[N;p];
        %lengK=[lengK;leng-k+1];
        %lengN=[lengN;leng-p+1];
      end
    end
end

if optR==1
test(leng,leng,n+1)=0;
test(1,1,n+1)=-i;
test(leng,leng,n+1)=-i;
n=n+1;
end;

e=[];
e(leng)=0;
e(1)=1;
e=e(:);
J=[];
Final=[];
for k=1:n
  dI1=[];
```

```
  dIN=[];
  dS11=[];
  dS21=[];
  for p=1:lg
     dI=[];
     dI=i.*invtotal(:,:,p)*test(:,:,k)*invtotal(:,:,p)*e;

     dI1(p)=sqrt(weigth1(p)).*dI(1);
     dIN(p)=sqrt(weigth2(p)).*dI(leng);

     if k==n & optR==1
        dR=-i.*invtotal(:,:,p)*e./R1;
        dI1(p)=dI(1)+dR(1);
        dR=-i.*invtotal(:,:,p)*e./sqrt(R1.*R2);
        dIN(p)=dI(leng)+dR(leng);
     end
  end
  dS11=-2.*R1.*dI1(:);
  dS21=2.*sqrt(R1.*R2).*dIN(:);
  testS11=(S11t==0);
  S11t=S11t+(1e-15).*testS11;
  dS11=real(abs(S11t).*dS11./S11t);
  dS21=real(abs(S21t).*dS21./S21t);
  %dS11=real(conj(S11t).*dS11./abs(S11t));
  %dS21=real(conj(S21t).*dS21./abs(S21t));

  J(:,k)=[dS11(:);dS21(:)];
end
gx=[];
gx=2.*J'*fx;
hx=[];
hx=4.*J'*J;
H=hx;
alpha=(gx'*gx)./(gx'*H*gx);
%if number==0
S=eye(length(H),length(H));
dx=-alpha.*S*gx;
delta=dx
%Different Optmization Program
%else
%gama=gx-previous;
%S=S+(1+(gama'*S*gama)/(gama'*delta))*(delta*delta')/(gama'*delta)-
(delta*gama'*S+S*gama*delta')/(gama'*delta);
%dx=-.25.*alpha.*S*gx;
%delta=dx;
%beta=(gx'*gx)./(previous'*previous);
%dx=-.25.*alpha.*gx-.25.*beta.*previous;
%end
%.....
dM=[];
dM(leng,leng)=0;
if optR==1
   n=n-1;
end
```

```
for k=1:n
   dM(K(k),N(k))=dx(k);
   dM(N(k),K(k))=dx(k);
   %dM(lengK(k),lengN(k))=dx(k);
   %dM(lengN(k),lengK(k))=dx(k);
end
Finalr=[R1,R2];

if optR==1
dR1=dx(n+1);
dR2=dx(n+2);
n=n+1;
R1=R1+dR1;
R2=R2+dR1;
end

Finalm=M;
format short;
M=M+dM
long=length(Mmin);
for j=1:long
   I=formmin(j,1);
   J=formmin(j,2);
   if M(I,J)<Mmin(j)
      M(I,J)=Mmin(j);
   end
end
long=length(Mmax);
for j=1:long
   I=formmax(j,1);
   J=formmax(j,2);
   if M(I,J)>Mmax(j)
      M(I,J)=Mmax(j);
   end
end
%M=Mfunction1(M)
format long;
%comp1=diag(M);
%comp2=diag(comp1);
%comp=((M-comp2)>=0);
%M=M.*comp;
%M=M+comp2;
count=count+1;
%maxfx=max(abs(fx));
%weigth1=(weigth1+(abs(fx(1:lg))-maxfx)./sum(abs(fx)));
%weigth2=(weigth2+(abs(fx(lg+1:2.*lg))-maxfx)./sum(abs(fx)));
[fx,invtotal,S11t,S21t]=Fxx1(M,R1,R2,w,w0,deltaw, Node);
F(count)=(fx')*(fx);
ep=(-F(count)+F(count-1));
previous=gx;
number=number+1;

pause;
end
```

```
----------FX1----------
    %The program in order to find the proper coupling matrix for the filter
%structure
format short;
N=input('please enter the number of resonatores plus non-resonators in the coupling
configuration:');
Recog=input('If you have the initial coupling matrix for optimization Press 1, otherwise Enter 0');

if Recog==0
M=[];
M=eye(2+N,2+N);
for i=1:(N+1)
M(i,i)=0;
M(i,i+1)=0.5;
M(i+1,i)=0.5;
end
M(2+N,2+N)=0;
end

while Recog==1
  M=input('please enter initial coupling matrix M :')
  if (length(M)-2)==N
    Recog=578;
  else
    input('Error! the size of coulpling matrix is not matched with the number of resonators you
have entered. Press ENTER');
  end
end

R1=input('please enter the normalized input resistor:');
R2=input('please enter the normalized output resistor:');
optR=input('Would you like to do optimzation of the input/output resistor? Yes press 1, No press
0.');
%for k=1:N+2
%   for p=k:N+2
%     if abs(k-p)==1
%        M(k,p)=.75;
%       M(p,k)=M(k,p);
%     end
     %%%%if k==p & k~=1 & k~=(N+2)
     %%%%   if k==3 |k==5 |k==7
     %%%%      M(k,p)=-.45;
     %%%%   else
     %%%%   M(k,p)=-.8;
     %%%%   end
     %%%%end
     %   end
     %end

Mmin=[];
Mmax=[];

P(N+2,N+2)=0;
Control=input(' Do you want to enter the control elements of coupling matrix? Yes press "1", No
Press "0"');
```

```
i=0;
j=0;
formmin=[];
formmax=[];
while Control==1
   form=input(' Please enter the coupled elements to control in Optimization in the form of [i,j]');
   I=form(1);
   J=form(2);
   if I<=(N+2) & J<=(N+2)
      P(I,J)=1;
      P(J,I)=1;
         sign=input(' Is there any minimum value for this coupling element? Yes press 1, No press
0');
         if sign==1
         min=input('How much is the minimum value considered of this coupling element in the
optimization program? ');
         formmin=[formmin;form];
         Mmin=[Mmin;min];
         end
         sign=input('Is there any maximum value for this coupling element? Yes press 1, No press
0');
         if sign==1
         max=input('How much is the maximum value considered of this coupling element in the
optimization program? ');
         formmax=[formmax;form];
         Mmax=[Mmax;max];
         end

   else
      input('you have entered wrong connection, Please ENTER to Continue');
   end
   Control=input(' Do you want to enter more control elements of coupling matrix? Yes press "1",
No Press "0"');
end

%Entering the maximum and minimum value of coupling elemnts into the filter
%topology;

long=length(Mmin);
for i=1:long
   I=formmin(i,1);
   J=formmin(i,2);
   if M(I,J)<Mmin(i)
      M(I,J)=Mmin(i);
   end
end
long=length(Mmax);
for i=1:long
   I=formmax(i,1);
   J=formmax(i,2);
   if M(I,J)>Mmax(i)
      M(I,J)=Mmax(i);
   end
end
```

```
%P=input('please enter the P matrix:');
%returnloss=input('please enter the return loss:');
%[centerfreq,band]=bandwidth(returnloss);
centerfreq=input('Enter the center frequency of the filter:');
band=input('Enter the bandwidth of the filter:');
sign=1;
f=[];
S11p=[];
S21p=[];

weigth1=[];
weigth2=[];
input('In the next step, please enter the important frequencies ( Poles and Zeros ) in the
optimization from min to max respectively and their scattering parameters : PRESS ENTER');
while sign==1
   fin=input('Please enter frequency :');
   f=[f;fin];
   Sin=input(' Please enter the magnitude of S11 of the frequency you entered :');
   weight=0;
   while weight==0
   wgt=input('How much is the weight on this element? Please enter a weight value between 1 to
10!');
      if wgt>=1 & wgt<=10
      weigth1=[weigth1;wgt];
      weight=1;
      else
      input('Error! Please Enter to go to input the right weight value!');
      end
   end
   S11p=[S11p;Sin];
   Sin=input('Please enter the magnitude of S21 of the frequency you entered :');
   weight=0;
   while weight==0
   wgt=input('How much is the weight on this element? Please enter a weight value between 1 to
10!');
      if wgt>=1 & wgt<=10
      weigth2=[weigth2;wgt];
      weight=1;
      else
      input('Error! Please Enter to go to input the right weight value!');
      end
   end

   S21p=[S21p;Sin];
   Yes=input('Do you want to add more frequency? Yes press 1 No press 0');
   if Yes==0
      sign=0;
   end
end
save testoffilter S11p S21p f;
w=f(:);
w0=centerfreq;
deltaw=band;
%load filey P;
```

```
P=abs(P);
eps=1e-28;
ep=1;
figure(1);
hold;
%%%%plot(w,20.*log10(abs(S21p(151:801))),'c');
%%%%plot(w,20.*log10(abs(S11p(151:801))),'g');
plot(w,20.*log10(abs(S21p(:))),'c');
plot(w,20.*log10(abs(S11p(:))),'g');
Yes=input('Is there any NON resonator node in the filter topology ? yes press 1 No press 0');
Node=[];

while Yes==1
   node=input('Please enter the Non-resonating node number :');
   Node=[Node;node];
   Yes=input('Is there any other NON resonator node in the filter topology ? yes press 1 No press
0');
end
i=sqrt(-1);
[fx,invtotal,S11t,S21t]=Fxx1(M,R1,R2,w,w0,deltaw, Node);
count=1;
F=[];
F(count)=(fx')*(fx);
leng=length(M);
number=0;
previous=[];
S=[];
lg=length(w);
while (ep)>eps
n=0;
K=[];
N=[];
lengK=[];
lengN=[];
test=[];
for k=1:leng%ceil(leng./2)
   for p=k:leng
      if P(k,p)==1
         n=n+1;
         test(leng,leng,n)=0;
         test(k,p,n)=1;
         test(p,k,n)=1;
         %test(leng-k+1,leng-p+1,n)=1;
         %test(leng-p+1,leng-k+1,n)=1;
         %lengK=[lengK;leng-k+1];
         %lengN=[lengN;leng-p+1];

         %if k==1 & p==2
         %   test(5,6,n)=1;
         %   test(6,5,n)=1;
         %   lengK=[lengK;5];
         %   lengN=[lengN;6];
         %else
         %   if k==1 & p==3
```

```
        %       test(3,6,n)=1;
        %       test(6,3,n)=1;
        %       lengK=[lengK;3];
        %       lengN=[lengN;6];
        %     else
        %       if k==2 & p==4
        %         test(4,5,n)=1;
        %         test(5,4,n)=1;
        %         lengK=[lengK;4];
        %         lengN=[lengN;5];
        %       else
        %         if k==1 & p==4
        %           test(4,6,n)=1;
        %           test(6,4,n)=1;
        %           lengK=[lengK;4];
        %           lengN=[lengN;6];
        %         else
  %                 if k==2 & p==2
  %                   test(6,6,n)=1;
  %                   lengK=[lengK;6];
  %                   lengN=[lengN;6];
  %                 else
  %                   lengK=[lengK;k];
  %                   lengN=[lengN;p];
  %                 end
  %               end
  %             end
  %           end
  %       end
        %test(leng-k+1,leng-p+1,n)=1;
        %test(leng-p+1,leng-k+1,n)=1;
        K=[K;k];
        N=[N;p];
        %lengK=[lengK;leng-k+1];
        %lengN=[lengN;leng-p+1];
      end
    end
end

if optR==1
test(leng,leng,n+1)=0;
test(1,1,n+1)=-i;
test(leng,leng,n+1)=-i;
n=n+1;
end;

e=[];
e(leng)=0;
e(1)=1;
e=e(:);
J=[];
Final=[];
for k=1:n
   dI1=[];
```

```
  dIN=[];
  dS11=[];
  dS21=[];
  for p=1:lg
     dI=[];
     dI=i.*invtotal(:,:,p)*test(:,:,k)*invtotal(:,:,p)*e;

     dI1(p)=sqrt(weigth1(p)).*dI(1);
     dIN(p)=sqrt(weigth2(p)).*dI(leng);

     if k==n & optR==1
        dR=-i.*invtotal(:,:,p)*e./R1;
        dI1(p)=dI(1)+dR(1);
        dR=-i.*invtotal(:,:,p)*e./sqrt(R1.*R2);
        dIN(p)=dI(leng)+dR(leng);
     end
  end
  dS11=-2.*R1.*dI1(:);
  dS21=2.*sqrt(R1.*R2).*dIN(:);
  testS11=(S11t==0);
  S11t=S11t+(1e-15).*testS11;
  dS11=real(abs(S11t).*dS11./S11t);
  dS21=real(abs(S21t).*dS21./S21t);
  %dS11=real(conj(S11t).*dS11./abs(S11t));
  %dS21=real(conj(S21t).*dS21./abs(S21t));

  J(:,k)=[dS11(:);dS21(:)];
end
gx=[];
gx=2.*J'*fx;
hx=[];
hx=4.*J'*J;
H=hx;
alpha=(gx'*gx)./(gx'*H*gx);
%if number==0
S=eye(length(H),length(H));
dx=-alpha.*S*gx;
delta=dx
%Different Optmization Program
%else
%gama=gx-previous;
%S=S+(1+(gama'*S*gama)/(gama'*delta))*(delta*delta')/(gama'*delta)-
(delta*gama'*S+S*gama*delta')/(gama'*delta);
%dx=-.25.*alpha.*S*gx;
%delta=dx;
%beta=(gx'*gx)./(previous'*previous);
%dx=-.25.*alpha.*gx-.25.*beta.*previous;
%end
%.....
dM=[];
dM(leng,leng)=0;
if optR==1
   n=n-1;
end
```

```
for k=1:n
   dM(K(k),N(k))=dx(k);
   dM(N(k),K(k))=dx(k);
   %dM(lengK(k),lengN(k))=dx(k);
   %dM(lengN(k),lengK(k))=dx(k);
end
Finalr=[R1,R2];

if optR==1
dR1=dx(n+1);
dR2=dx(n+2);
n=n+1;
R1=R1+dR1;
R2=R2+dR1;
end

Finalm=M;
format short;
M=M+dM
long=length(Mmin);
for j=1:long
   I=formmin(j,1);
   J=formmin(j,2);
   if M(I,J)<Mmin(j)
      M(I,J)=Mmin(j);
   end
end
long=length(Mmax);
for j=1:long
   I=formmax(j,1);
   J=formmax(j,2);
   if M(I,J)>Mmax(j)
      M(I,J)=Mmax(j);
   end
end
%M=Mfunction1(M)
format long;
%comp1=diag(M);
%comp2=diag(comp1);
%comp=((M-comp2)>=0);
%M=M.*comp;
%M=M+comp2;
count=count+1;
%maxfx=max(abs(fx));
%weigth1=(weigth1+(abs(fx(1:lg))-maxfx)./sum(abs(fx)));
%weigth2=(weigth2+(abs(fx(lg+1:2.*lg))-maxfx)./sum(abs(fx)));
[fx,invtotal,S11t,S21t]=Fxx1(M,R1,R2,w,w0,deltaw, Node);
F(count)=(fx')*(fx);
ep=(-F(count)+F(count-1));
previous=gx;
number=number+1;

pause;
end
```

```
----------FXX1----------
function [fx,invtotal,S11,S21]=Fxx1(M,R1,R2,w,w0,deltaw, Node)
i=sqrt(-1);
N=length(M)-2;
R=[];
R(1,1)=R1;
R(2+N,2+N)=R2;
U=eye(2+N,2+N);
U(1,1)=0;
U(2+N,2+N)=0;
long=length(Node);
if long~=0
   for j=1:long
      U(Node(j),Node(j))=0
   end
end

e=[];
e(2+N)=0;
e(1)=1;
e=e(:);
wp=[];
wp=(w0./deltaw).*((w./w0)-(w0./w));
%wp=((w./w0)-(w0./w));
leng=length(wp);
I=[];
invtotal=[];
for k=1:leng
   invertA=inv(wp(k).*U-i.*R+M);
   invtotal(:,:,k)=invertA;
   I(:,k)=-i.*invertA*e;
end
S21=[];
S21=2.*sqrt(R1.*R2).*I(2+N,:);
S11=[];
S11=1-2.*R1.*I(1,:);
plot(w,20.*log10(abs(S21)),'r');
%hold;
plot(w,20.*log10(abs(S11)),'b');
load testoffilter;
S11t=abs(S11(:))-abs(S11p(:));
S21t=abs(S21(:))-abs(S21p(:));
%S11t=abs(S11(:))-abs(S11p(:));
%S21t=abs(S21(:))-abs(S21p(69:2:97));
%S11t=(S11(:))-(S11p);
%S21t=(S21(:))-(S21p);
S11=S11(:);
S21=S21(:);
fx=[(S11t);(S21t)];
fx=fx(:);
---------- OPTFILTER----------
%Matlab Program for the Direct Simulation of the Coupling matrix
format short;
M=input('please enter M coupling matrix after the final Optimization:');
```

```
N=length(M)-2;
%M=[];
M(1,1)=0;
M(2+N,2+N)=0;
R1=input('please enter the normalized input resistor:');
R2=input('please enter the normalized output resistor:');
%for k=1:N+2
%   for p=k:N+2
%      if abs(k-p)==1
%         M(k,p)=.5;
%         M(p,k)=M(k,p);
%      end
%   end
%end
R=[];
R(1,1)=R1;
R(2+N,2+N)=R2;
U=eye(2+N,2+N);
U(1,1)=0;
U(2+N,2+N)=0;
Yes=input('Is there any NON resonator node in the filter topology ? yes press 1 No press 0');
Node=[];

while Yes==1
   node=input('Please enter the Non-resonating node number :');
   Node=[Node;node];
   Yes=input('Is there any other NON resonator node in the filter topology ? yes press 1 No press
0');
end
long=length(Node);
if long~=0
   for i=1:long
      U(Node(i),Node(i))=0
   end
end

e=[];
e(2+N)=0;
e(1)=1;
e=e(:);

w=input('please enter the frequency range:');
deltaw=input('please enter the bandwidth of the filter:');
w0=input('please enter the center frequency of the filter:');
wp=(w0./deltaw).*((w./w0)-(w0./w));
%wp=((w./w0)-(w0./w));
%w=w.*(1e9);
%w0=w0.*(1e9);
%deltaw=deltaw.*(1e9);
leng=length(wp);
I=[];
tetag=[];

for k=1:leng
```

```
   invertA=inv(wp(k).*U-i.*R+M);
   tetag(:,k)=2.*sqrt(R1.*R2).*i.*invertA*U*invertA*e;
   I(:,k)=-i.*invertA*e;
end

S21=[];
S21=2.*sqrt(R1.*R2).*I(2+N,:);
tetag=-imag(tetag(2+N,:)./S21);
S11=[];
S11=1-2.*R1.*I(1,:);
figure(1);
plot(w,20.*log10(abs(S21)),'g');
hold;
plot(w,20.*log10(abs(S11)),'r');
figure(2);
plot(w,tetag,'y');
hold;
load testoffilter S11p, S21p, f;
f1=[];
f1=(w0./deltaw).*((f./w0)-(w0./f));
n=length(f);
tetag1=[];
S21p=abs(S21p);
S11p=abs(S11p);
for k=1:n-1
   tetag1(k)=(S21p(k+1)-S21p(k))./(f1(k+1)-f1(k));
   tetag1(k)=-imag(tetag1(k)./S21p(k));
end
tetag2=[];
for k=n:-1:2
   tetag2(k)=(S21p(k)-S21p(k-1))./(f1(k)-f1(k-1));
   tetag2(k)=-imag(tetag2(k)./S21p(k));
end
tetag=[];
tetag(1:n)=0;
tetag(1)=tetag1(1);
tetag(n)=tetag2(n);
tetag(2:n-1)=(tetag1(2:n-1)+tetag2(2:n-1))./2;
plot(f,tetag(:),'g');
format short;
----------ELECTRIC AND MAGNETIC COUPLING COEF----------
a=22.5
w=.2;
h=.508;
epsr=2.2;
s=.05:.001:3;
Fe=(-.09605+1.4087.*sqrt(a./h)-.2443.*(a./h));
De=(.1608-.06945.*sqrt(a./h)).*((s./h).^1.15);
pe=1.0886+.03146.*((w./h).^4);
Be=(1.0678+.226.*log((epsr+1)./2)).*((s./h).^pe);
Ae=.2259-.01571.*epsr+.1.*sqrt(epsr+1).*w./h;
Ke=pi.*Fe.*exp(-Ae).*exp(-Be).*exp(-De)./16;
figure(1);
plot(s,Ke);
```

```
Fm=-.5014+1.0051.*sqrt(a./h)-.1557.*(a./h);
Dm=(1.154-.8242.*sqrt(a./h)+.1417.*a./h).*(s./h);
pm=.8885-.1751.*sqrt(w./h);
Bm=1.2.*((s./h).^pm);
Am=(-.06834+.14142.*(w./h)+.08655.*((w./h).^3));
Km=pi.*Fm.*exp(-Am).*exp(-Bm).*exp(-Dm)./16;
figure(2);
plot(s,Km);
Kb=.5.*Km+.6.*Ke;
figure(3);
plot(s,Kb);
-----------------------------------Epsr effective Calculation-----------------------------------
function [epseff,epsef]=espf(f,h,W,epsr);
n=length(W);
h=h./10;
w=W./10;
f=f./(1e9);
epsef=[];
epseff=[];
for k=1:n
w=W(k);
k1=(1+12.*h./w).^-.5;
k2=(1-w./h).^2;
if w./h<=1
   epsef(k)=(epsr+1)./2+((epsr-1)./2).*(k1+.04.*k2);
else
   epsef(k)=(epsr+1)./2+((epsr-1)./2).*(k1);
end
p4=1+2.751.*(1-exp((-(epsr./15.916).^8)));
p3=.0363.*(exp(-4.6.*w./h)).*(1-exp(-(f.*h./3.87).^4.97));
p2=.33622.*(1-exp(-.03442.*epsr));
p1=.27488+(.6315+.525./((1+.157.*f.*h).^20)).*w./h-.065683.*exp(-8.751.*w./h);
pf=p1.*p2.*((.1844+p3.*p4).*(10.*f.*h)).^1.5763;
epseff(k,:)=epsr-(epsr-epsef(k))./(1+pf);
end
-----------------------------------------------------------------------------------------------------------
```

List of Publications

Journal Papers:

[1] M. Mokhtaari, J. Bornemann, K. Rambabu, and S. Amari, "Coupling-matrix design of dual and triple pass-band filters", IEEE Trans. Microwave Theory Tech., Vol. 54, pp. 3940-3946, Nov. 2006.

[2] M. Mokhtaari, J. Bornemann, and S. Amari, "Quasi-elliptic dual-band filter design using stepped-impedance resonators and coupling topologies for narrow-to-wide-band applications", Accepted to be published at IET Proceeding on Microwave, Antennas & Propagations.

[3] M. Mokhtaari, J. Bornemann, and S. Amari, "Compact ultra-wideband filters in microstrip technology", to be submitted to the Int. Journal of Electronics and Communications.

Conference Papers:

[1] M. Mokhtaari, J. Bornemann and S. Amari, "Advanced filter design using cross-coupled networks with higher-order resonances", Proc. 35th European Microwave Conf., pp. 1423-1426, Paris, France, Oct. 2005.

[2] J. Bornemann and M. Mokhtaari, "Initial design and optimization of broad-band and dual-band square-to-circular waveguide transitions", Proc. 2005 Asia-Pacific Microwave Conf., pp. 726-728, Suzhou, China, Dec. 2005.

[3] J. Bornemann and M. Mokhtaari, "The bifurcated E-plane T-junction and its application to waveguide diplexer design", Proc. German Microwave Conf. (GeMiC), 1a-5, 4 p., Karlsruhe, Germany, Mar. 2006.

[4] M. Mokhtaari, J. Bornemann and S. Amari, "Coupling-matrix design of dual/triple-band uni-planar filters", 2006 IEEE MTT-S Int. Microwave Symp. *Dig.*, pp. 515-518, San Francisco, USA, June 2006.

[5] M. Mokhtaari, J. Bornemann and S. Amari, "New reduced-size step-impedance dual-band filters with enhanced bandwidth and stopband performance", 2006 IEEE MTT-S Int. Microwave Symp. *Dig.*, pp. 1181-1184, San Francisco, USA, June 2006.

[6] M. Mokhtaari, J. Bornemann and S. Amari, "Compact planar ultra-wide pass-band filters with source-load coupling and impedance stubs", Proc. 2006 Asia-Pacific Microwave Conf., pp. 155-158, Yokohama, Japan, Dec. 2006.

[7] M. Mokhtaari, J. Bornemann and S. Amari, "Folded compact ultra-wideband stepped-impedance resonator filters", 2007 IEEE MTT-S Int. Microwave Symp. *Dig.*, pp. 747-750, Honolulu, USA, June 2007.

[8] K. Rambabu, M. Mokhtaari and J. Bornemann, "Simplified computation of electromagnetic band-gap properties of via-holed metal patches", 2007 IEEE EMC-S Int. Symp. Dig., TU-AM-5-2, 4 p., Honolulu, USA, July 2007.

[9] M. Mokhtaari, J. Bornemann and S. Amari, "Dual-band stepped-impedance filters for ultra-wideband applications", Proc. 37th European Microwave Conf., pp. 779-782, Munich, Germany, Oct. 2007.

[10] M. Mokhtaari, J. Bornemann and S. Amari, "Quasi-elliptic dual-band stepped-impedance filters with folded parallel high-impedance segments", Proc. 37th European Microwave Conf., pp. 862-865, Munich, Germany, Oct. 2007.

[11] M. Mokhtaari, K. Rambabu, J. Bornemann and S. Amari, "Advanced stepped-impedance dual-band filters with wide second stopbands", Proc. 2007 Asia-Pacific Microwave Conf., pp. 2285-2288, Bangkok, Thailand, Dec. 2007.

[12] M. Mokhtaari, J. Bornemann, "Directional ultra-wideband antennas in planar technologies", Proc. 38th European Microwave Conf., Amsterdam, Netherlands, Oct. 2008.

[13] M. Mokhtaari, J. Bornemann, "Ultra-wideband and notched wideband filters with grounded vias in microstrip technology", Accepted at the Asia Pacific Microwave Conference (APMC), Dec. 2008.

[14] M. Mokhtaari, J. Bornemann, "A tunable notched wideband filter in microstrip technology", submitted to the International Microwave Symposium (IMS), June 2009.